Flow System to Study the Role of the Vascular Endothelial Glycocalyx in Transendothelial Migration of Cancer Cells in-vitro

A Major Qualifying Project Report:

Submitted to the Faculty of

WORCESTER POLYTECHNIC INSTITUTE

In partial fulfillment of the requirements of the

Degree of Bachelor of Science in

Biomedical Engineering

By
Helga Becka
Kerry Bushway
Samantha Cocchiaro
Jacob Elliott

Advisor
Professor Solomon A. Mensah

April 25, 2024

Table of Contents

Authorship

Section	Subsection	Primary Author(s)	Primary Editor(s)
Acknowledgements		Kerry	Samantha
Abstract		Kerry, Samantha	Helga
Chapter 1: Introduction		All	All
Chapter 2: Literature Review	2.1 Cancer and Its Causes	Kerry	Samantha
	2.2 The Vascular System	Samantha	Kerry
	2.3 The Glycocalyx	Samantha	Kerry
	2.4 Prior Art	Jacob, Helga	Samantha
Chapter 3: Project Strategy	3.1 Initial Client Statement	All	Samantha
	3.2 Design Requirements	All	Kerry
	3.3 Engineering Standards	Samantha	Kerry
	3.4 Revised Client Statement	Samantha	Kerry
	3.5 Management Approach	Kerry	Samantha
Chapter 4: Design Process	4.1 Need Analysis	Helga	Kerry, Jacob
	4.2 Alternative Designs	All	Kerry, Jacob
	4.3 Design Process and Final Design Models	All	Kerry
	4.4 Determining Flow System Geometry	Jacob	Kerry

	4.5 Arts and Crafts Model	Kerry	Helga, Samantha
	4.6 CAD Models	Samantha, Helga	Kerry
	4.7 3D Printing	Jacob	Kerry
Chapter 5: Testing	5.1 SolidWorks Fluid Flow Simulation	Kerry	Jacob
	5.2 Flow Tests	Kerry	Jacob
	5.3 Membrane Tests	Jacob, Helga	Kerry
	5.4 Staining Test	Jacob	Helga
Chapter 6: Final Design	6.1 Final Model Components	All	Helga, Kerry
	6.2 Device Manufacturing	Samantha	Helga
	6.3 Flow System Components	All	Helga, Kerry
	6.4 Final Design Setup	Samantha, Kerry	Helga
	6.5 Final Design Test	Jacob	Helga
Chapter 7: Design Validation and Verification	7.1 Flow System	Samantha, Kerry	Kerry, Helga
	7.2 Cells	Helga	Kerry
	7.3 Membranes	Helga	Kerry
	7.4 Imaging	Helga	Kerry
Chapter 8: Safety and Ethics Statement	8.1 Health and Safety Concerns	All	Samantha
	8.2 General Ethical Concerns and Mitigation	All	Samantha

Chapter 9: Results	9.1 HLMVEC Flow tests	Jacob, Samantha	Helga
	9.2 HLMVEC and MDA-MB-231 Flow Tests	Jacob, Helga	Samantha
Chapter 10: Discussion	10.0 Discussion	Helga	Samantha
Chapter 11: Conclusions and Recommendations	11.1 Conclusions	Jacob	Helga
	11.2 Recommendations	Kerry	Helga
References		All	Kerry
Appendix I: Fluid Flow Calculations		Jacob, Kerry	All
Appendix II: Breast Cancer Cell Culture Protocol		Jacob	All
Appendix III: HLMVEC Culture Protocol		Jacob	All
Appendix IV: CellTrace Protocol		Jacob	All
Appendix V: Cell Freezing Protocols		Jacob	All
Appendix VI: Cell Thawing Protocols		Jacob	All
Appendix VII: MDA-MB-231 Media Preparation		Jacob	All
Appendix VIII: Flow Rate Test Protocols		Jacob	All
Appendix IX: Full System Test		Jacob, Kerry	All
Appendix X: Flow System Setup Protocol		Kerry	All
Appendix XI: Static Migration Tests		Jacob, Helga	All
Appendix XII: Staining WGA and DAPI Procedures		Jacob	All
Appendix XIII: Quantification Procedures		Samantha, Helga	All

Acknowledgments

Abstract

Cancer is a complex disease characterized by uncontrolled cell growth, posing a significant health challenge worldwide. One of cancer's deadliest aspects is its ability to metastasize wherein cancer cells spread from their primary site to other parts of the body, forming secondary tumors that often prove fatal due to their aggressive and invasive nature. The endothelial glycocalyx, a crucial component of the blood vessel wall, plays a pivotal role in this process by mediating interactions between circulating cancer cells and endothelial cells, influencing cancer cell adhesion, extravasation, and ultimately, secondary tumor formation. The aim of this project is to develop an in-vitro device that is able to study the role of the endothelial glycocalyx in transendothelial migration of cancer cells. The results of our research show that the glycocalyx is thicker when exposed to shear stress as opposed to static conditions where no shear stress is present, and that more cancer cells are able to complete transendothelial migration when the glycocalyx is less robust and has not been exposed to shear stress. This novel device allows for viewing of transendothelial migration of cancer cells and the team believes that using this framework future research and further experimentation will allow the role of the endothelial glycocalyx in cancer metastasis to be studied.

List of Figures

List of Tables

Chapter 1: Introduction

Cancer is a disease in which normal cells divide uncontrollably forming a tumor [1]. This tumor formation typically starts in one location and then moves throughout the body in the vascular system leading to the formation of secondary tumors called metastasis [1]. Movement of circulating cancer cells is enhanced by blood flow, although the actual blood vessels themselves serve as the mechanism of transport [1]. Included in the vascular system is a series of branched pathways including arteries, veins, and capillaries. Within each of these vessels is a carbohydrate-rich layer that lines the vessel walls called the endothelial glycocalyx [2]. The endothelial glycocalyx plays a large part in how cancer cells are able to spread throughout the body forming secondary tumors [3].

The glycocalyx is a barrier that shields the vascular endothelium of blood vessels from negatively charged molecules in the blood [4]. Cancer cells are negatively charged and when they enter the vessel walls they have to degrade the glycocalyx in order to access the vascular endothelium [5]. Once they degrade the glycocalyx, they migrate out of the blood vessel. This process is called transendothelial migration because it involves the cancer cells pushing between vascular endothelial cells to migrate into the surrounding tissues leading to secondary tumor formation [6].

There have been efforts in the past to study transendothelial migration of cancer cells in vitro as a first step in understanding secondary tumor formation. Among the first models that assess how malignant cells can transmigrate through an endothelial cell monolayer is a modified Boyden chamber, also known as a Transwell migration assay [7]. 3D in vitro microvascular networks that replicate human vasculature have also been utilized to investigate transendothelial migration of cancer cells [8]. Additionally, microfluidic devices have been developed and used to explore how breast cancer cells metastasize and invade bone tissue [9]. While all these studies represent great efforts that have been done in the past regarding transendothelial migration of cancer, they do not give any indications of the importance of the glycocalyx in this process.

This project aims to generate a model for studying the role of the endothelial glycocalyx in the transendothelial migration of cancer cells in-vitro. Following the engineering design process, the team began by generating the final design in CAD software, SolidWorks, and then using a simulation as a first step in analysis. This SolidWorks fluid flow simulation showed proof of concept in allowing the team to understand the flow dynamics within the model. The simulation also helped to ensure that flow dynamics are psychologically relevant to the application in capillaries. After the device was manufactured, flow tests, leak tests, and several membrane tests were completed with cells before moving forward to full device testing. Human lung microvascular endothelial cells (HLMVECs) and breast cancer cells from the MDA-MB-231 cell line were utilized in testing. HLMVECs were seeded onto a 3.0-micron porous membrane at a

concentration of 100k/mL. Attaching a peristaltic pump, to emulate pulsatile flow in the body, the system was screwed together, and tubing attached. Following the device setup protocols, the full device was set up inside the hood before being transferred to the incubator. A calculated flow rate of 270.3 ml/min was then applied to precondition the system. After one hour, the flow was stopped, one million live labeled cancer cells in one ml of media were added into the syringe reservoir and then the flow was decreased to a rate of 60.1ml/min and ran for another hour. Immediately following the second hour of flow, the system was taken apart, the cells on the membrane were fixed, and the reservoir was removed. The membrane and the reservoir were transferred to a Keyence BZ-X800 microscope to image. This imaging was completed to evaluate the overall interaction between the circulating cancer cells and the endothelial glycocalyx. A static test was used as a control and was completed in parallel with the dynamic flow test. Finally, the number of cancer cells that passed through the membrane were quantified and graphs were created to further analyze the results.

Chapter 2: Literature Review

In order to appreciate the depth of the need for this project, it is important to understand the research done by the team. This includes what cancer is, what affects cancer, how it spreads, and the general principles of the vascular system. Additionally, the team explored previous flow systems and strategies that already exist in order to classify and describe the greater need for this type of system in cancer research.

2.1 Cancer and Its Causes

Cancer is the second leading cause of death worldwide accounting for nearly ten million deaths in 2020 alone [10]. In the United States, it has been predicted that in 2024 alone, 611,720 people will die from cancer, which is approximately 1,680 people per day [11]. Everyone faces an equal risk of being diagnosed with cancer because it affects every race, gender, and age across the globe. On a cellular level cancer is the result of changes in a cell's DNA. DNA is the carrier of all genetic information and makes up chromosomes [12]. Certain changes in a cell's DNA can lead to cells that are dividing normally to become cancer cells that divide rapidly or abnormally. The cancer cell formation process can be seen in Figure 1 below.
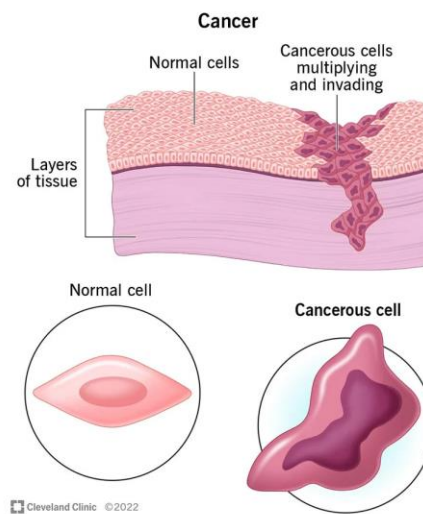
Figure 1: Cancer Cell Formation. The above image depicts the difference in shape of normal cells versus cancerous cells. It also shows how cancerous cells multiply and invade the layers of tissue throughout the body [12].

Although mostly unknown, some factors and other environmental impacts can lead to certain people being more susceptible to developing [13]. For example, UV radiation is a proven human carcinogen causing types of cancer that appear on the skin due to damage from the sun [13]. Wearing sunscreen and staying out of direct sunlight when the UV index is high will decrease your chances of experiencing too much UV radiation leading to cancer cell development [14]. Another factor that can make someone more likely to develop cancer is smoking. Tobacco and

cigarette smoke contain poisons that weaken the body's immune system. With a weakened immune system, it is harder for one's body to have a proper immune response and therefore is more difficult to kill the cancerous cells [14]. Although cancer isn't contagious and cannot be passed down directly from parent to child, genetic changes increase the risk of cancer if an individual inherits a growth control gene with a mutation from one parent [13]. This occurs in a small percentage of cancer patients but is not impossible. Ultimately, living a healthy lifestyle will lead to people being less likely to develop cancer throughout their lifetimes. This includes habits such as eating a healthy diet, getting regular exercise, and only consuming alcohol in moderation, if at all [14].

2.1.1 Physiology of Cancer

Tumors can be described as either malignant or benign [14]. Malignant tumors are cancerous while benign tumors are non-cancerous [14]. In general, cancer is a disease that occurs when normal cells divide incorrectly forming cancerous cells. These cancerous cells typically grow uncontrollably and invade the layers of tissues ultimately forming tumors. Additionally, cancer cells can be characterized by their large nucleus and overall irregular size and shape. There are four different stages of cancer that help to characterize how much the cancer has spread throughout a patient's body [12]. The first stage is characterized when the cancer is localized to a small area that has not spread to the lymph nodes or other tissues [3]. Stage II cancer has grown to form a small tumor, but it still has not spread to other parts of the body [12]. The third stage is distinguished by the increased growth of the tumor, and it has possibly spread to the lymph nodes or other tissues [12]. Lastly, stage four is characterized when the cancer has spread to other organs and areas of the body. This fourth stage is often referred to as metastatic or advanced cancer [12].

2.1.2 Clinical Presentation and Diagnosis

Although cancer presents itself differently in each patient it impacts, there are a variety of general symptoms that seem to characterize a patient's cancer diagnosis, many of which appear as common symptoms of other diseases [10]. These can include fatigue or overall chronic tiredness which can be characterized by light sensitivity, headaches, muscle and joint pain, difficulty concentrating, and mood swings [13]. In some cases, there may be a lump of cells or an area of thickening that can be felt under the skin. Unexpected and unexplained weight changes or changes in different areas of the skin may also occur [13]. Persistent pain that cannot seem to be understood and unexplained bleeding or bruising is also one form of the clinical presentation of cancer [13]. It is important to note that cancer symptoms may vary depending on the person and the location of the cancer cells.

Diagnosis of cancer often occurs using blood and imaging tests and biopsies [12]. Each of these tests may be requested by a physician in the event that any one of the above symptoms is present

[12]. Blood testing may involve collecting a blood sample from a patient and conducting a complete blood count looking for potential tumor markers. Some types of cancer may cause either high or low values in the number of white blood cells. This includes a higher than normal number of lymphocytes or monocytes whereas some cancer types cause low numbers of neutrophils [15]. Typically, blood tests are considered along with other testing, such as a CT scan, an MRI, a nuclear scan, a bone scan, a PET scan, or an ultrasound [15]. A CT scan can view your organs using a machine similar to an X-ray machine that takes a series of pictures that can be analyzed by a technician for abnormalities [16]. Similarly, an MRI uses a powerful magnet and radio waves in order to take pictures of your body in slices [15]. For a nuclear scan, a small amount of radioactive material will be injected into the bloodstream and during the procedure, a scanner will detect and measure the radioactivity throughout the body [15]. Bone scans are a specific type of nuclear scan that checks specifically for abnormality in the bones. Furthermore, a PET scan is also a type of nuclear scan that works on the general principle that cancer cells take up more glucose than healthy cells. Before the actual scan, radioactive glucose will be injected into the bloodstream and the scanner will be able to take 3D pictures of specific areas where excess glucose is present [15]. Lastly, ultrasounds use high-energy sound waves which echo off the tissues inside your body. Based on the echoes that the computer receives, a technician can determine if a specific area of the body may have cancerous cell growth [15]. Biopsies are typically a more invasive procedure where cells are removed from the potential tumor and tested to determine if the cells are cancerous or benign [17]. Cancer symptom presentation, screening, and diagnosis (Figure 2) are helpful practices in allowing for early detection and treatment of potentially cancerous formations [10].
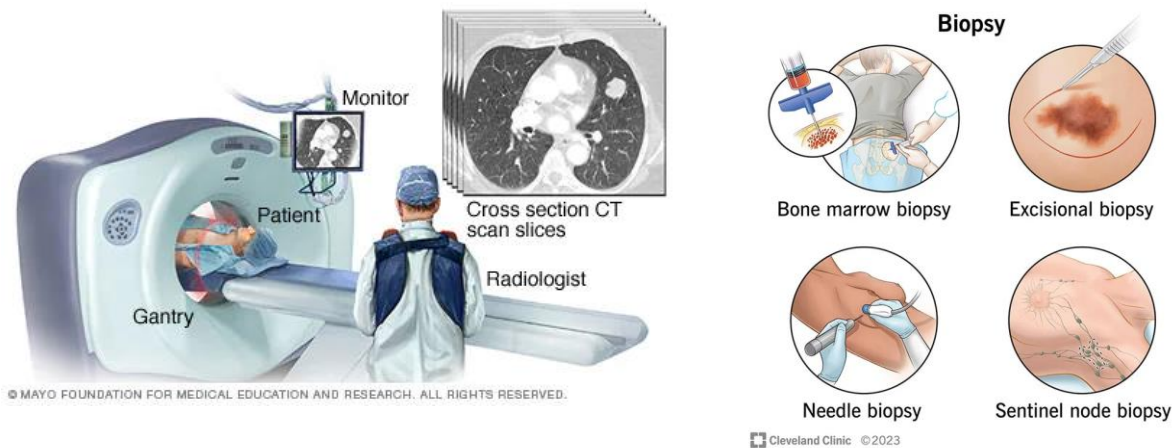
Figure 2: Methods of Cancer Diagnosis. Based upon the type of cancer that is suspected to be invading tissues in the body, different methods may be used to diagnose cancer. Some methods are invasive, and some involve imaging of the area of concern [17] [16].

2.1.3 Treatment and Clinical Outcomes

Once a cancer diagnosis has been given to a patient there are several steps forward towards treatment and ridding the body of all cancerous cells [18]. This can be completed through a variety of therapy and treatment options (Figure 3). Hormone, chemo, targeted, radiation, and immunotherapy are all types of therapy treatments with the same intention to rid cancer in the body [19]. Surgery and bone marrow transplantation are also forms of cancer treatment for specific types of cancer [12]. Hormone therapy is a type of treatment that stops the spread of cancer cells by targeting hormones by slowing or stopping them from being active [19]. Chemotherapy uses drugs to kill cancer cells and is often effective in killing cancer cells but it also kills the surrounding healthy cells. Targeted cancer treatments look for genes, proteins, and other tumor markers that provide information about cancer and how it is spreading. These are then used to specifically target the cells with these markers [20]. Radiation therapy uses high doses of radiation to kill cancer cells ultimately shrinking tumors. Immunotherapy focuses specifically on your immune system and how this body system can help fight cancer [19]. In a surgical procedure, the surgeon will physically remove a cancerous tumor from the body. A bone marrow transplant is another form of procedure that is also used for the treatment of cancer. It is a special type of therapy that involves taking cells that are normally found in the bone marrow and filtering them [21]. All of these types of treatment options have positives and negatives associated with and depending upon the type of cancer that is being treated [12]. This is a general overview of the various types of treatment that are generally used to treat cancer but with further research being completed each and every day, new treatments and methods for treating cancer are being developed.

Figure 3: Common Cancer Treatment Options. For patients diagnosed with cancer, the next step is to understand the options for treatment. Again, specific to the type of cancer, a variety of treatment options are available to help rid the body of these abnormal cells [19].

Cancer impacts every part of a person's life. Learning more about treatment options and how they target cancer cells in the body brings up the question of the economic impact this has on a patient. In 2015, direct medical costs for cancer treatment in the United States alone were 80.2 billion dollars [22]. The out-of-pocket costs spent on cancer treatments in the United States as of 2018 were estimated to have an average upper limit of 2600 USD [23]. For many patients, a cancer diagnosis often comes with financial hardships due to the medical costs associated with hospital bills and treatment paths [20]. Not only is there a financial burden on anyone who is diagnosed with cancer but there is a mental, physical, and emotional impact as well. Due to treatment and or experienced symptoms of cancer, some patients might have limitations on daily activities [20]. This might include everything from not being able to lift heavy objects to not being able to go to work due to the time it takes for treatment [24].

2.1.4 Cancer Metastasis

Primary tumor formation first occurs when normal healthy cells grow uncontrollably after dividing incorrectly [14]. Metastasis (as referenced in Figure 4) is the process in which cancer cells break away from the primary tumor and spread to other parts of the body to establish new tumors which are called secondary tumors [3]. This secondary tumor formation is a result of the cancer cells traveling through the vascular system [3]. Migration of cells happens first and then those cancerous cells invade into other tissues and organs leading to secondary tumor formation. These cells travel through the bloodstream or through the lymph vessels. Cancer metastasis ultimately leads to further spreading of cancer throughout the body via the vascular system [14].
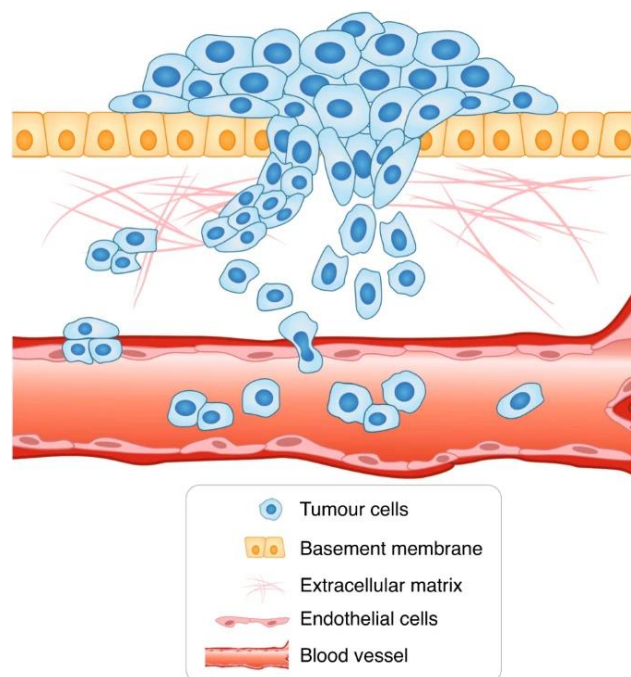
Figure 4: Cancer Cell Metastasis. The image above shows cancer spreading through the wall of a vessel. Once the cancer cells enter the blood vessels, they begin spreading throughout the body. The movement of cancer cells is enhanced by blood flow where these vessels serve as a mechanism for transportation throughout the body [25].

2.2 The Vascular System

The cardiovascular system is composed of the heart, blood, and blood vessels [26] [27]. The main role of this system is to deliver nutrients and oxygen to tissues throughout the body and to transport waste away from tissues in the blood via arteries and arterioles [26] [27]. This project will focus more on the Peripheral Vascular System which is composed of the blood vessels that are outside of the heart and can be seen in Figure 5. The classifications of the peripheral vascular system are the aorta and its branches which include arterioles, capillaries, and the venules and veins that return blood to the heart [27]. We chose to focus on the Peripheral Vascular System due to the role capillaries play in cancer metastasis.
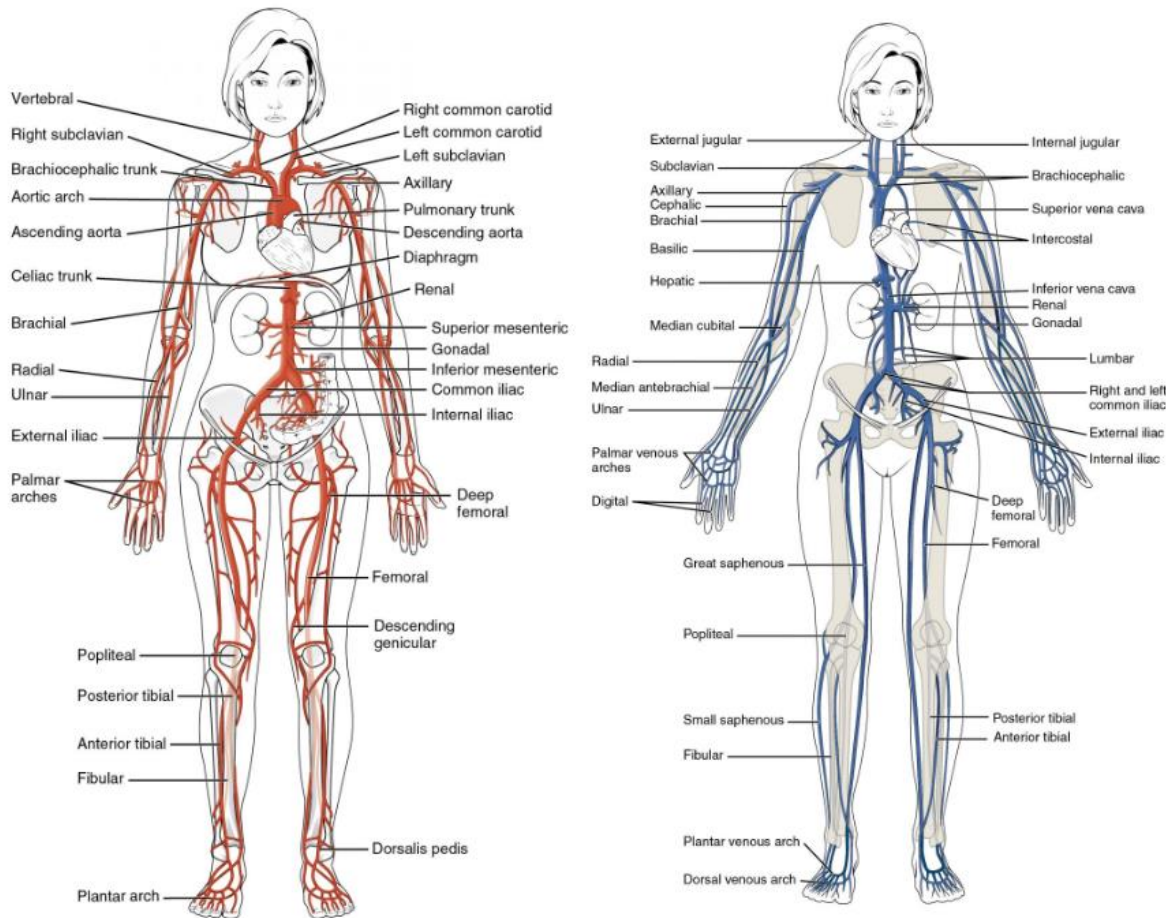
Figure 5: Peripheral Vascular System. The image above is a diagram of the peripheral vascular system and shows the arteries in red (on the left) and the veins in blue (on the right). Notice how the heart is not colored in, as it is not a part of the peripheral vascular system [28].

2.2.1 Capillaries

Capillaries are thin-walled blood vessels that are made up of a single layer of simple squamous endothelial cells, tunica intima, and pericytes [26]. Since capillaries are thin, diffusion is the main method for exchanging nutrients [26] [27]. Due to their thin walls and the ease of diffusion, capillaries are the main vessels used for the loading and unloading of both nutrients and oxygen in and out of tissues [26] [27]. There are three types of capillaries, as can be seen in Figure 6, which include continuous non-fenestrated, continuous fenestrated, and discontinuous/sinusoid [26] [29]. Most organs in the human body consist of continuous non-fenestrated capillaries so those will be the ones that are focused on in this project [26]. Continuous non-fenestrated capillaries have a basement membrane connected via cellular junctions and lack fenestrations, which are pores, on their plasma membrane [26]. These capillaries also allow solutes and water that are smaller than 3nm to pass freely through the vessel wall through the process of diffusion, and any molecule over 3nm can pass through selectively via a transporter [27].
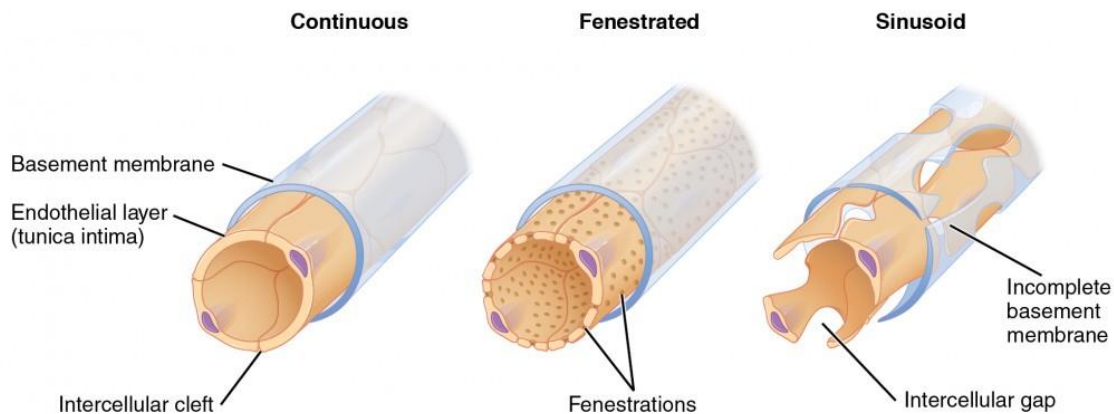
Figure 6: Three Types of Capillaries. The image above shows the three different capillaries; continuous nonfenestrated (left), continuous fenestrated (middle), and discontinuous/sinusoid (right). This image also shows the endothelial layer of the capillary along with the basement membrane [29].

The intra-capillary forces, also called the Starling forces, dictate molecular movement inside the vessel [26]. The main determinant of these forces is the difference in oncotic and hydrostatic pressures between the capillary and the tissue [26]. The hydrostatic pressure of the capillary is the pressure that the fluid exerts on the capillary endothelium [26]. The oncotic pressure is the osmotic pressure that is exerted on the fluid by colloids and proteins [26]. Together, the oncotic and hydrostatic pressures, which can vary over the length of the capillary, control the mechanism by which nutrients diffuse through the membrane [26].

2.2.2 The Endothelium

As mentioned previously in section 2.2.1, capillaries consist of a single layer of simple squamous endothelial cells which can be seen in Figure 6 [26]. These endothelial cells fall under the

category of vascular endothelium because they are the innermost structure of the interior walls of the capillary [30]. The luminal membrane of the endothelial cells is directly in contact with the blood and molecules flowing through the capillary and is also the site for the glycocalyx [30]. The basolateral surface of the endothelial cells is separated from other tissues by the basement membrane, which we previously referred to as the tunica intima in section 2.2.1 [30]. The endothelium is responsible for controlling the degree of vascular relaxation and constriction of the capillary, the extravasation of solutes, and other things such as: fluid, macromolecules, and hormones [30].

2.3 The Glycocalyx

The glycocalyx is a villiform substance that consists of polysaccharide protein complexes, that covers the surface of the vascular endothelium as shown in Figure 7 [31] [32]. It is a proteoglycan polymer, and its core proteins consist of heparan sulfate, chondroitin sulfate, and hyaluronan [31]. The glycocalyx is considered to be the skeletal structure of the endothelial cell surface and therefore is a key factor in fluid regulation and vascular permeability [32]. The dimension and composition of the glycocalyx can fluctuate with changing shear forces which can cause it to shed and resynthesis [30]. The glycocalyx has three main functions in vasculature. The first function is it acts as a bridge between circulating cells in the blood and the endothelium [32]. The second function is that the glycocalyx acts as a selectively permeable barrier for the wall of the blood vessel [32]. Finally, the third function is that it acts as a mechanical sensor of blood shear force [32].
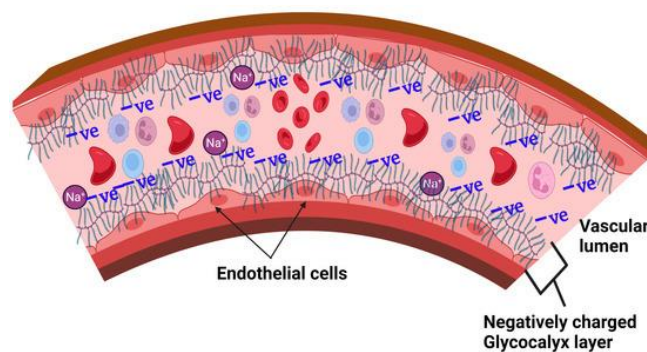
Figure 7: Glycocalyx as a Barrier. This figure shows how a glycocalyx sits on top of the vascular endothelium inside a blood vessel. Since the glycocalyx is negatively charged it repels molecules in the blood and keeps them away from the vascular endothelium [33].

2.3.1 The Glycocalyx Serves as a Barrier

The glycocalyx acts as a barrier between molecules in the blood, such as leukocytes and platelets, and the vascular endothelium [30] [31]. The glycocalyx is negatively charged which is why it is able to repel leukocytes and platelets as can be seen in Figure 7, because they are also negatively charged molecules [30] [31]. The glycocalyx is also described as being a complex

mesh structure which acts as a macromolecular sieve that determines the permeability of blood vessels [30] [31]. Through experiments and testing it has been determined that cancer cells are all negatively charged which means that cancer cells are also repealed by the glycocalyx [4]. However, when the glycocalyx is damaged, there is an increased ability for molecules to move from the plasma to outside the blood vessels because the glycocalyx is no longer there to act as a permeability barrier and repel negatively charged molecules [31].

2.3.2 Degradation of The Glycocalyx

The glycocalyx can be degraded due to a variety of health conditions. For the purpose of this research focus, emphasis will be placed on how cancer and inflammation degrade the glycocalyx. Although glycocalyx impairment can be due to cancer it is generally due to the underlying inflammation which cancer causes [32]. When blood vessels are inflamed, the glycocalyx sheds as a response [31]. The inflammatory mechanisms/sheddases responsible for the shedding and degradation of the glycocalyx include MMPs (Matrix metalloproteinases), HPSE (Heparanse), and HAse (Hyaluronic Acid) [30]. The shedasses are activated by reactive oxygen species and pro-inflammatory cytokines such as TNF-α (Tumor Necrosis Factor Alpha) [31]. TNF-α is produced by cancer cells and activates the inflammation in the blood vessels which in turn degrades the glycocalyx [5]. Degradation of the negatively charged glycocalyx allows cancer cells to attach to the vascular endothelium since there is no longer a negative charge repelling them [31].

2.3.3 A Degraded Glycocalyx Enhances Cancer Attachment

When the glycocalyx is degraded, cancer cells have a much better chance at attaching to the vascular endothelium. TNF-α not only activates inflammation which degrades the glycocalyx, but it also stimulates the proliferation, growth, metastasis, and invasion of cancer cells [34]. Once the glycocalyx is damaged, vascular endothelial cell intercellular adhesion molecule 1 (ICAM-1) and vascular cell adhesion molecule 1 (VCAM-1) are exposed [32]. The exposure of these adhesion molecules allows molecules in the blood circulation (like cancer cells) to attach to the vascular endothelium easier, especially since there is no negative force repelling them [32]. Overall, this creates what can be considered an environment that promotes the development of cancer and allows cancer cells to complete transendothelial migration [34].

2.3.4 Transendothelial Migration

Transendothelial migration, which is also called diapedesis, occurs when migrating cells in the blood move from the luminal side to the abluminal side of the vascular wall [6]. A visual representation of transendothelial migration can be seen in Figure 8. Transendothelial migration starts when the cancer cells invade the blood vessel [6]. Once in the blood vessel, the cancer cells are able to get closer to the adhesion molecules on the vascular endothelium because the

glycocalyx has been damaged and they have the opportunity to attach [6]. Once connected to the adhesion molecules, the cancer cells will crawl along the vascular endothelium as they are still being moved by the shear force of the blood in the blood vessel [6]. Finally, the cancer cell will complete transendothelial migration by moving through the vascular endothelium [6]. There are two types of transendothelial migration: paracellular and transcellular [6]. Paracellular is when the migrating cells move between endothelial cells, and transcellular is when the migrating cells move through the endothelial cells [6]. For the majority of cancer cells, the paracellular method of transendothelial migration is used but it is not impossible for cancer cells to complete transcellular transendothelial migration [35].
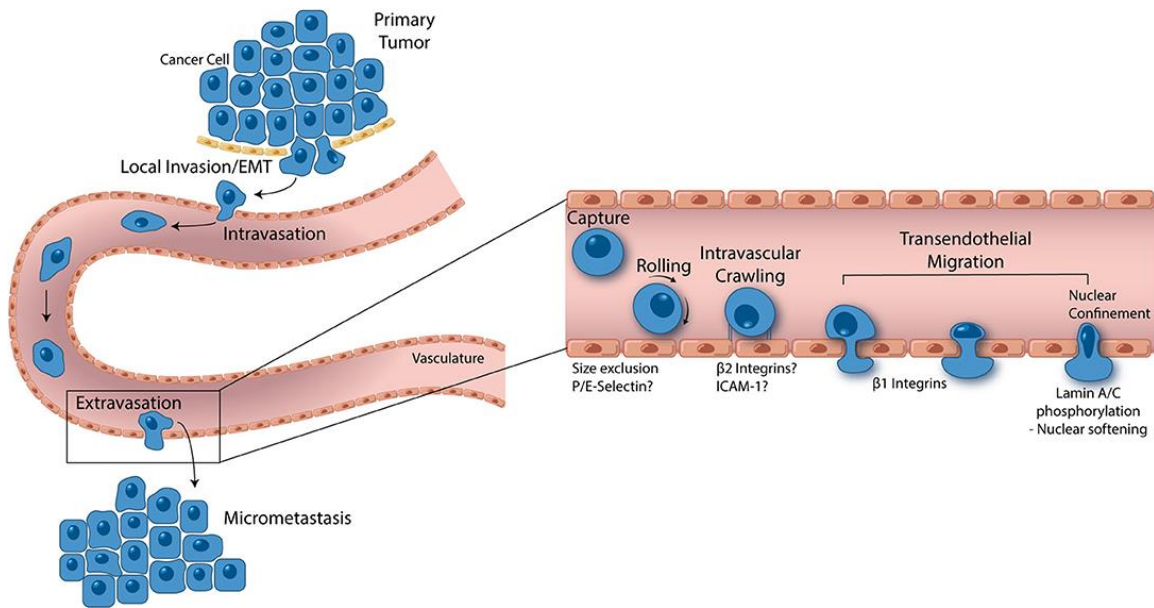
Figure 8: Transendothelial Migration of Cancer Cells. The image above shows the entire process of cancer cells completing transendothelial migration. The image shows the cancer cells entering into the blood vessel, rolling along the exposed vascular endothelium, being captured by adhesion molecules, and crawling across the vascular endothelium, and completing paracellular transendothelial migration [6].

2.4 Prior Art

Despite having knowledge of how cancer is able to degrade the glycocalyx and therefore complete transendothelial migration, there is no current model that allows this to be studied. All current models help to study the overall process but not specifically how the degradation of the endothelial glycocalyx plays a role in secondary tumor formation. In this section, the team reviewed the relevant prior art in the field of in-vitro models for studying transendothelial migration of cancer cells, laying the foundation for our novel approach and highlighting the key advancements and gaps in current research.

2.4.1 Flow Systems in In-Vitro Metastasis Research

In the field of cancer research, the study of in-vitro metastasis models has emerged as a critical avenue for gaining deeper insights into the complex and multifaceted process of cancer metastasis. Utilizing in-vitro systems to model in-vivo phenomena, such as cancer metastasis, is crucial as it not only provides a controlled and manipulable environment for dissecting underlying mechanisms but also allows for the development and testing of targeted therapeutics, The result is an advancement of our understanding of specific diseases and facilitating the discovery of potential treatments. Current models in studying cancer metastasis in vitro consist of flow systems, 2D and 3D cell culture models, and Transwell or modified Boyden chamber assays [36].
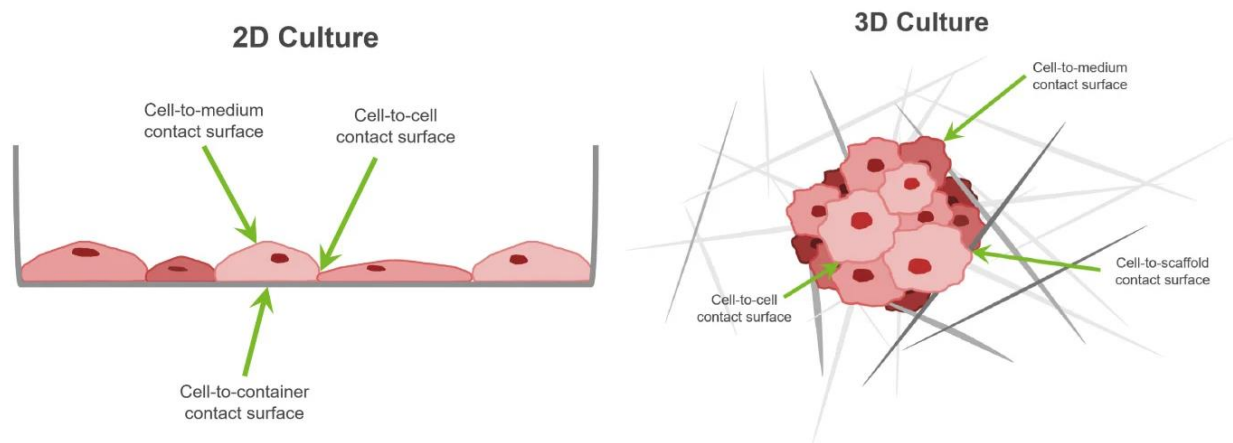
Figure 9: 2D and 3D Cell Culture. The above image depicts the difference between 2D cell culture models and 3D cell culture models [37].

2D cell culture models, as seen in Figure 9 above, involve the cultivation of cells on a flat surface, providing a simplified and controlled environment for various cellular studies and experiments. They possess advantages such as simplicity, low cost, and ease of functional testing [38]. These models also have various downsides including lack of resemblance to natural tissue structures, altered cell morphology, lack of shear stresses, and loss of phenotype diversity [38]. Various 2D cell culture assays are commonly used in metastasis research. These consist of migration assays, invasion assays, adhesion studies, gap closure or cell exclusion zone assays, and Transwell chambers which will be highlighted later in this chapter due to their unique applications in this area of study [36].

Migration assays, also referred to as scratch/wound healing assays, are 2D cell culture models that can be used to assess the migratory potential of cancer cells [39]. In these assays, a monolayer of cancer cells is grown on a flat surface, and a "wound" is created in the cell layer [39]. The closure of this wound over time provides insights into the cells' ability to migrate and close the gap, which is a critical step in the metastatic process [36]. The gap closure or cell

exclusion zone assay involves creating a cleared or "exclusion" zone within a confluent monolayer of cultured cells which track the movement of cells into this cleared area over time. The assay provides valuable insights into cell migration dynamics, motility, and the factors influencing these processes [36].

To provide a more suitable in-vitro testing environment to better replicate in vivo conditions, including cell interactions, researchers in recent years have been using 3D culture methods due to their advantages. 3D culture methods include suspension cultures, cultures in concentrated medium or gel-like substances, and cultures on scaffolds, and overall better mimic natural tissue and tumor structures [38]. Although 3D cultures are generally seen in a positive manner, they do have their downsides such as lower repeatability and higher costs. Figure 10 below provides a comparison of 2D and 3D cell culture methods based on the type of culture and their varying characteristics.

Type of culture	2D	3D	Ref.
Time of culture formation	Within minutes to a few hours	From a few hours to a few days	[11, 34, 57]
Culture quality	High performance, reproducibility, long-term culture, easy to interpret, simplicity of culture	Worse performance and reproducibility, difficult to interpret, cultures more difficult to carry out	[12]
In vivo imitation	Do not mimic the natural structure of the tissue or tumour mass	*In vivo* tissues and organs are in 3D form	[35]
Cells interactions	Deprived of cell-cell and cell-extracellular environment interactions, no *in vivo*-like microenvironment and no "niches"	Proper interactions of cell-cell and cell-extracellular environment, environmental "niches" are created	[13, 28, 29, 36, 37]
Characteristics of cells	Changed morphology and way of divisions; loss of diverse phenotype and polarity	Preserved morphology and way of divisions, diverse phenotype and polarity	[1, 14–17, 20, 38]
Access to essential compounds	Unlimited access to oxygen, nutrients, metabolites and signalling molecules (in contrast to *in vivo*)	Variable access to oxygen, nutrients, metabolites and signalling molecules (same as *in vivo*)	[10, 46]
Molecular mechanisms	Changes in gene expression, mRNA splicing, topology and biochemistry of cells	Expression of genes, splicing, topology and biochemistry of cells as *in vivo*	[23–26, 42–45]
Cost of maintaining a culture	Cheap, commercially available tests and the media	More expensive, more time-consuming, fewer commercially available tests	[8, 48, 58, 75]

Figure 10: Comparison of 2D and 3D Cell Culture Methods. Based on the various types of culture, the figure above shows the differences between 2D and 3D cell culture [38].

Suspension cultures on non-adherent plates are performed by first seeding single cells on non-adherent plates with a culture medium. After approximately 3 days of culture, 3D structures can

be observed. This method is simple, repeatable, and cells can be easily extracted for further testing [38]. Using this method, researchers can establish a monolayer of endothelial cells on a porous membrane or culture dish. Then, cancer cells can be added to the top of the endothelial monolayer, and they can then assess the ability of cancer cells to breach the endothelial barrier. Cultures in concentrated medium or in gel-like substances contain single cells that grow in a medium containing gelling substances like agarose or Matrigel [38]. Cancer cells can be embedded within a Matrigel or similar gel-like substance containing endothelial cells to create a 3D co-culture model. Researchers can then monitor cancer cell migration through the endothelial cell-containing gel and assess the impact of different conditions on transendothelial migration during cancer metastasis. Cultures on scaffolds involve using a scaffold constructed of biodegradable materials where cells can migrate among fibers and attach to them [38]. This method can more accurately resemble cells growing in vivo, with proper cell-cell and cell-environment interactions. In terms of transendothelial migration of cancer cells during metastasis, endothelial cells can be incorporated into the scaffold alongside cancer cells. The scaffold's 3D structure would allow for more complex interactions between these cell types [38].

As mentioned previously, the Transwell or modified Boyden chamber assay has a unique application in the study of transendothelial migration of cancer cells during metastasis. This assay is a 2D cell culture assay that involves a two-chamber system separated by a microporous membrane (usually coated with an ECM matrix component to enhance attachment). Endothelial cells are first seeded into an upper chamber, and their movement is monitored as they migrate to a lower well. In order to promote cell movement, a chemotactic gradient is established by adding serum or specific chemotactic factors in the lower well [36]. After a certain incubation period, the cells that have migrated through the porous membrane can be stained and counted [36]. The setup of this test can be visualized in Figure 11. This assay possesses unique features which can be incorporated into the design of a system that can be utilized to study transendothelial migration of cancer cells during cancer metastasis.
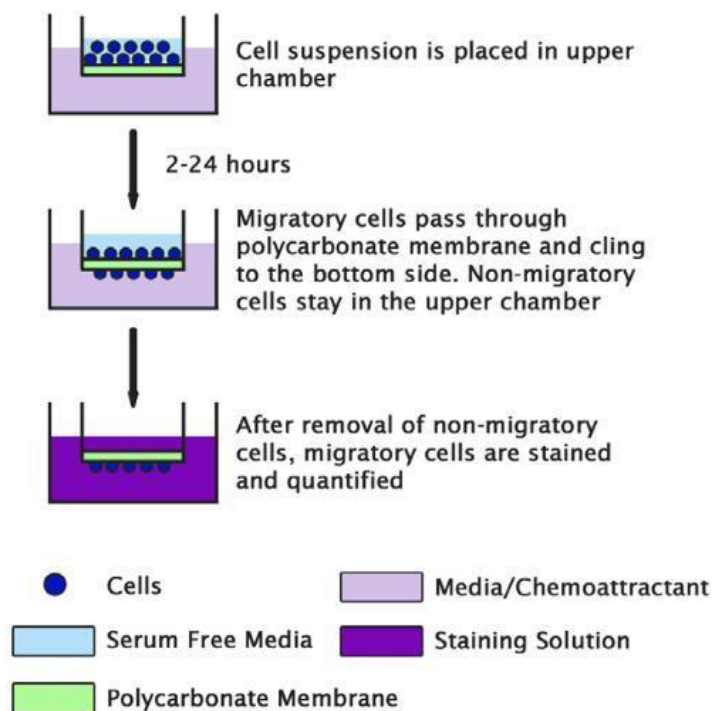
Figure 11: Schematic Diagram of Cell Migration Assay. The cell migration assay has features that can be applied to the application of modeling transendothelial migration during cancer metastasis [40].

Although many of the previously described models to study cancer metastasis in vitro provide valuable insights, they lack several unique features that play a major role in this process. All of the aforementioned processes fail to exhibit the physiological conditions of blood flow in blood vessels and lymphatic vessels and more specifically the impact of the degradation of the glycocalyx on metastasis. This capability is particularly relevant for studying the transendothelial migration of cancer cells, as it replicates the mechanical forces cells encounter during intravasation and extravasation. These static culture conditions fail to mimic flow dynamics and shear stress which ultimately influences cell behavior and migration patterns. In current research, flow systems are popularly utilized to account for these factors. There are three types of flow chambers that are most relevant in cancer metastasis research: microfluidic devices, parallel plate flow chambers, and cone and plate devices [41].

2.4.2 Types of Flow Systems

Understanding the intricacies of cancer metastasis in vitro necessitates the use of flow systems as essential models, enabling researchers to simulate the multifaceted aspects of natural phenomena with precision and relevance. As mentioned previously, flow systems are able to mimic the shear stresses of blood flow seen within the body through the vasculature. Therefore, when

experiments are being conducted for research in areas such as cancer metastasis, the in-vivo conditions can be more accurately reproduced so as to create a physiologically relevant system that can be used to study what exactly happens within the body.

There are currently three widely utilized flow chamber apparatuses including parallel-plate flow chambers, cone-and-plate devices, and microfluidic devices [41]. To begin, a parallel-plate flow chamber (PPFC) (Reference Figure 12 & 13) consists of three main components, a distributor, a gasket, and a glass coverslip. One side of the PPFC contains the distributor which has an inlet port, an outlet port, and a vacuum slot. The other side contains the glass coverslip where the vascular cells are seeded. In between these lies the gasket which prevents fluid leakages and determines the height of the flow path. Flow is generated through an inlet and outlet port on the gaskets that are connected to tubing and a pump [41]. When flow is initiated, the fluid enters the flow chamber through a tube and then flows between two parallel plates, passing over cells cultured on the glass slide. The fluid friction against the cells generates shear stress, and the small gap between the cells and the gasket permits laminar flow [42]. The PPFC system can be adjusted to vary the amount of shear stress the cells experience, which can be visualized in the Navier Stokes equation:

$$(\tau = \frac{6Q\mu}{wh^2})$$

From this equation, τ is the shear stress, μ is the viscosity, Q is the flow rate, w is the width of the channel, and h is the height of the channel formed by the gasket [42]. When the height of the channel is increased the shear stress will decrease immensely as these two values are inversely related. In addition, the entrance length ensures fully developed laminar flow which closely mimics the flow conditions in blood vessels, where laminar flow is predominant [41]. This precise control of shear stress as well as the development of laminar flow is crucial for studying the effects of shear stress on cells, particularly endothelial cells that line blood vessels, which is a crucial factor when studying transendothelial migration of cancer cells.
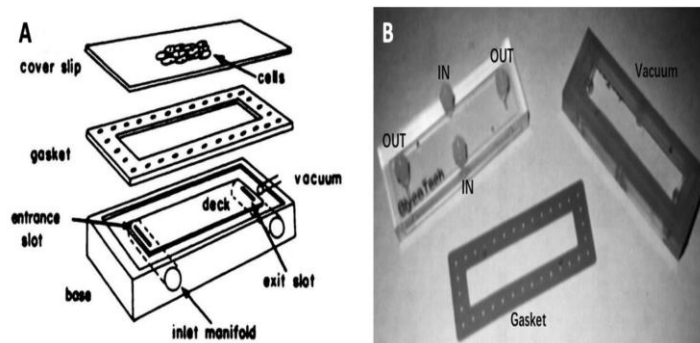
Figure 12: Presentation of the Parallel-Plate Flow Chamber. (A) Schematic diagram of the parallel-plate flow chamber. (B) Parallel-plate flow chamber equipment [43].

The next type of flow system is a microfluidic device. Microfluidic systems revolutionize fluid manipulation by enabling precise control of minute volumes. This highly miniaturized and precise platform is designed for manipulating and controlling small volumes of fluids, typically at the microliter (10^{-6}) to nanoliter (10^{-9}) scale. Within the study of microfluidics, systems called "Lab on Chips" (LoCs) are heavily utilized [44]. These devices can replicate many of the functions of a traditional laboratory but in a much smaller and portable format. A typical Lab-on-Chip consists of a silicon substrate that integrates mechanical elements, microchannels, reaction chambers, actuators, pumps, sensors, and micro-and nano-electronics [45]. The integration of the previously listed features is dependent on the area of research for the LoC. LoCs are typically fabricated using microfabrication techniques such as photolithography and chemical etching techniques [45]. Due to the decrease in size of these systems, there is a different interplay of forces. Surface effects become more important as forces such as gravity and inertia are less relevant. Similar to the PPFC, these devices favor laminar flow due to the vast decrease in channel diameter [44].

A

Entrance Slit Flow Channel Exit Slit

Flow Inlet

Flow Outlet

Gasket

Glass Slide

Cells

B

ω

θ

Cells

$$\tau = \frac{6\mu Q}{wh^2}$$

where τ : shear stress
μ : viscosity of fluid
Q: flow rate
w: width of the channel
h: height of the channel
(formed by the gasket)

$$\tau = \frac{\mu \omega}{\theta}$$

where τ : shear stress
μ : viscosity of fluid
ω: rotational speed
θ: angle of the cone
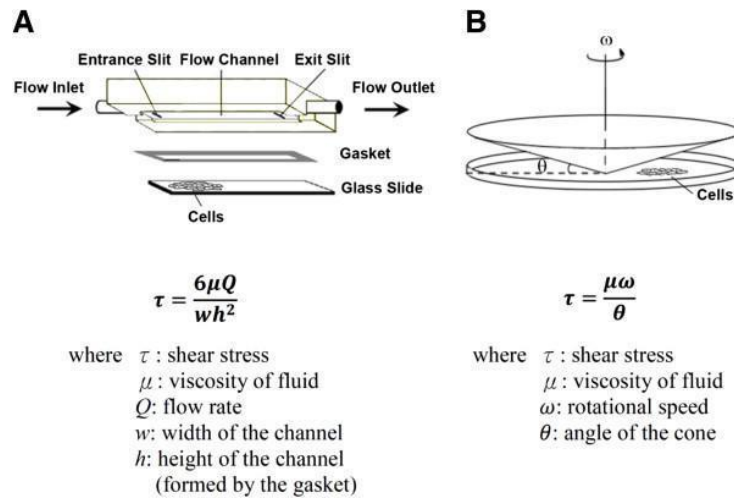
Figure 13: Flow System Setups. (A) Parallel plate flow chamber (PPFC) with applicable equations. (B) Cone and plate device (CPD) with appropriate equations [46].

The final type of flow system that will be explored is the cone and plate device, shown in Figures 13 and 14. This system consists of a rotating cone typically constructed of stainless steel. Each cone has a unique angle at its apex which can vary depending on the specific experimental requirements. Beneath the cone lies a plate/substrate which acts as a flat surface onto which the material under study is applied (primarily endothelial cells) [41] [47]. In many designs, this plate is fixated to a base with the use of a vacuum pump to ensure there is no movement. The cone is attached to a motor or a drive system that allows it to rotate at a controlled speed. Often, spacers are used between the cone and the plate/substrate to maintain a gap between the cone and the dish avoiding cell monolayer damage [47]. As the cone rotates, it induces a shearing effect within the underlying material. This shearing force prompts the material to either flow or deform,

33

contingent upon its rheological characteristics. The degree of flow or deformation is subsequently quantified and analyzed to gain insight into how the material reacts to shear stress [47]. These devices are designed to be small enough to put into an incubator as well as permitting the separation of the CPD base from the motor for sterility during cell culture procedures. The CPD is governed by the following equation:

$$\tau = \frac{\mu\omega}{\Theta}$$

As seen in Figure 13, τ is the shear stress, μ is the viscosity of the liquid, ω is the rotational speed of the cone, and Θ is the angle at the apex of the cone [41] [47]. Researchers and engineers use CPD to measure and characterize the rheological properties of materials. This information is vital for understanding how materials behave in various applications.
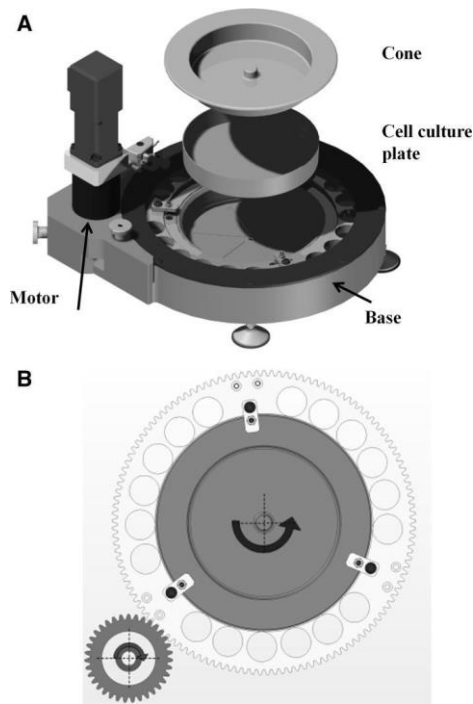
Figure 14: Cone and Plate Device (CPD) Configuration. The image above shows a schematic of what a CPD device typically looks like. There are several components including the motor, base, cell culture plate, and cone [47].

2.4.3 Challenges and Considerations in Establishing Flow Systems

In addressing three types of flow systems popularly used in cancer metastasis research, it is important to look at the benefits and downsides of each system to observe which system works best for the type of research being performed. Various studies have combined different attributes from each of these flow systems to engineer their own novel flow systems that can be utilized to

better study cancer metastasis. Table 1 below provides the pros and cons of each type of flow system that was discussed in the previous section.

Table 1: Pros and Cons of Three Flow Systems. Below is an in-depth list of the pros and cons of all three types of flow systems [41].

Type of Flow System	Pros	Cons
Microfluidic Systems	-Precise control (crucial for studying metastasis, which involves complex cellular processes.) -Good imaging -Complex geometries -Isolate cell-specific biological responses for research -Reduced consumption of samples and reagents -Lower power consumption -High reproducibility	- Complex Fabrication - Limited Complexity -Limited amount of area to seed cells -No 3D micro-environment to study cells
Parallel Plate Flow Chamber	-Realistic/Tunable Shear Stress -Good visualization (larger scale) -Simple in design and operation -Can be easily imaged	- There is no precise control - Simplified geometry, cannot mimic complex systems
Cone and Plate Devices	-Precise Rheological Measurements	-Limited to Steady-State Flow

	-Sample Volume Flexibility	-Expensive -Accumulation of secreted molecules can occur within the operating fluid -Poor cell visualization

2.4.4 Previous Studies

Among the first studies to assess tumor cell transendothelial migration is a paper by Li and Zhu that utilizes a modified Boyden chamber [7]. In this study, comparisons were made between seven human cell lines derived from malignant and non-malignant tissues, to transmigrate through bovine aortic endothelial cell (BAEC) monolayers. For the Boyden chambers, polycarbonate membrane filters were used to form dual compartments within a 24-well tissue culture plate. The BAECs were seeded in the upper compartment and allowed to reach confluency before introducing the cell lines (Figure 15). The percentage of cells that had penetrated through the filter into the lower compartment after being incubated for various time intervals was quantified by assessing the radioactivity of the cells in the lower compartment compared to the radioactivity of all cells present in the dual chamber at the end of the experiment (HB1). The disruption of the endothelium during transmigration was quantified by counting the numbers of the retracted areas (holes) on the monolayer and by measuring their sizes. It was found that there was a higher level of transendothelial migration for the malignant Calu-1 cell line than its non-malignant counterpart L-132 cell line. Out of all cell lines, fibrosarcoma HT-1080 cells exhibited the highest percentage of transendothelial migration, and lung carcinoma Calu-1 was the second highest [7].

This paper provides useful insight when it comes to choosing aggressive cell lines for the purposes of our project. However, there are a number of limitations of this study, the most evident being the lack of flow in this system. There are also no indications of the role of the glycocalyx in the transendothelial migration of tumor cells.
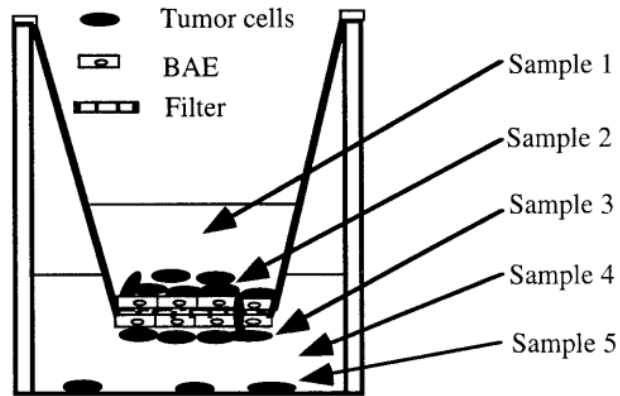
Figure 15: Transendothelial Migration Assay. The above image is a schematic representation of the in vitro transendothelial migration assay [7].

A 2021 study by Hajal et al. explores the effects of luminal and trans-endothelial fluid flows on the extravasation and tissue invasion of tumor cells by using 3D *in vitro* microvascular networks (MVNs) that replicate human microvasculature [8]. To form the MVNs, microfluidic devices (DAX-1, AIM Biotech) with three-channel chips on the same coverslip were used (Figure 16). A monolayer of human umbilical vein endothelial cells (HUVECs) was added to the MVNs and a few days later, tumor cells (TCs) were perfused in the MVNs. A controlled hydrostatic pressure was applied along and across the endothelium to recapitulate luminal and trans-endothelial flows, respectively. The systems were continuously imaged and the behavior of tumor cells, particularly extravasation and migration, were characterized. This study concluded that intravascular flow could promote tumor cell extravasation. Additionally, flow-induced endothelial junctional reorganization and elicited mechanotransduction responses in TCs under increased shear stresses can play a major role in promoting TC extravasation. Finally, transendothelial flow was found to increase both the speed at which TCs transmigrate as well as their migratory speeds once in the surrounding matrix [8].

This study gives useful insight in terms of understanding how intravascular flows and shear stresses affect the extravasation of TCs and thus metastasis. However, it does not explore the importance of the glycocalyx and its degradation in this complex process.
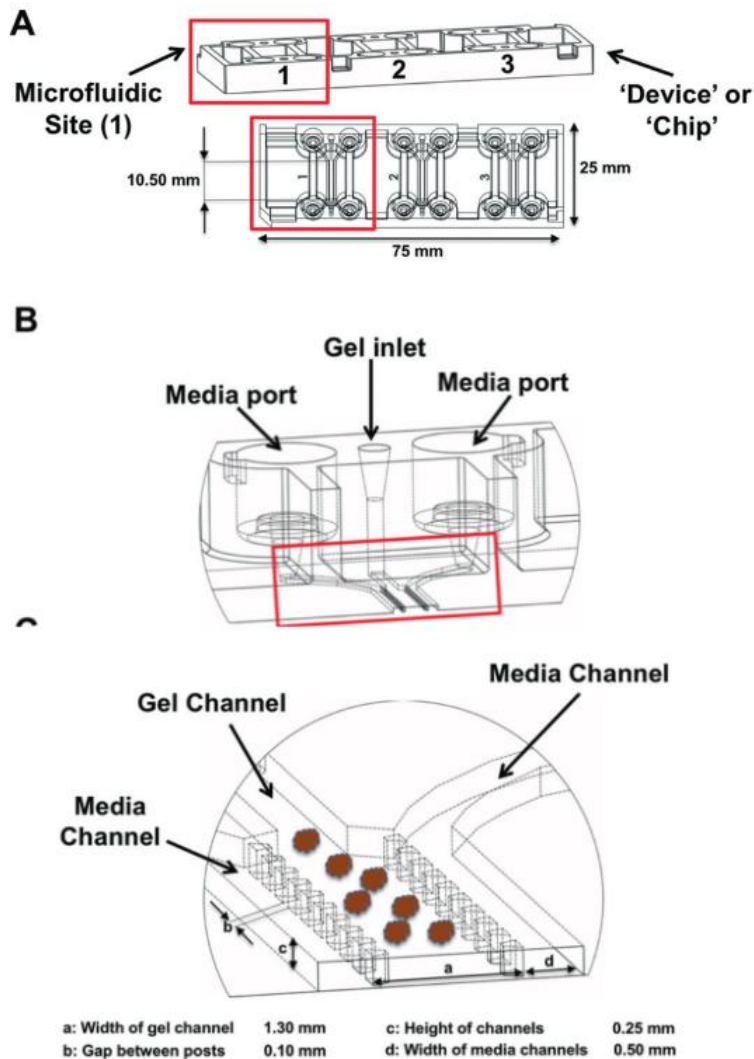
Figure 16: Microfluidic Device. (A) The 3D cell culture chip (AIM Biotech) is shown with three independent microfluidic chambers per chip. Red rectangle identifies a single microfluidic chamber in the 3D cell culture chip. (B & C) Each device contains a center gel region with posts separating the gel region from the anti-parallel side channels. Gel loading port and media ports labeled (B) along with center and side channels (C) [48].

Next, the team reviewed a study by Bersini et al. which used a microfluidic 3D in vitro model consisting of a central media channel and eight independent gel channels to explore breast cancer metastasis to bone [9]. Osteocytes embedded in collagen type I solution with Phosphate Buffered Saline and 1N NaOH were injected in four different gel channels. Endothelial cells were introduced into the central media channel (previously treated with Matrigel) in order to generate a monolayer covering channel walls and gel-channel interfaces. After that, cancer cells were injected in the same media channel and their transendothelial migration into the osteo-cell environment was analyzed (see Figure 17) [9]. It was found that extravasated cancer cells can

proliferate and generate micrometastases within the osteo-cell conditioned microenvironment [9]. This study provides useful insight in terms of demonstrating transendothelial migration of cancer cells to tissue (i.e. bone tissue) by utilizing a 3D microfluidic device. However, it does not provide any information about the role of the glycocalyx in this process.
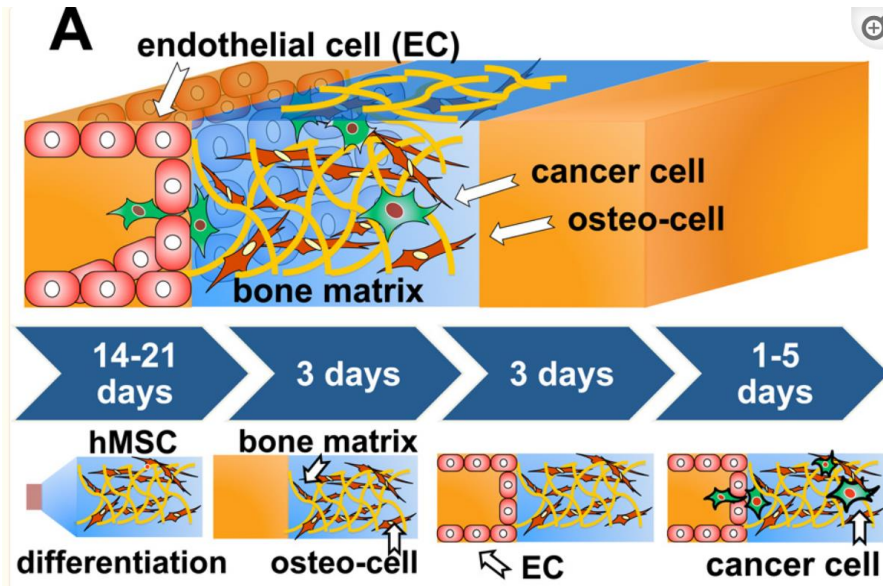
Figure 17: Generation of the Osteo-Cell Conditioned Microenvironment. HBM-MSCs (brown) were cultured for 2–3 weeks within osteogenic medium and seeded within microfluidic devices where they started depositing extracellular matrix (yellow filaments). After 3 days endothelial cells (ECs) (red) were seeded and a monolayer covering the media channel was generated. Finally, cancer cells (green) were introduced after 3 additional days and their extravasation ability and micrometastasis generation were monitored for 1 to 5 days [9].

A study by Mensah et al. focuses on the endothelial glycocalyx and presents evidence that disturbed flow induces glycocalyx degradation, which leads to tumor cell attachment to the endothelium, a first step in secondary tumor formation [49]. Disturbed flow occurs as a result of irregular vessel geometries and is prevalent in distant organs such as the lungs or the liver, where metastasis is more likely to occur due to the branched or curved blood vessels present (see Figure 18). A vertical step flow chamber covered in a HUVEC monolayer was used to introduce disturbed and uniform flows. The flow systems were continuously imaged and a comparison between TC behavior under disturbed and uniform flow was made. It was found that in areas of the vasculature with a disturbed flow, there was an increase in cancer cell attachment to the endothelium, which results from decreased glycocalyx expression [49]. While this study gives helpful insight into understanding the relationship between glycocalyx degradation and TC attachment to the endothelium, it does not explore the transendothelial migration of cancer cells.
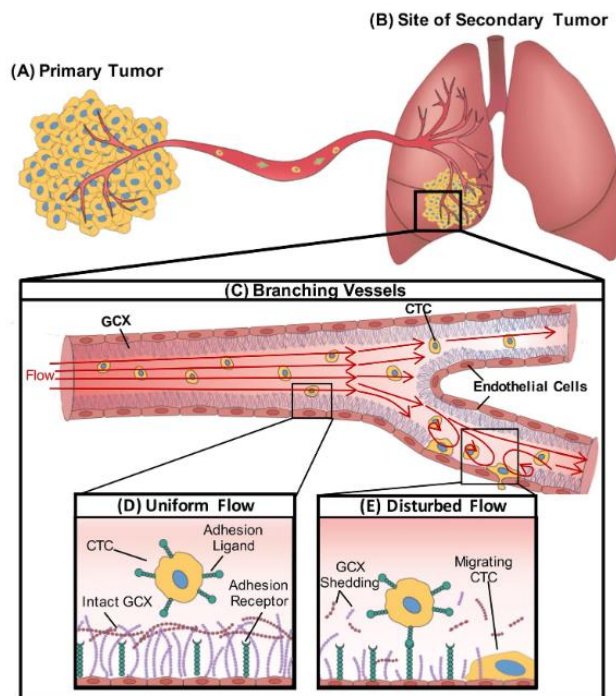
Figure 18: Effect of DF Patterns on Endothelial GCX and Circulating Cancer Cell Attachment. (A) Cancer cells within the primary tumor gain migratory properties and leave the primary tumor, intravasate through a nearby blood vessel, enter the bulk flow and (B) form secondary tumor sites in distant organs including the lungs. (C) Geometric changes within the blood vessels result in different flow patterns. (D) UF regions of blood vessels are known to have intact GCX resulting in the inability of CTC to attach to the endothelium. (E) Branched areas will produce DF; it is hypothesized that this DF will result in degradation of the endothelial GCX enhancing attachment of CTC to the endothelium [49].

Finally, the team reviewed a study by Siren et al. which focused on developing an in vitro system for studying the properties of the endothelial glycocalyx in arteries, veins, and capillaries [50]. A multi-height microfluidic platform (Figure 19) was designed and a HUVEC suspension was introduced into the chambers. Unique shear stresses at magnitudes that replicated the physical environment in arterial, capillary, and venous regions of the vasculature were introduced into the system. This promoted the growth of glycocalyx with different characteristics. The high shear environment on the chip pertaining to the arterial region, yielded the thickest glycocalyx, while the medium shear environment (pertaining to the capillary region) and low shear environment (venous region) yielded progressively less thick glycocalyx [50]. This study provides a good overview of the effects of shear stresses with different magnitudes on the robustness of the glycocalyx; however, it does not explore the role of the glycocalyx in transendothelial migration and metastasis of cancer, which is the main focus of our project.
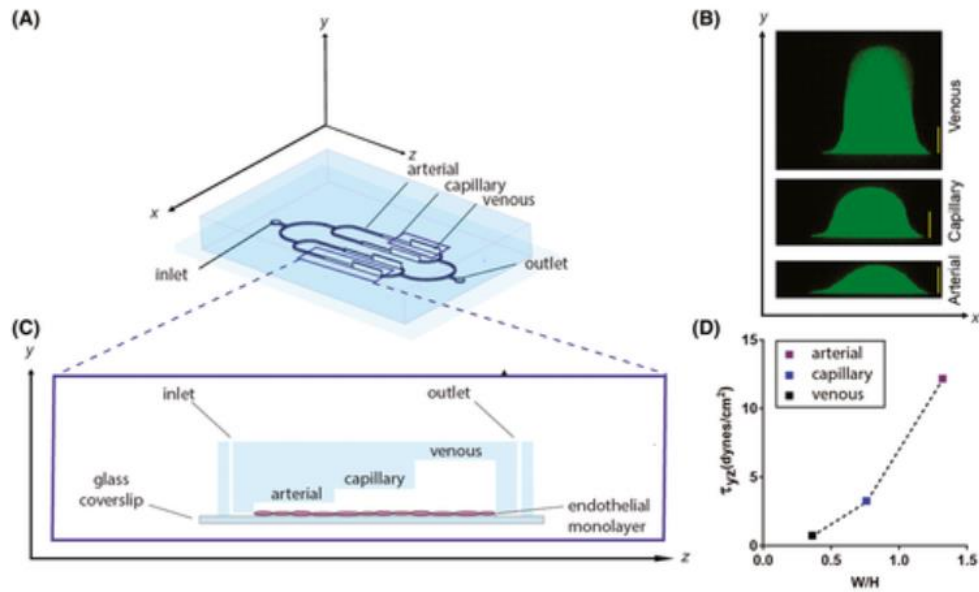
Figure 19: Integrated Multi-Shear Microfluidic Design. (A) The microfluidic platform comprises 4 channels, each with 3 regions (arterial, capillary, venous) of varying height (y-axis). (B) the height of each region post-fabrication was verified by perfusing the device with fluorescein (green) and acquiring z-stacks along the y-axis by confocal microscopy. (C) Side profile of the microfluidic channel illustrating the varying channel height in the arterial, capillary, and venous regions of the channel and the location of the endothelial monolayers along the z-axis. (D) Shear stress imposed on the cell surface within different regions of the channel at a constant flow rate (600uL/h) and viscosity (0.02 Pa*s) [50].

Chapter 3: Project Strategy

This chapter delineates the ideas that the team generated, consisting of the initial client statement, design requirements, design objectives and constraints, as well as the intended project approach.

3.1 Initial Client Statement

An in-vitro model that replicates the in-vivo environment, enabling the precise investigation of transendothelial migration and focusing on understanding how the glycocalyx facilitates the migration of cancer cells through the vascular bed is needed. The development of such a model is essential to advance cancer research by properly simulating the accurate physiological conditions.

3.2 Design Requirements

To initiate the design process, objectives, constraints, and specifications were generated and adapted to provide a basis for the proposed design models.

3.2.1 Objectives

Since our project's goal is to develop a model that can be utilized for further research on cancer metastasis our stakeholders consist of various groups such as oncologists, academic institutions, vascular biologists, and biomedical engineers. In order to cater to the needs of each of these groups, design objectives were identified and adapted over the duration of the design process. These objectives were first sorted into primary objectives, which were broader, and were then broken down into secondary objectives to be more specific. The primary and secondary objectives are summarized in Figure 20 below.
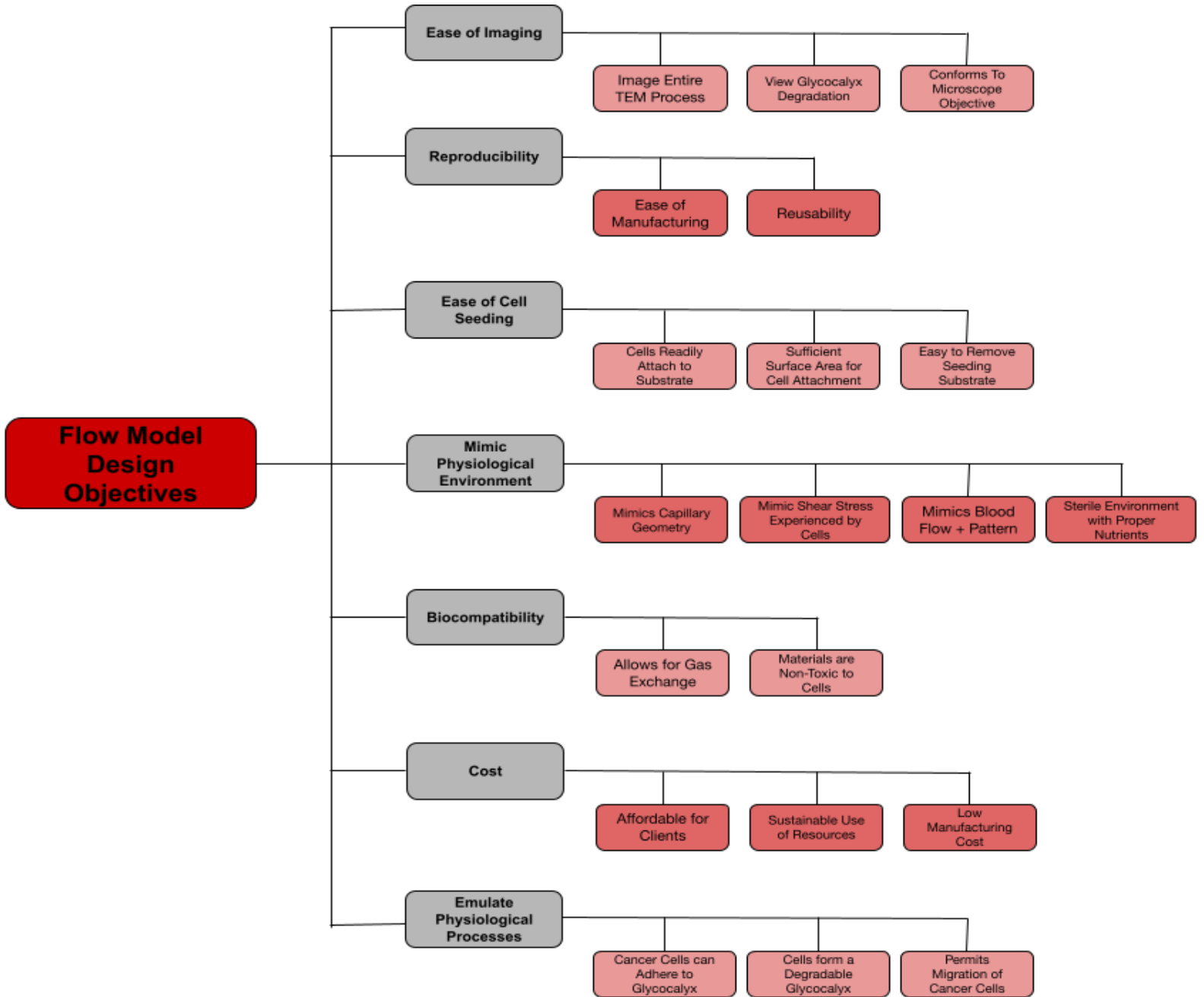
Figure 20: Flow Chart of Primary and Secondary Objectives. The primary objectives are denoted by the gray boxes, and the secondary objectives are denoted by the red boxes.

The primary and secondary objectives and their definitions can be observed as followed:

Ease of Imaging: The device must allow for the imaging of the entire transendothelial migration process, and degradation of the glycocalyx with the use of a microscope.

> **Image Entire TEM Process:** The device must allow for the entire Transendothelial migration process to be imaged with the use of a microscope.

> **View Glycocalyx Degradation:** The device must permit the viewing of the degradation of the glycocalyx.

> **Conforms to Microscope Objective:** The device must be able to fit under the objective of a microscope without obscuring the images that will be taken.

Reproducibility: The device must be able to be manufactured consistently, and it must be designed for repetitive use.

> **Ease of Manufacturing:** The device must be easily constructed within a reasonable time frame.

> **Reusability:** The device must be designed so that it can be used various times before replacing components.

Ease of Cell Seeding: The device must allow for proper cell attachment/adherence to the surface.

> **Cells Readily Attach to Substrate:** The substrate should be constructed of a material (or coated with one) that will permit the adherence of HLMVECs.

> **Sufficient Surface Area for Cell Attachment:** The substrate should be geometrically designed to have sufficient surface area so that the HLMVECs can evenly spread over the surface.

> **Easy to Remove Seeding Substrate:** The device must allow easy removal of the seeding substrate.

Mimic Physiological Environment: The device must mimic the geometry and shear stresses seen within human capillary.

> **Mimics Capillary Geometry:** The device must be designed to mimic the dimensions typically seen within a human capillary.

> **Mimics Shear Stress Experienced by Cells:** The device must be designed so that the HLMVECs experience shear stresses that are seen in vivo.

> **Mimics Blood Flow + Pattern:** The device should allow for blood flow rates and flow patterns observed within human capillaries.

> **Sterile Environment with Proper Nutrients:** The device must provide a sterile environment with proper nutrients that can emulate what is found in the human body.

Biocompatibility: The device must not pose a toxic environment to both the HLMEVCs and metastatic cancer cells.

> **Allow for Gas Exchange:** The device must be permeable to the atmosphere to allow for proper gas exchange and the exchange of nutrients.
>
> **Non-Toxic Materials:** The device must be constructed of materials that do not pose toxicity concerns to the HLMVECs and metastatic cancer cells.

Cost: The device must be cost effective and avoid unnecessary costs in the materials and construction process**.**

> **Affordable for Clients:** The device must be affordable to the people who will be utilizing it.
>
> **Sustainable Use of Resources:** The device must be designed to eliminate wasted resources and be economically sustainable.
>
> **Low Manufacturing Cost:** The manufacturing cost of the device must be reasonable.

Emulate Physiological Processes: The device must permit the attachment of metastatic cancer cells to the glycocalyx and allow the entire transendothelial migration process to occur.

> **Cancer Cells Adhere to Glycocalyx:** The device must allow the metastatic cancer cells to attach to the glycocalyx of the HLMVECs.
>
> **Cells form a Degradable Glycocalyx:** The device must allow for the formation of a degradable glycocalyx.
>
> **Permits Migration of Cancer Cells:** The device must enable the metastatic cancer cells to travel through the endothelial cells into a secondary chamber.

3.2.2 Constraints

The team's primary constraints can be divided into two categories: project limitations and design constraints. Project limitations include the time constraint based upon Worcester Polytechnic Institute's academic calendar and the budget that is allotted to each MQP group. Design constraints include restrictions such as cell seeding, biocompatibility, available microscope imaging devices, and the importance of emulating the physiological environment in the flow model created.

Due to the fact that the Major Qualifying Project (MQP) at Worcester Polytechnic Institute must be completed within one academic year, the team's timeline and breakdown of the entire design process was based upon this limitation. One academic year is approximately a total of 8 months. Additionally, per the WPI Biomedical Engineering department guidelines, each team member is allotted $250 USD to contribute to all project related costs. With a total of four team members, this makes the budget for this project a total of $1,000 USD.

The design specifications are listed below in Table 2. These specifications are all related to a design constraint such that the created device meets all of the requirements. For example, one design constraint involves the processes of seeding endothelial cells in the flow model. If the cells cannot be seeded properly then when the cancer cells are introduced into the model, they will have nothing to migrate through in order to complete transendothelial migration. Additionally, there needs to be a sufficient concentration of endothelial cells. This is a constraint because the correct materials and seeding methods need to be selected in order for testing to be successful. Similarly, another constraint is biocompatibility which needs to be accounted for when selecting materials. If any portion of the device that comes into contact with cells is not biocompatible, it could cause the cells to die while ruining the experiment. The availability of a microscope is a constraint because of the location of imaging with the microscopic objective viewing from the bottom. This had to be taken into consideration when brainstorming potential designs. Lastly, emulating the physiological environment is a design constraint because if the flow model was not representative of the correct capillary environment, then the testing would not be as accurate in terms of the degradation of the glycocalyx and transendothelial migration.

3.2.3 Product Specifications

In order to better define the constraints and understand the design specifications further, Table 2 was created in order to help organize requirements for the flow system design. The table includes both functional and performance specifications for each requirement. To begin, the flow system geometry is an important specification for our system. The device shall allow for the flow conditions to mimic a capillary. To achieve this, the gasket geometry was calculated based on that of a capillary; it has a width of 13.01 mm and a height of 2 mm. The second specification we discuss is related to cancer cells' flow. An aggressive type of cancer that has the ability to perform transendothelial migration should be chosen. For this project, the team utilized MDA-MB-231, which is a commonly researched human breast cancer cell line, derived from metastatic breast cancer, mammary gland epithelial cells. After two hours of flow, the cancer cells shall collect in the petri dish reservoir, and from there they can be counted for quantification. The next specification is associated with cell seeding. The device would allow a certain adherent cell type that can form a proper glycocalyx to be seeded within the membrane. Human Lung Microvascular Endothelial Cells (HLMVECs) were selected since they are adherent cells that can form a proper endothelial layer and a proper glycocalyx. The device would also allow seeding of at least 100k HLMVECs. The next specification is related to cell concentrations. This device should contain a distinct concentration of adherent cells, and a certain concentration of metastatic cancer cells should flow through the system. The concentration of both HLMVECs and breast cancer cells shall be at least 100k/mL. Next, the identification of cancer cells for imaging is another important specification for our system. The device shall allow for easy immunofluorescence staining on cells to be able to differentiate cancer cells from endothelial cells when seeing them under the microscope and to observe the degradation of the glycocalyx. For this reason, Far Red CellTrace, which is used for in vitro labeling of cells, was selected to

label cancer cells in order to image them using the Keyence microscope and confirm transendothelial migration. As for the shear stress specification, the flow rate going through the device shall provide a shear stress value similar to that seen in capillaries. The shear stress experienced in the flow chamber is in the range of 0.2-0.6 Pa (2-6*10^{-7} MPa) as seen in a typical capillary [51]. Next, we discuss another important specification which is related to mimicking capillary flow. The device shall emulate proper blood flow rates through the utilization of a certain method of flow (pump). The flow system will allow for the use of a peristaltic pump at a laminar flow rate of 260.25 mL/min (factor of .75 mm/s which is typically observed in capillaries). As for the imaging specification, the device would allow for easy imaging of cells from underneath using a microscope. The microscope that was utilized for this project was a Keyence microscope, at an established working distance of 1 mm. Moreover, the flow time is another specification of great importance. The device shall allow for continuous and intact flow to be able to observe all of the stages of transendothelial migration. It shall also allow for 6 hours of uninterrupted flow via a peristaltic pump. Lastly, the membrane shall emulate the capillary wall, permitting cancer cell migration. A 3.0-microns porous membrane allows for a HLMVEC monolayer to be established on top while the breast cancer cells can pass through it.

Table 2: Functional and Performance Specifications. This table shows all specifications that need to be satisfied in order for the device to meet validation and verification requirements.

	Functional	Performance
Flow System Geometry	The device allows for flow conditions to mimic a capillary.	The gasket geometry is calculated based on that of a capillary. The gasket has a width of 13.01 mm and a height of 2 mm.
Cancer Cells Migration	An aggressive type of cancer that has the ability to perform transendothelial migration.	After 2 hours of flow, at least 10 breast cancer cells will collect in the petri dish.
Cell Seeding	The device would allow a certain adherent cell type to be seeded within it that can form a proper glycocalyx.	Device will allow seeding of at least 100k HLMVECs.
Cell Concentrations	This chamber should contain a distinct concentration of adherent cells, and a certain concentration of metastatic cancer cells should flow through the system.	The concentration of HLMVECs will be at least 100k/mL.

The concentration of breast cancer cells will be at least |

		100k/mL.
Identification of Cancer Cells for Imaging	The device shall allow for easy immunofluorescence staining on cells to be able to differentiate cancer cells from endothelial cells when seeing them under the microscope and to observe the degradation of the glycocalyx.	Far Red CellTrace will be applied to the cancer cells to image using the Keyence to confirm TEM.
Shear Stress	The flow rate going through this device shall provide a shear stress value similar to that seen in capillaries.	The shear stress experienced in the flow chamber is in the range of 0.2-0.6 Pa (2-6 x 10^{-7} MPa) as seen in a typical capillary.
Mimicking Capillary Flow	The device shall emulate proper blood flow rates through the utilization of a certain method of flow (pump).	The flow system will allow for use of a peristaltic pump and a laminar flow rate of 260.25 mL/min (factor of .75 mm/s which is typically observed in capillaries) [51].
Imaging	The device would allow for easy imaging of cells from underneath using a microscope.	A Keyence Microscope will be utilized at an established working distance of 1 mm [52].
Flow Time	The device would allow for continuous and intact flow to be able to observe all of the stages of TEM.	The device will allow for at least 2 hours of flow via a peristaltic pump.
Membrane	The membrane will emulate the capillary wall, permitting attachment of HLMVECs, while also permitting cancer cell migration.	A 3.0-microns pore size membrane allows for a HLMVEC monolayer to be established on top while the breast cancer cells can pass through. The membrane also needs a thickness between 10-15 microns.

3.3 Engineering Standards

Since the device is not designed to be tested on human subjects or with blood, the main focus for our engineering standards are biocompatibility and cytotoxicity. That means that our team was primarily focused on ISO 10993-1, which focuses on evaluating the biocompatibility of a device to manage any biological risk. For our team this included autoclaving the device, keeping everything sterile, and preventing using materials that would negatively interact with cells. Our team also followed ISO 9001:2015 (Quality Management Systems Requirements) and ISO 13485 (Medical Devices). These standards help us ensure that our device is safe, and the processes involved in making the device and handling it are safe and regulated.

3.4 Revised Client Statement

The goal of this project is to design an in-vitro system that models the in-vivo environment of a capillary. The system will be able to accurately study transendothelial migration by studying the role of the glycocalyx in enhancing the movement of cancer cells through the vascular bed for secondary tumor formation. The system will allow for the process of transendothelial migration to occur and for the process to be imaged.

3.5 Management Approach

In order to keep the team organized throughout the completion of the major qualifying project, the team used a Gantt Chart to track tasks each week. A Gantt chart uses a series of horizontal lines which are marked based on specifically set aside time periods. The team split up the work by term and within each term based upon recommended deadlines suggested by the advising team. As shown in Figure 21, this approach allowed the team to stay on track and complete the project within the allotted academic year.

	TASK TITLE	START DATE	DUE DATE	DURATION	COMPLETE?
1	**Project Conception and Initiation**				
1.1	Discuss Team Dynamics, Update Syllabus, Create A-term Schedule	8/27/23	8/30/23	4	✓
1.2a	Literature review (annotated bibliography)	8/27/23	9/9/23	13	✓
1.2b	Complete Background	9/3/23	9/9/23	7	✓
1.2c	Complete Introduction	9/3/23	9/9/23	7	✓
1.2d	Complete Client Statement	9/3/23	9/9/23	7	✓
1.3a	Complete Initial Design Concepts (IDC) Section: Objectives	9/10/23	9/16/23	7	✓
1.3b	Complete IDC Section: Functions	9/17/23	9/23/23	7	✓
1.3c	Complete IDC Section: Means	9/24/23	9/30/23	7	✓
1.3d	Complete IDC Section: Design Alternatives	10/1/23	10/7/23	7	✓
1.3e	Complete IDC Section: Revised Client Statement	10/1/23	10/7/23	7	✓
1.4a	Plan B-term Methods and Experiments	10/8/23	10/13/23	6	✓
1.4b	Plan Work Breakdown and Gantt Chart for B term	10/8/23	10/13/23	6	✓
1.5	Self and Team Assessment Forms	10/5/22	10/13/22	8	✓
2	**Alternative Designs, Proof of Concept, and Prototypes**				
2.1a	Create Material List	10/23/23	10/25/23	3	✓
2.1b	Make Presentation Video	10/24/23	10/27/23	4	✓
2.1c	Order Material List	10/25/23	11/5/23	12	✓
2.1d	Finalize Functional and Performance Specifications	10/25/23	10/30/23	6	✓
2.1e	Advisor Revisions to A-Term Paper Draft	10/26/23	11/12/23	7	✓
2.2a	Initial CAD Design	10/26/23	11/15/23	20	✓
2.2b	Fluid Flow Simulations COMSOL	10/30/23	11/15/23	16	✓
2.2c	Refined CAD Design	11/7/23	11/15/23	9	✓
2.3a	Make Initial Prototype	11/13/23	11/21/23	8	✓
2.3b	Proof of Concept Testing	11/27/23	12/4/23	8	✓
2.4a	Draft of Chapter 4	11/27/23	12/15/23	19	✓
2.4b	Draft of Chapter 5	11/27/23	12/15/23	19	✓
2.4c	Draft of the Beginning of Chapter 6	11/27/23	12/15/23	19	✓
2.5	Self and Team Assessment Forms	12/11/22	12/15/22	4	✓
3	**Completeing the Design**				
3.1a	3D Print Final Design	1/10/24	1/12/24	3	✓
3.1b	Meet with Ian/Contact Ian	1/10/24	1/12/24	3	✓
3.1c	Fabricate Final Design	1/14/24	1/18/24	5	✓
3.1d	Leak Test w/Water	1/19/24	1/24/24	6	✓
3.1e	Revise Model (if leaks)	1/24/24	1/26/24	3	✓
3.1f	Finish final design concept chapter	1/27/24	3/1/24	35	✓
3.2a	Retrieve Cells	1/27/24	1/28/24	2	✓
3.2b	Culture + Split Cells	1/29/24	2/5/24	7	✓
3.2c	Seed Cells	2/6/24	2/6/24	1	✓
3.3a	Control Test w/Media	2/7/24	2/9/24	3	✓
3.3b	Test w/Cancer Cells	2/12/24	2/14/24	3	✓
3.4a	Test w/Cancer Cells and Cytokines	2/15/24	2/17/24	3	✓
3.4b	Fix, Stain, Image with Keyence	2/7/24	3/1/24	25	✓
3.4c	Repeat Testing	2/7/24	3/1/24	25	✓
3.4d	Compile Results in Chapter	2/12/24	3/1/24	20	✓
3.5	Self and Team Assessment Forms	2/26/24	3/1/24	6	✓
4	**Finalize Design and Deliverables**				
4.1a	HLMVEC Membrane Testing	3/11/24	3/13/24	3	✓
4.1b	MBA-MD-231 Membrane Testing	3/12/24	3/14/24	3	✓
4.1c	HLMVEC + MBA-MD-231 Membrane Testing	3/13/24	3/17/24	5	✓
4.1d	Biocompatibility Tests with Gaskets	3/18/24	3/19/24	2	✓
4.1e	Cell Concentration Testing	3/20/24	3/21/24	2	✓
4.1f	System Geometry Tests	3/22/24	3/22/24	1	✓
4.2a	Full Device Testing	3/23/24	3/29/24	7	✓
4.2b	Stain Cancer Cells	3/24/24	3/30/24	7	✓
4.2c	Image Using Keyence	3/27/24	3/29/24	3	✓
4.3a	Lisa Initial URPS Information	3/11/24	3/15/24	5	✓
4.3b	Final Project Title/Department	3/16/24	3/28/24	13	✓
4.3c	Two-Page IEEE Abstract	3/30/24	4/8/24	9	✓
4.4a	Final Presentation	3/11/24	4/5/24	25	✓
4.4b	Practice Presenting	3/16/24	4/18/24	33	✓
4.4c	Project Presentation Day	4/19/24	4/19/24	1	✓
4.4d	Submit Final Report and eCDR	4/20/24	4/24/24	5	✓
4.5	Self and Team Assessment Forms	4/27/24	5/1/24	5	✓

Figure 21: Gantt Chart. Above is a condensed version of the team's Gantt chart which helped keep the team organized throughout the academic year.

Chapter 4: Design Process

The content in this chapter aims to break down the complete design process from understanding the need of this project to selecting a final design. Using the background knowledge shared above, specifications were spelled out and the team brainstormed four potential designs that meet such specifications. Finally, using analysis techniques, a final design was selected.

4.1 Need Analysis

In order to determine the final design of the device, the team developed certain design specifications required to meet the client's need for building an in vitro model that emulates transendothelial migration of cancer cells and allows for the exploration of the role of the endothelial glycocalyx in this process. The design specifications are shown in Table 2 above. The team then determined which of these design specifications were primary versus secondary by compiling a Pairwise comparison chart as will be discussed next.

4.2 Alternative Designs

An important part of the design process is brainstorming several different options for potential designs. This process is an exercise in coming up with a variety of different solutions to the same problem, each possessing certain advantages and disadvantages. In brainstorming, it is important to note that no ideas are bad ideas and the team was encouraged to think outside of the box to come up with the following alternative designs. A later section of this paper describes the steps the team took in order to select the final design for the flow system.

4.2.1 Parallel Plate Flow Chamber + Transwell Modified Assay

One of the primary ideas that was devised consisted of the combination of a parallel plate flow chamber combined with a Transwell or modified Boyden chamber assay. The flow system will consist of a distributor containing an inlet and an outlet, and a gasket, as commonly seen in a PPFC. It will also contain a reservoir filled with culture media, and a microporous membrane, in place of the commonly used glass slide; these attributes are derived from the Transwell Modified Assay. The structure of this flow system can be observed in Figure 22. The microporous membrane would be coated with an ECM matrix component to enhance attachment of the HLMVECs (e.g. fibronectin). This would be a viable option due to the precise control of the shear stresses experienced by the HLMVECs, as the shear stress can be altered based on the height of the gasket. Also, imaging would be relatively easy as the porous membrane and reservoir would be able to be easily detached and placed under the objective of a microscope.
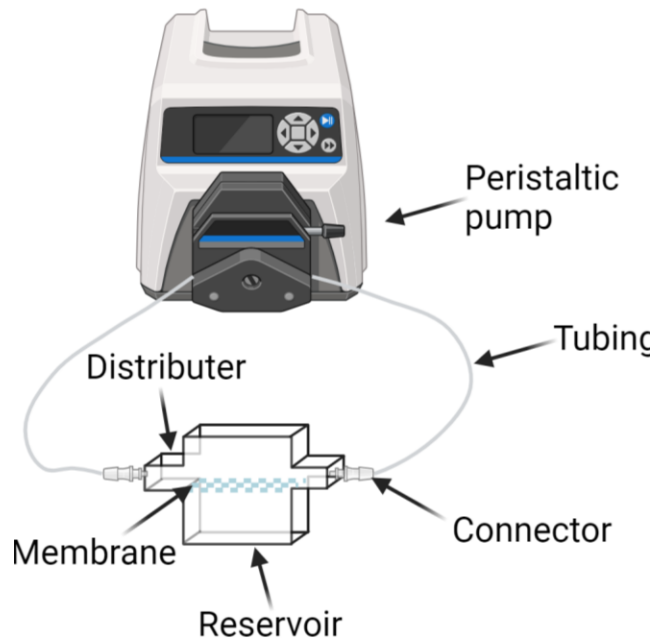
Figure 22: Parallel Plate Flow Chamber + Transwell Migration Assay. Design of PPFC + TMA consisting of a distributor, gasket, microporous membrane, and reservoir containing CM and a chemotactic factor.

4.2.2 Organs-on-Chips

Our next design idea for a flow system that would model transendothelial migration of cancer cells was organs-on-chips. Organs-on-chips are a type of flow system that are designed to mimic human physiology by using a microfluidic device to control cell microenvironments and maintain certain tissue functions [53]. As can be seen in Figure 23, the system consists of a glass slide, a microfluidic device, an inlet reservoir and tubing, and an outlet reservoir and tubing. The microfluidic device would have a channel with a membrane on one side that leads to another media filled channel. Using Figure 23 as an example, the vascular endothelium would be seeded along the membrane, cancer cells would then flow through the dark pink channel and would transendothelial migrate to the light pink channel. For setting up the system, the microfluidic device can either be plasma bonded to the glass slide or clamped [54]. The system runs using capillary action which is fluid flow through a narrow space that is caused by surface tension, adhesion, and cohesion [55].
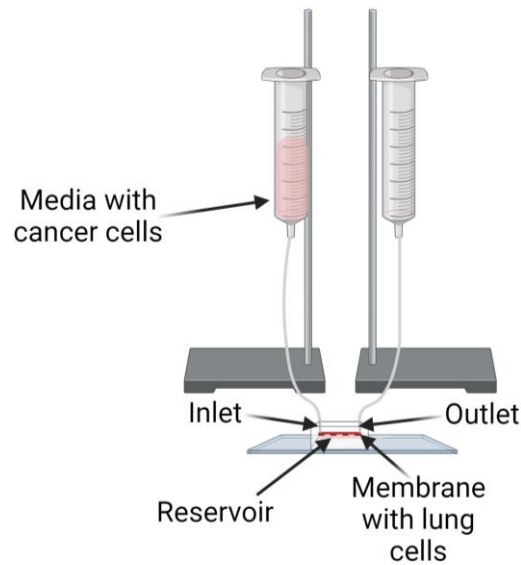
Figure 23: Organs-on-Chips. This image shows the potential set up for the organs-on-chips flow system which includes: a glass slide, a microfluidics device, an inlet reservoir and tubing, and an outlet reservoir and tubing.

4.2.3 Multi-Channel System

Another potential idea would be to design a microfluidic system with multiple access channels that would allow for different types of cells to be simultaneously seeded in different regions of the device. Figure 24 below shows how such a system is designed and how different channels communicate with each other. Each access channel has an inlet and outlet that allows for flow regulation. The gel region connects the channels with each other [56]. For our project, this region would be filled with a gel that acts like a porous membrane. Then, endothelial cells could be seeded in one of the channels and after a certain amount of time, aggressive cancer cells could be introduced in that same channel. The system would run until the cancer cells had migrated through the endothelial layer and the porous gel and collected in the other channel. This type of device would allow for relatively easy imaging under the microscope in order to observe the transendothelial migration of the cancer cells through the porous gel region. For the purposes of our project, the device would be made to mimic the physiological environment including size, geometry, and flow rates of the capillaries.
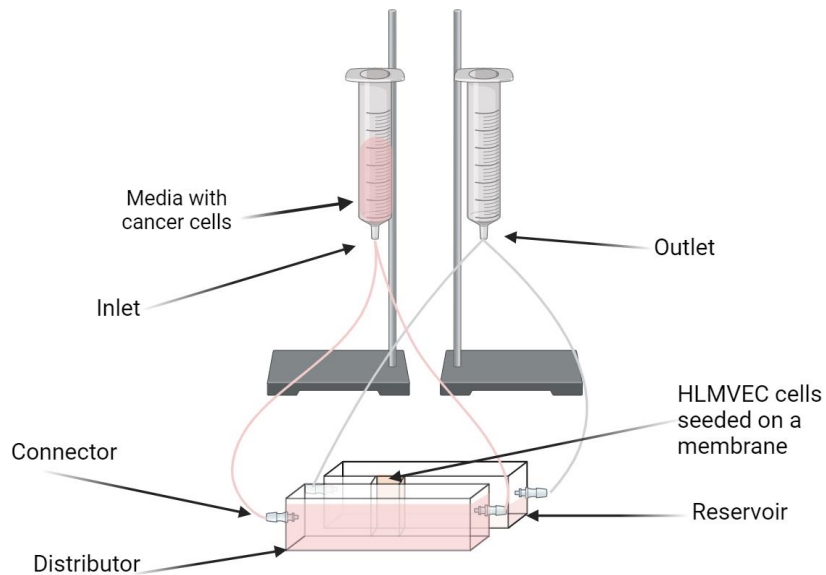
Figure 24: Multi-Channel System Alternative Design. The top image shows more specifically how this multi-channel system would work. Each channel allows for a gel region with two access channels on either side. The bottom image is a representation of this model using CAD software.

4.2.4 Well Plate

The Well Plate design idea combines a microfluidic device and a well plate. The main advantage of this design is that many experiments can all be completed at the same time [57]. Ultimately, this would help save time in terms of the amount of testing that needs to be completed before determining the best results. With the potential of being able to purchase a well plate and modify it as needed for this specific experiment, it would reduce the need for tubing and sterilization would not be necessary [58]. The design, as seen in Figure 25, consists of a 'normal' well plate that has several holes. The difference is that two holes are connected with a channel that runs near the bottom. Additionally, there can be a layer with microfluidics followed either by a cover slip glass or a PDMS bottom layer [59].
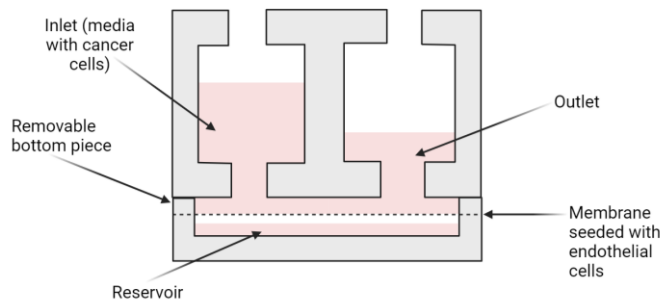
Figure 25: Well Plate Alternative Design. This design involves curating the flow system within the small little wells of a well plate. The major benefit of this system over other potential designs is the fact that multiple experiments can be running simultaneously.

As shown in Figure 25, our design will harness this same general design concept of the two wells being connected and then the bottom most layer will have endothelial cells seeded to emulate the capillary wall. This endothelial layered substrate as the bottom layer is how the design aims to emulate transendothelial migration. Similar to some of the other designs mentioned, this bottom plate will be removable to ensure easy imaging.

4.3 Design Process and Final Design Models

In this section, we discuss in detail the design process, specifically the Pairwise Comparison chart we compiled in order to determine the most important design specifications, as well as the Pugh Analysis we conducted which helped us select the final design of our device.

4.3.1 Pairwise Comparison

A Pairwise comparison chart is a decision-making method used to determine the most important design specifications by comparing two specifications simultaneously to determine relative preferences. Design objectives are placed on both the horizontal and vertical axis. Essentially, this chart helps compare each objective to the others which helps the design team figure out which objectives are the most crucial to the final design. The ranking system involves a zero score if the horizontal requirement is less important compared to the vertical requirement, a one if the horizontal requirement is more important compared to the vertical requirement, and finally a one half if the requirements are equally important. The horizontal rows are then added together to produce a total score. This numerical value of the total score will reveal which design objective is crucial to have in the final design. Table 3 shows the Pairwise comparison chart

which helps in the determination of what the final design really needs versus what would be nice to have.

Table 3: Pairwise Comparison Chart. The table below shows the Pairwise comparison chart that the team used in order to determine total scores and overall importance of each objective.

	Ease of Imaging	Reproducibility (ease of construction)	Ease of Cell Seeding	Mimic Physiological Environment	Biocompatibility	Cost	Emulate Physiological Processes	Total Score
Ease of Imaging	X	1	0	0	0	1	0	2
Reproducibility (ease of construction)	0	X	0	0	0	1	0	1
Ease of Cell Seeding	1	1	X	1	0	1	0	4
Mimic Physiological Environment	1	1	0	X	0	1	0	3
Biocompatibility	1	1	1	1	X	1	1	6
Cost	0	0	0	0	0	X	0	0
Emulate Physiological Processes	1	1	1	1	0	1	X	5

Based upon Table 3 the most important design objective is biocompatibility. Following biocompatibility is the system emulating the physiological process and then ease of cell seeding. The next most important is that the system emulates the physiological environment, is easy to image and then is able to be reproduced and easy to construct. Cost is the final design objective meaning that it is the least important.

Biocompatibility means that all the materials being used in the design of this flow system must be suitable with living tissue and not be toxic or harmful to the human body cells. Additionally, the design must emulate the physiological process which includes things such as fluid flow rates that are appropriate for that of capillary geometry. The cells must be able to be seeded easily on a material that allows them to adhere at a concentration applicable to the normal physiology of the human body. The team has chosen to model a capillary and therefore it is important that the system emulates that of a capillary including the diameter and a length that is sufficient to reach a specific flow rate. Also, it is important to take into consideration how easy it is to image which may require a removable portion of the device. Being able to reproduce the device and clean it so

it can be reused and allowing it to be easy to put together is another consideration to take into account. Finally, the cost is something to take into consideration within the constraints of the MQP team budget.

4.3.2 Pugh Method

The Pugh Method is an approach used by designers to select a final model after brainstorming several potential models. After determining the primary and secondary design specifications, the team weighs the user and design requirements based on the number of requirements. The highest weight is assigned to the most important specification and the lowest to the least important specification. The gold standard, an already existing design against which all the alternative designs are compared to, is chosen. Then, each specification is compared to the baseline by using two values: +1 indicates that the alternative design is superior compared to the gold standard, and -1 indicates that the gold standard is superior to the alternative design. These values are then multiplied by the weight and final scores are assigned. The highest score determines which design should be chosen to move forward. The teams Pugh chart can be seen in Table 4 below.

Table 4: Pugh Chart. The Pugh chart is used to determine the most suitable design by comparing each requirement to the baseline.

| Requirement	Weight	Baseline (Transwell Migration Assay)	PPFC + TMA	OoC + TMA	Multi-Channel Device	Well Plate
Biocompatibility	7	0	0 (0)	0 (0)	0 (0)	0 (0)
Emulates Physiological Processes	6	0	1 (+6)	1 (+6)	1 (+6)	-1 (-6)
Ease of Cell Seeding	5	0	0 (0)	0 (0)	-1 (-5)	0 (0)
Mimics Physiological Environment	4	0	1 (+4)	1 (+4)	1 (+4)	-1 (-4)
Ease of Imaging	3	0	0 (0)	-1 (-3)	-1 (-3)	1 (+3)
Reproducibility (ease of construction)	2	0	-1 (-2)	-1 (-2)	-1 (-2)	1 (+2)
Cost	1	0	-1 (-1)	-1 (-1)	-1 (-1)	0 (0)
Rank Score	-	-	7	1	-1	-5

Our team initially utilized this approach to determine the final design we were going to proceed with. The Pugh analysis can be seen in Table 4 above. A Transwell migration assay, also known as a modified Boyden chamber, that was discussed previously, was chosen as the gold standard. As determined earlier, biocompatibility is the most needed design requirement, therefore it has the highest weight. Similarly, cost was determined to be the least important requirement, therefore, it was assigned the lowest weight. After comparing each design to the gold standard, final scores were assigned. The parallel plate flow chamber + Transwell modified assay design received a score of 7, the organ-on-chip + Transwell modified assay design received a score of 1, the multi-channel device received a score of -1, and finally the well plate design received a score of -5. Based on the highest score, the most suitable design would be the parallel plate flow chamber combined with a Transwell modified assay, which is the design the team chose to proceed with for our in vitro model.

4.4 Determining Flow System Geometry

To initiate the construction of the in-vitro flow system, quantitative parameters had to be calculated, and simple experiments had to be performed to ensure that the flow system had suitable geometries so that realistic capillary stresses and imaging could be achieved.

4.4.1 Height of Reservoir Experiments

The first parameter that was calculated was the height of the reservoir. For imaging the stained HLMVECs proceeding flow trials, it was decided that the Keyence BZ-X810 (Figure 26) microscope would be utilized. According to Keyence manufacturing, the working distance of this Keyence microscope with an objective of 20x is 1 mm which was tested during this experiment [52]. In addition, it is important to note that the microscope views from the bottom with the light source on the top. The resolution had to be defined so that the height of the reservoir could be properly determined. This was done such that the cells on the top of the reservoir could be located in the microscope. To test this, HLMVECs were seeded into a T-75 flask which has a height of 40 mm (1.575'). After the cells were properly seeded, they were brought to the Keyence BZ-X800 microscope. The T-75 containing the cells was inverted so that the cells were on the top of the T-75 and it was placed on the correct mount. The Keyence imaging software was opened, and the cells were brought into focus. For this initial test, the cells could not be located, therefore, showing that the Keyence microscope has a maximum viewing distance of less than 40 mm (1.575'). The same experiments were performed with a T-25 and a petri dish, with heights 30 mm and 11 mm, respectively. The cells could also not be located within these tests, once again showing that the maximum viewing distance for the Keyence is 1 mm.
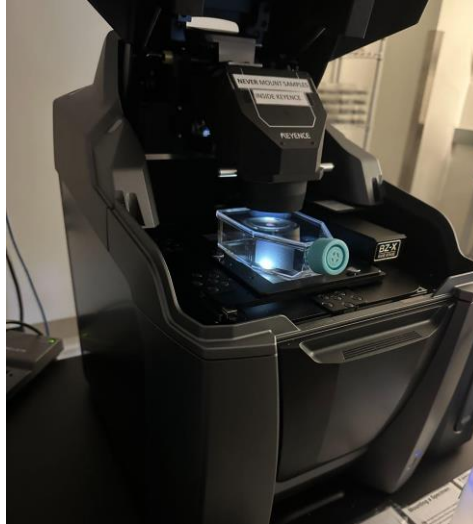
Figure 26: Keyence Microscope Image Testing. The above image shows the team using a T-75 flask to test the working distance on the Keyence microscope. This was important in the design of our system to ensure that it could be properly imaged.

Since none of these tests passed, it was decided that the reservoir would be removable from the flow system to ensure ease of imaging for both the metastatic cancer cells in the reservoir and the monolayer of endothelial cells located on top of the porous membrane.

4.4.2 Initial Gasket Dimension + Flow Rate Calculations

The gasket dimensions and peristaltic pump flow rate in the in-vitro flow system play a significant role in determining the shear stress (τ) experienced by the HLMVECs and, therefore, play a crucial role in how the MDA-MB-231 cells interact with the HLMVECs and metastasize. To achieve these values, the Navier Stokes equation was used.

$$\left(\tau = \frac{6Q\mu}{wh^2}\right)$$

In this equation, τ is the shear stress, μ is the viscosity, Q is the flow rate, w is the width of the channel, and h is the height of the channel formed by the gasket was utilized [42]. Before performing calculations, various assumptions were made such as steady-state flow (velocity is not a function of time), laminar flow, incompressible fluid (density remains the same), Newtonian fluid, the viscosity of media is equivalent to the viscosity of water (1×10^{-9} Mpa - s). Next, values from the literature were determined and constants were chosen based on previously constructed parallel plate flow chambers. These literature values consisted of the velocity of blood flow in capillaries being 0.75 mm/s, and the typical shear stress at the wall of the capillary being 5×10^{-7} MPa [60] [61]. The other constants consisted of the interior diameter of the size 17 tubing being 6.40 mm, and the gaskets total height being made 2 mm to permit an appropriate amount of distance for the manufacturing process to be feasible. Also, based on previously

constructed PPFCs in literature a gasket width of about 13 mm was chosen. Utilizing all these variables the calculations and spreadsheet can be located in Appendix I.

With the gasket height being 2 mm and the width of the gasket being set at about 13 mm based on other PPFCs found in literature, the flow velocity was determined to be 134.8 mm/s (a factor of 180 greater than typical flow rates observed in vivo). Knowing the inner diameter of the tubing that we are utilizing (6.40 mm), the cross-sectional area was determined, and utilizing the volumetric flow rate equation ($Q = VA$), the volumetric flow rate was calculated to be 4337.47 mm^3/s. This flow rate was then converted to 260.6 mL/min so that it could easily be inputted into the peristaltic pump. With all of the constants from the literature, the velocity and volumetric flow rate were able to be obtained and the SolidWorks model and simulation could be completed.

4.5 Arts and Crafts Model

In order to better visualize the initial model that the team had in mind, household materials were used to create a replica with a 1:1 scale. We made the model to scale such that we could have a better understanding of the relative sizing. This model involved cardboard, straws, and tape. As seen in Figure 27, the cardboard was used to represent the top and bottom pieces and the gaskets while the straws were used to represent the tubing where fluid will flow.
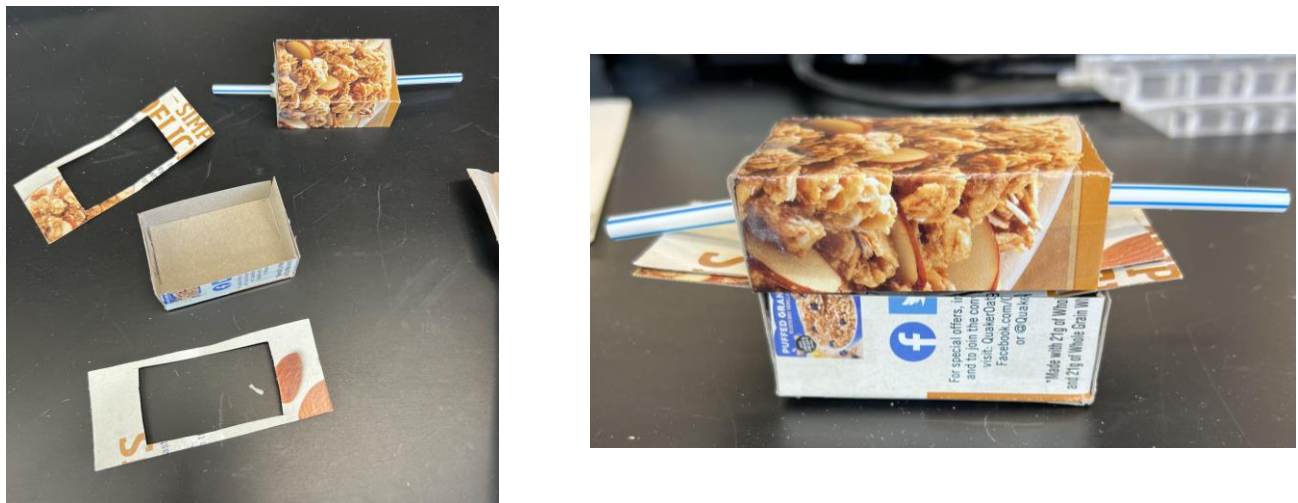
Figure 27: Arts and Crafts Model. Cardboard, straws, and tape were used to create the first replica of the fluid flow chamber the team designed.

Through the process of creating this cardboard model, we were able to better understand how each component could best be imaged and what kind of fasteners could best be utilized to keep all the components together. The team also explored potential areas where the device might leak

and where modifications needed to be made. Our team realized we needed a better way to secure the membrane, and we needed to be able to remove the reservoir easily. Overall, this was an important step in the design process to help us visualize and determine where there might be faults in the design. The next step was to create a CAD model to allow for future fabrication.

4.6 CAD Models

After making our cardboard model the next step was to model our design in SolidWorks. Modeling our design in SolidWorks would allow us to be exact with dimensions and get a better understanding of how our flow system would actually work. Our team went through many CAD model iterations before finally manufacturing the device. The different iterations and the changes we made will be explained in the following section.

4.6.1 Version 1

The goal of our first CAD model was to bring our initial rough sketches to life. We were less focused on it being perfect and accurate and more focused on making a model, so we had a place to start. This first version of the CAD model was two pieces and can be located in Figure 28. The top piece was the distributor, and the bottom piece was a reservoir. The measurements used to make this were not picked for any specific reason, it was just to see what our ideas would look like as a 3D model.

There were a lot of flaws with this initial design that needed to be addressed. For starters there was no gasket which is an important component for a parallel plate flow chamber. There was nothing technically holding the membrane besides just clamping the two pieces together and there was also an unnecessary gap between the inlet/outlet and the top of the distributor. This first iteration was good because it allowed us to have a starting point, even if it had a lot of flaws.
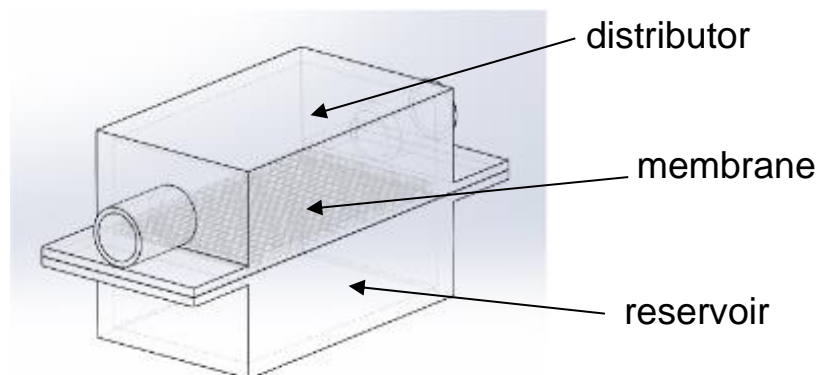
Figure 28: Version 1- Initial Design. Initially, the basic backbone of the device included only a distributor, membrane, and a reservoir.

4.6.2 Version 2

The second version of our CAD model (Figure 29) was developed based on the flaws identified in the initial design. We moved the inlet and an outlet from the side of the distributor to the top, and we also designed a double gasket with a hole in the middle, in order for the porous membrane to sit in between the two gaskets. The bottom piece was also updated to have a smaller reservoir that matched the size of the holes of the gaskets and two support "leg" extrusions were added on each end for support and balance.

The main flaw identified at this point was associated with the way the top gasket was designed, which would not allow for laminar flow to the membrane. Having laminar flow is a significant aspect of our project, therefore, the top gasket was redesigned to meet these criteria, as described in the next version of our model.
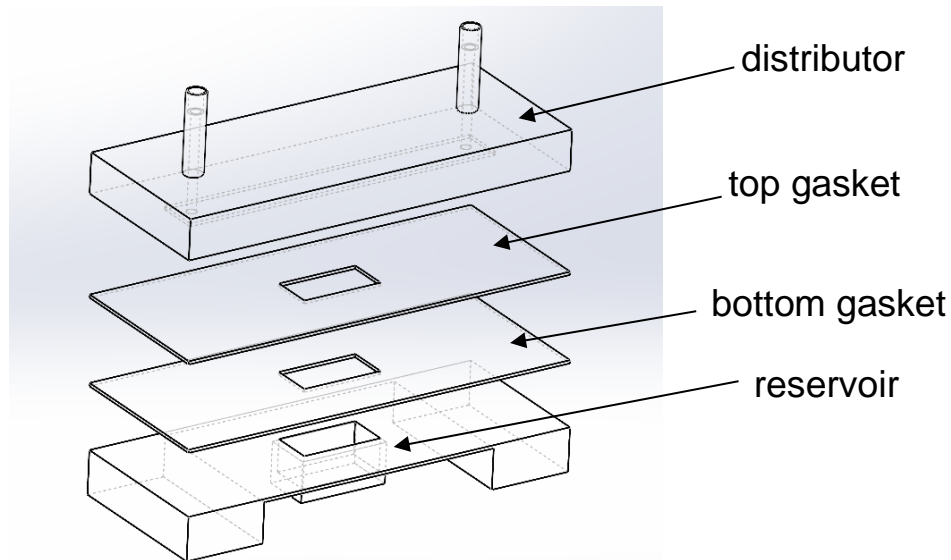
Figure 29: Version 2- Two Gaskets. The second iteration of the design added gaskets and a smaller reservoir. It also decreased the size of the distributor and changed the inlet and outlet location.

4.6.3 Version 3

This next version of our CAD model, we focused on redesigning the top gasket so that it would allow for laminar rather than disturbed flow. To do that, we added a low slope to the top gasket as seen in Figure 30. This was done in order to allow the liquid media to smoothly flow to the membrane, without causing excessive stress on the cells and allowing the flow to be laminar. The other components of the device were not changed during this iteration, as the team was just focused on making sure this gasket was properly designed.
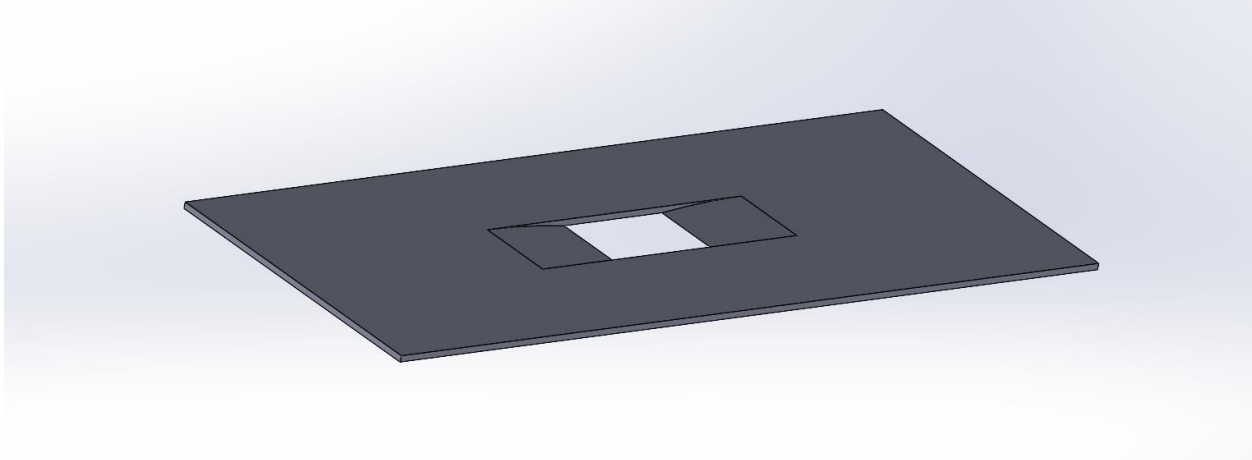
Figure 30: Version 3- Sloped Gasket. Above shows the dipped gasket modeled in SolidWorks.

4.6.4 Version 4

In the next version of the CAD model, the team updated the top distributor (Figure 31). Instead of having the inlet and outlet on the top of the distributor, it was decided to have them on the sides. Curvature was added to the holes to create a pipe-like structure that would allow for smoother flow and would not introduce excessive stress to the cells. This modification was made in order to allow for a continuous and intact flow to meet the flow time specification as described in section 3.2.3.
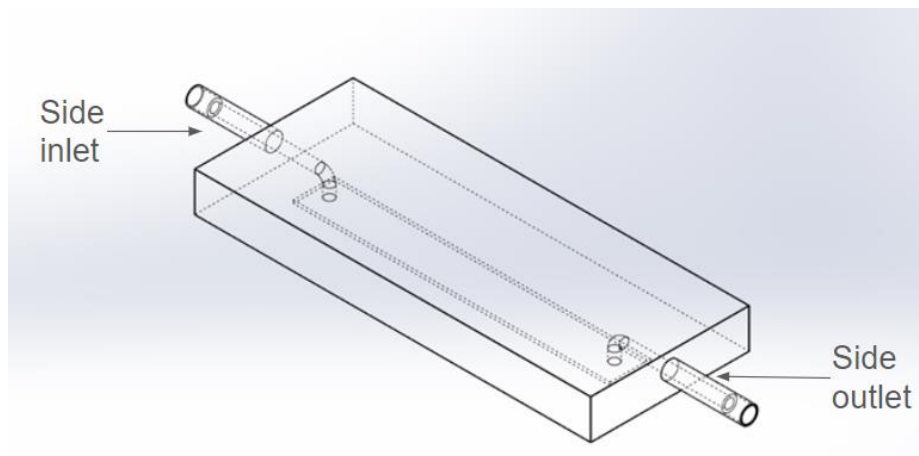
Figure 31: Version 4- Distributor Side Inlet/Outlet. Screenshot of the distributor with side inlets; modeled in SolidWorks.

4.6.5 Version 5

The original idea was to use clamps on the device to hold it together. After careful consideration, we decided to use screws as they would hold the device more tightly and securely, reducing the

chances of leaking. In this version of our CAD model, we added eight screw holes on each of the four parts of our device (the distributor, the two gaskets, and the bottom part). We made careful measurements and ensured that the holes would not interfere with the flow or with the imaging portion of our device. Additionally, we decided that the way we had previously modeled the distributor would make it hard to machine, therefore, we redesigned the inlet and outlet to allow for easier manufacturing. We removed the side extrusions and added two threaded holes on each side that matched the dimensions of our tube connectors. We also cut holes inside each side of the distributor in a way that they would perpendicularly intercept each other. This would allow for easier manufacturing while not disturbing the flow of the system. The updated distributor can be seen in Figure 32 below.
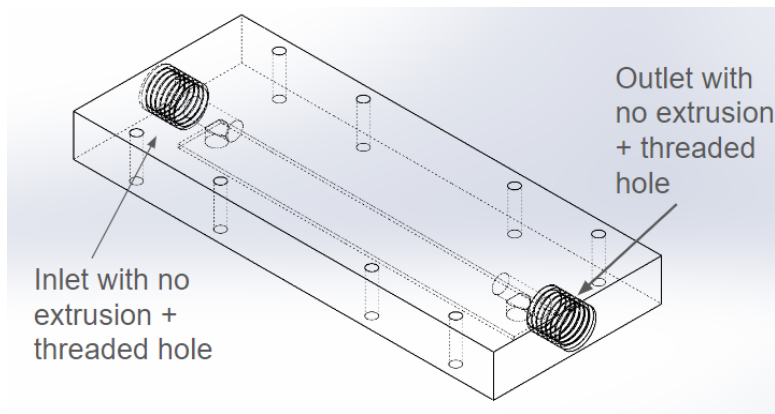
Figure 32: Version 5A- Distributor Holes and Threading. Screenshot of the distributor with two threaded holes for connector attachment and eight screw holes for device assembly; modeled in SolidWorks.

Another major change that we made in this version of our CAD model was changing the bottom. We realized that we needed a better design that would allow for easier imaging of the cells. We decided to use a 35 mm cell culture plate as a reservoir where cancer cells would be collected, therefore, any changes to the bottom were made in order to ensure a perfect fit with the culture plate. We added a pocket-like structure with a lip that would allow for sliding the culture plate into it, as seen in Figure 33. The lip was designed to go around the culture plate and ensure a perfect fit in order to avoid leaks. Additionally, the leg extrusions were minimized in order to save material. This change was mainly made to meet the imaging specification, stating that the device would allow for easy imaging of cells from underneath using a microscope.
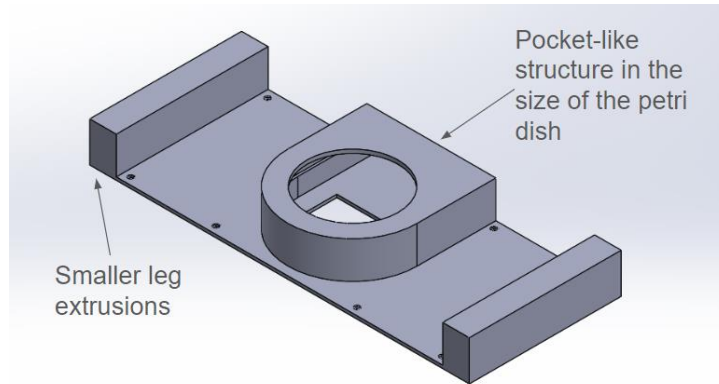
Figure 33: Version 5B- Bottom Redesign. Screenshot of the bottom part with the pocket-like structure; modeled in SolidWorks.

4.6.6 Version 6

Once the CAD design was finalized, we took it to the machine shop for manufacturing. From our conversation with Ian Anderson, we got some helpful feedback regarding certain changes in our design that would make manufacturing easier. Firstly, we needed to break apart the bottom piece of our device, modeling the support legs and the base separately. We added a jigsaw pattern to the legs and the base for a stronger and more secure attachment. Ian suggested that we get rid of the pocket structure as it couldn't be machined. Instead, he suggested we create a perfect seal between the culture plate and the base part of our device. For this, we needed to model a square piece with four screw holes that would serve as a compressor for the culture plate ensuring a tight fit with no leaks. Additionally, we would need a silicone seal to be placed around the culture plate to prevent any leakages. The updated assembly can be seen in Figure 34, while the exploded view of the assembly can be seen in Figure 35.
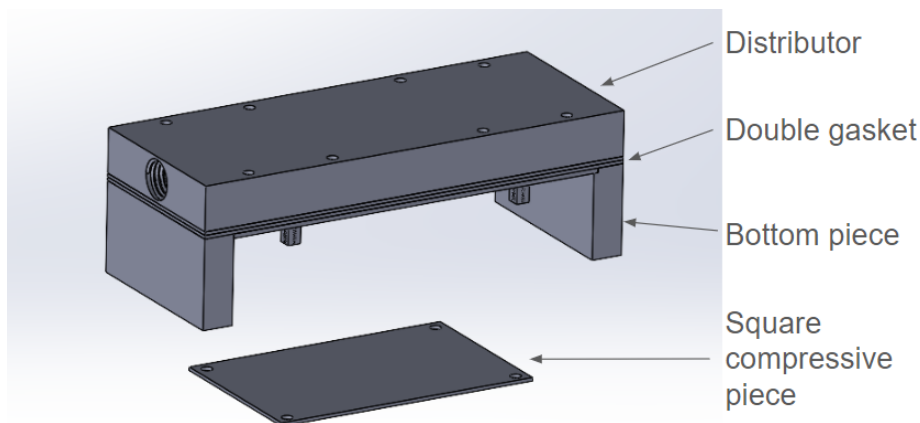
Figure 34: Version 6A- Assembly. Screenshot of the device assembly from SolidWorks.
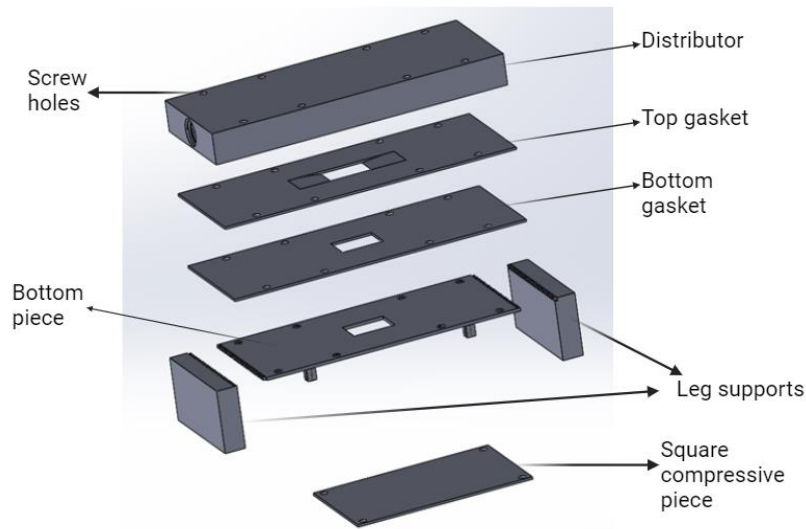
Figure 35: Version 6B- Exploded View. Exploded view of the final model modeled in SolidWorks. Each component is broken apart into pieces that are easier to machine.

4.7 3D Printing

This section focuses on the use of 3D printing technology, specifically employing a Prusa MK4 printer with a 0.4 mm diameter nozzle and PLA filament. This type of prototyping was done to fabricate multiple iterations of the custom flow system for studying cancer metastasis rapidly. The iterative design process allowed for refinement and optimization, ultimately enhancing the system's performance.

In terms of the 3D printing setup, as mentioned previously, the 3D printing process was executed using a Prusa MK4 3D printer, known for its precision and reliability in creating intricate designs. Polylactic acid (PLA) filament, a biodegradable thermoplastic derived from renewable resources, was chosen as the printing material due to its favorable balance of strength, durability, and ease of use [62].

The development of the flow system involved a systematic iterative design approach. Initial design concepts were translated into digital models using SolidWorks. These digital models were then converted into printable files compatible with the Prusa MK4 printer (.amf). Each iteration of the flow system underwent a series of refinements based on feedback from preliminary experiments and SolidWorks fluid flow simulations, allowing for continuous improvement.

During the 3D printing process, the PrusaSlicer software was employed. This software is specifically designed for Prusa 3D printers, including the MK4, facilitating the transformation of intricate 3D models into printable layers by generating G-code instructions for precise and

optimized printing. Within this software various settings were altered to provide precise and accurate geometries with higher resolutions. The settings that were altered consisted of the resolution being set to 0.07 mm ULTRADETAIL, permitting high resolution and precise geometries to be produced. In terms of the infill, 15% was used to enable faster printing times so that multiple iterations could be printed in a shorter amount of time. Supports were also generated using the "auto generated supports" feature on the software. The temperatures of both the heat bed and nozzle were automatically calibrated on the software based on the type of filament being used. An image of the editor view in the Prusa software can be seen in Figure 36, while a sliced view can be seen in Figure 37.
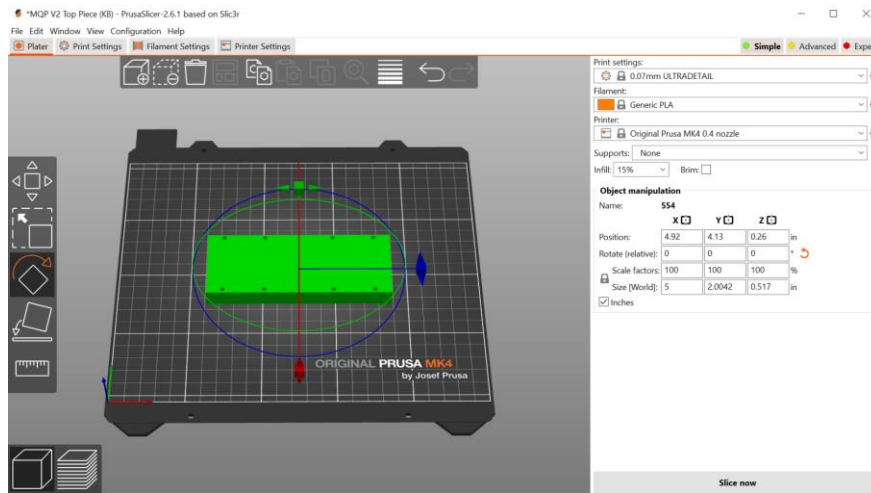
Figure 36: 3D Editor View in PrusaSlicer. An .amf file of the top piece of the flow system is displayed on the print bed within the PrusaSlicer software and the printer settings are adjusted for higher resolution.
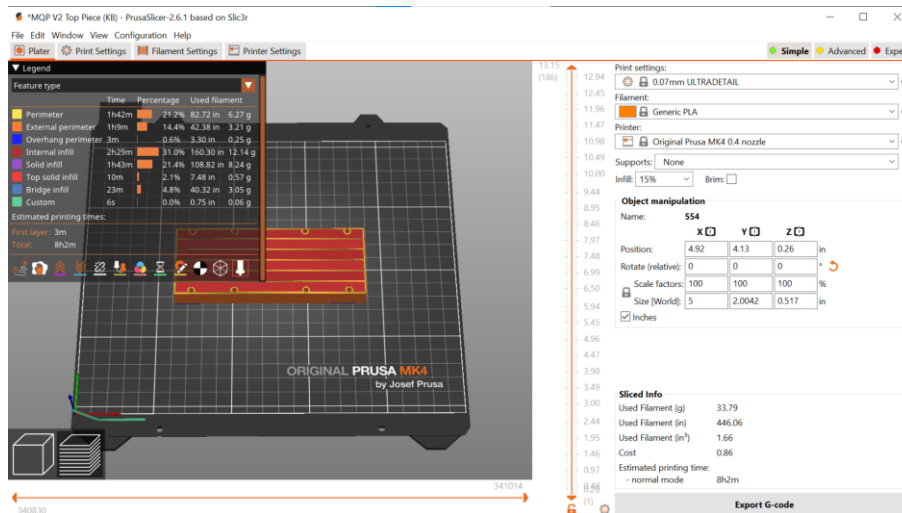
Figure 37: Sliced View in PrusaSlicer. A sliced view of the .amf file from Figure 36 before exporting into a G-code file for printing.

Chapter 5: Testing

This chapter aims to study the different tests the team completed prior to verifying and validating our device. The tests described in this chapter are not directly related to the spelled out functional and performance specifications. The fluid flow simulation, leak tests, and membrane tests are reported in the following sections.

5.1 SolidWorks Fluid Flow Simulation

Following the design process and creation of the CAD model, the team ran simulations in order to understand if the device that had been designed would be feasible in regard to it emulating that of a capillary. This test was critical in order to move forward with the manufacturing of the design. First, the team had to understand the software before moving forward to setting up the model.

5.1.1 Understanding the Available Software

SolidWorks is a versatile software that primarily develops and markets 3D CAD design software. In addition to being available for use with CAD, the software also contains analysis tools to help analyze the design you created. The team used both. First to create a 3D design of the device and then to analyze the device based on researched values for characteristics of a capillary. Using the SolidWorks student access through Worcester Polytechnic Institute, the team utilized the SolidWorks Fluid Flow Simulation to easily simulate liquid flow through the design. In addition to using SolidWorks, the team began the simulation portion of this project using COMSOL Multiphysics. In the end, the team decided to stick with SolidWorks because of the ease of use and the ability to create boundaries easier for where the flow needed travel.

5.1.2 SolidWorks Fluid Flow Model Setup

The simulated flow model was set up in three phases. The first phase was the initial CAD model setup with specific requirements in order to use the flow package and properly analyze the team's design. Next was the second phase where the input data was defined. This included things such as the initial flow rate and volume pressures. Finally, the results section was arranged to help define what type of results the model provided.

The initial step in constructing this model was to input the designed CAD model into the SolidWorks Flow Simulation package. Then in order to define the boundaries where the fluid would flow, lids were inserted into the holes in the device where the barbs and tubing would normally connect. A membrane was also created which in SolidWorks was represented by a thin sheet such that the hole in the bottom of the device would have a boundary. Although the final membranes the team used were circular, the rectangular representation was sufficient in representing the membrane. Three lines were drawn along the top of the membrane. One line

directly in the middle of the membrane and spanning across the entire opening in the device and two more lines near the edges. These lines were drawn along the direction of flow as seen in Figure 38 below to help in the analysis later. An additional line was also drawn perpendicular to the direction of flow along the middle of the membrane.
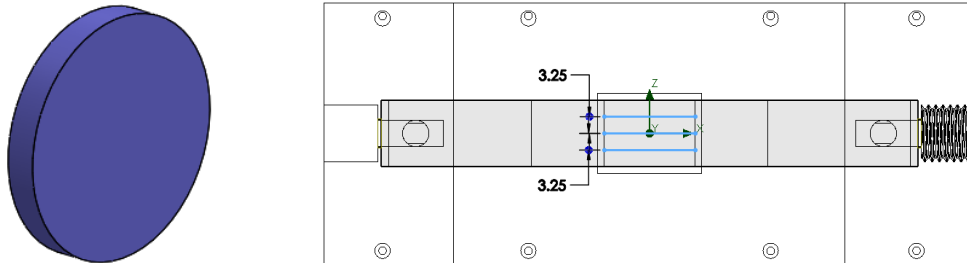
Figure 38: Phase One Simulation Set Up. The image on the left shows the lids as they were inserted where the barbs and tubing would be on the device. On the right are the three lines along the membrane.

The next phase of set up involved inputting data into the software to further classify boundary conditions and goals. Two boundary conditions were defined. One of the boundary conditions was the inlet flow volume which was set to 4.34×10^{-6} m^3/s based on the team's calculations (Figure 39) (see Appendix I). The flow was set as normal to the face inlet where the lid was placed on one end of the device. In addition, the flow was classified as uniform. The second was the environmental pressure which was set to 101325 Pa and the temperature to 293.2 K. These values are standard atmospheric temperature and pressure.
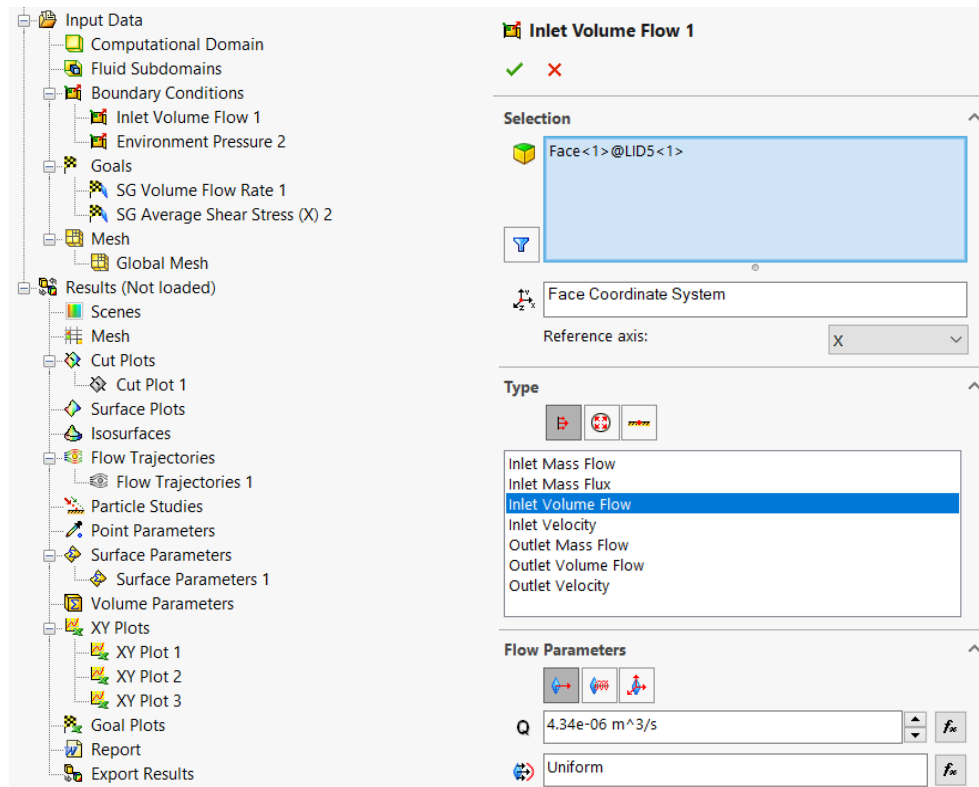
Figure 39: Input Data Simulation Set Up. This shows a closeup of the tree menu items as they appear on SolidWorks as well as the selection options for the inlet flow volume that the team defined.

The goals were set to define the volume flow rate and the average shear stress in the x-direction. The purpose of these goals was to define where the simulation should measure the volume flow rate and the average shear stress. More specifically, measurements of the flow rate and shear stress were wanted along the surface of the membrane. Therefore, both goals were defined along the membrane as defined in the CAD model.

The third phase consisted in constructing the results in the simulation (Figure 40). The ability to define results allowed the team to customize and select for certain results to be shown following the solving process. The cut plot was set to the front plane as defined by the CAD orientation. One flow trajectory was set with the starting point defined as the face of one of the lids placed in an earlier step. From there two surface parameters were defined on the membrane: velocity and volume flow rate.
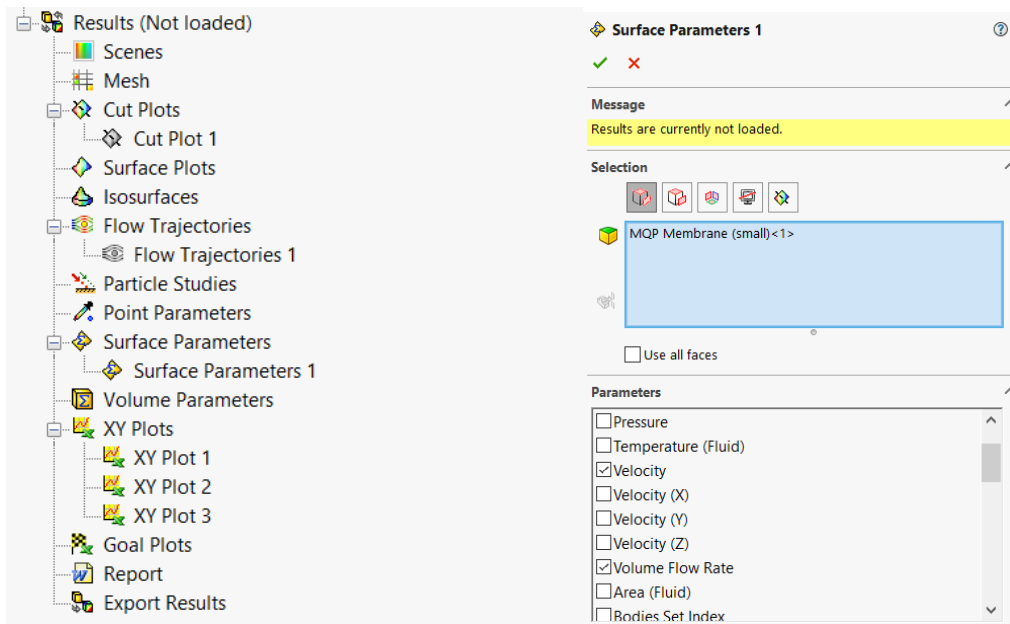
Figure 40: Simulation Results Set Up. This shows a closeup of the tree menu items as they appear on SolidWorks as well as surface parameters for the model.

XY plots were also created in order for the software to produce graphs showing the results of the simulation with numerical values. This involved one XY plot graphing shear stress along the three lines: one in the middle and two near the outer edges all in the same direction as the flow. The second XY plot was of the velocity in the x-direction also along the same three lines. A third plot graphed the velocity along the line perpendicular to the flow along the membrane. Any setting that was not mentioned in this section of the report was left as the pre-set from SolidWorks Fluid Flow Simulation. The final step was running the simulation to get the results that were set up.

5.1.3 SolidWorks Fluid Flow Model

Once the model was set up, the team was able to run the simulated flow through the CAD model. The results of this model, as seen in Figure 41, helped the team move forward with the manufacturing of the device because the model showed that the proper shear stress would be achieved.
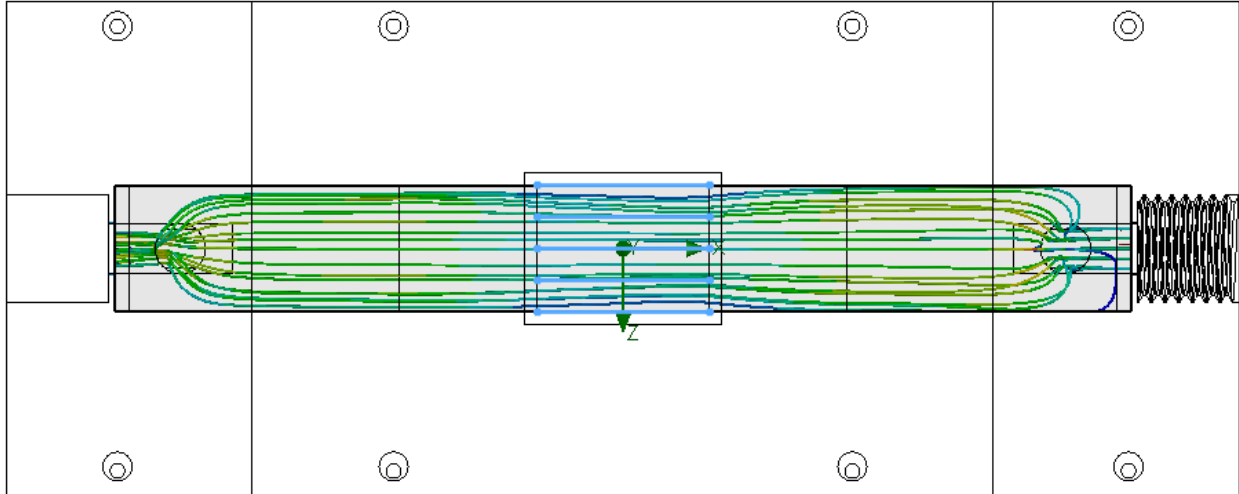
Figure 41: **Preliminary Simulation Results.** Above is a depiction of the flow area viewed from the bottom of the device. The blue lines running parallel to the direction of the flow represent the lines where shear stress was measured across the flow channel.

5.2 Flow Tests

In order to confirm that there were no leaks in the deceive and accompanying system, a series of flow tests were conducted. The first type of test the team conducted consisted of a basic test using a hose attached to the sink, simply to ensure that flow could run through our device after it was manufactured. Then the team moved to testing the entire system which included the device, tubing, peristaltic pump, and syringe reservoir. Many iterations of these tests were conducted until the device consistently no longer leaked. In between iterations, the design was modified. Food coloring was used because we ran each of these tests for 24 hours at a time and if the device leaked with just water there was a chance we would not know because it would dry by the time the test was finished. However, with the use of the food coloring, when the device leaked, it would leave behind a stain on the paper towel below the device.

5.2.1 Flow Test 1: Green

The first test that the team ran was a flow test using green food coloring as shown in Figure 42. This initial test utilized MasterFlex L/S 16 tubing and two 1/8" barb X 1/8" NPT male thread adapter connector pipe fittings. This was an initial test and upon initiating flow, it leaked everywhere. Part one of this test utilized a rubber O-ring that was inserted into the divot in the bottom of the device. This helped the leaking somewhat but another form of gasket was later implemented to help with this issue.
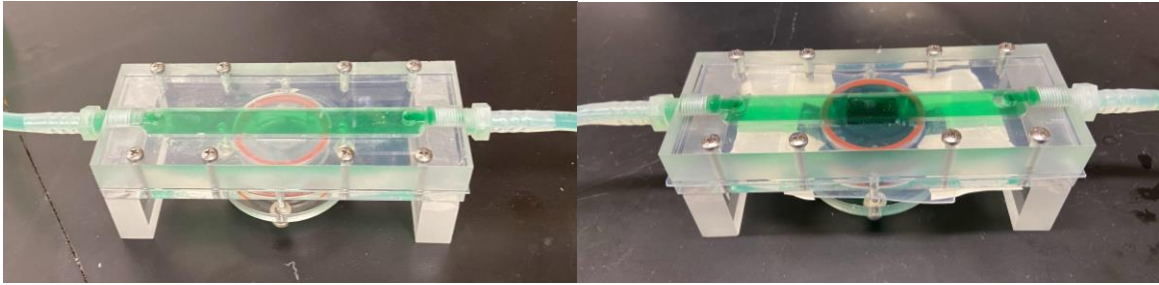
Figure 42: Flow Test 1: Green. The image on the left shows phase one of the first flow test and the image on the right shows phase two with the additional taped on gasket.

A silicone rubber strip was cut and placed around the hole on the bottom of the device. A hole was cut out in the shape of the petri dish in order to have the silicone material be up against the bottom of the device. Then it was secured using tape to assess if the addition of the seal would help with the leaking. Therefore, phase two of this first flow test helped to greatly decrease the amount of leakage from the device.

5.2.2 Flow Test 2: Orange

The second flow test was performed using orange food coloring to differentiate it from the first test. In between flow test 1 and flow test 2, the team carefully glued the silicone piece that we cut in the first flow test to the bottom of the device. Silicone loctite glue was used to ensure that it would stay in place.
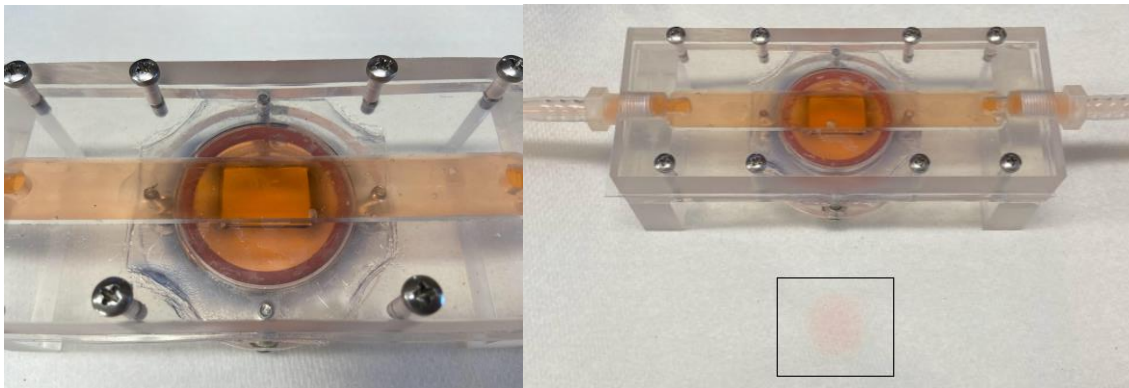
Figure 43: Flow Test 2: Orange. The image on the left shows the gasket that the team glued onto the bottom of the device. The image on the right shows the leak that occurred over the 24-hour flow test period.

This flow test yielded much more promising results but still resulted in a small leak as shown in Figure 43 above. It appeared that the device only leaked a few drops over the 24-hour period but, although it was a small leak, it was still problematic. This prompted discussions regarding the

possible reason for this leak and ways to proceed differently with the next flow test. The next step was to determine if the reservoir attachment piece needed to be screwed on tighter.

5.2.3 Flow Test 3: Pink

The next flow test involved switching the tubing and respective connectors. Due to the system and pump requirements, the group realized that with the smaller tubing and barb size the system was not reaching the appropriate flow rate as it was limited by the RPM of the peristaltic pump head. New tubing and connecting barbs were ordered to ensure that the proper flow rate could be reached given the system constraints. The new tubing was the MasterFlex L/S 17, and the barbs were ¼" barb by ⅛" NPT male thread barbs. Once the new tubing and barbs were installed, another flow test was run to verify that the system did not leak as a result of the connections.

Right from the start of this test, the device leaked. As a result, the barbs were removed, and Teflon tape was added to the barbs to ensure that the liquid was not leaking from the barbs to the device. The barbs were screwed in such that they were flesh to the acrylic portion of the device.
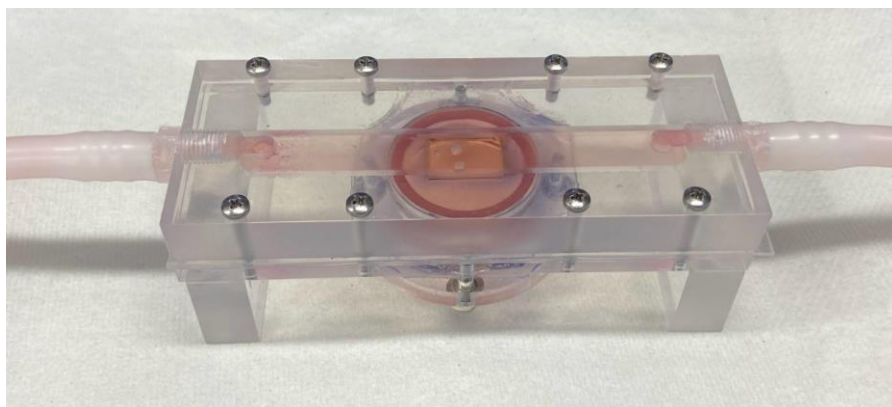
Figure 44: Flow Test 3: Pink. After changing the hose barbs and tubing size another test was completed to test for leaks.

The result of this 24-hour test, as seen in Figure 44 above, was that the device did not leak and no stains were found on the paper towel. One thing the team did learn as a result of this test is that with the larger tubing, the peristaltic pump eats away at the tubing causing small shavings to detach in the section that remains clamped down to allow for pulsatile flow. It is important to note that the tubing is compatible with the peristaltic pump the team is using. Each time succeeding this flow test the team ensured that the same degraded portion of the tubing is not in the pump clamp again to prevent hole formation in the tubing.

5.2.4 Flow Test 4: Pink

Due to the fact that the previous flow test did not leak, the team decided to move forward with the next flow test. The next step in this process was to put a membrane, with no cells seeded, into the device. This test was completed to ensure that the membrane did not break or buckle under the pressure and shear stress of the flow. Initially this test utilized the non-transparent 0.4 micron membranes because these were the membranes we had planned to use at this point in the flow testing.
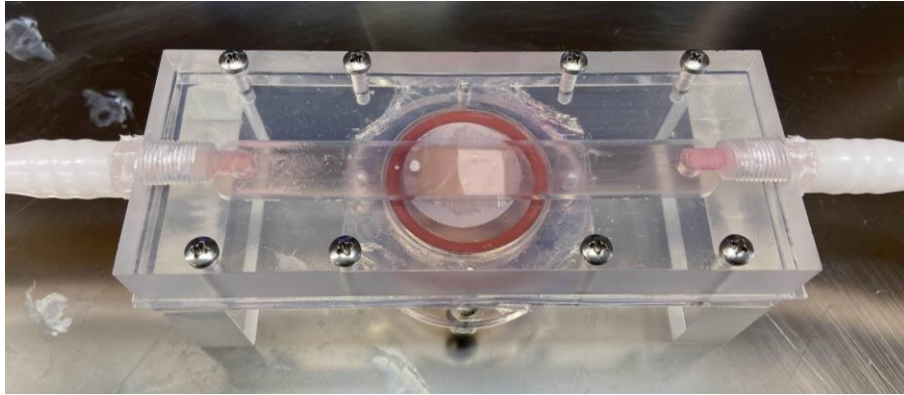
Figure 45: Flow Test 4: Pink. This was the first flow test completed with a membrane in place. The membrane is the non-transparent circle in the center of the rubber O-ring.

The result of this test (Figure 45) displayed the membranes would not break as a result of the shear stress being applied to them as a result of the flow rate. Additionally, there were no leaks in this testing which meant the team had run two consecutive tests where there were no leaks. The petri dish filled up almost completely with water about 30-45 minutes into the test.

5.2.5 Flow Test 5: Blue

The next flow test, in Figure 46 below, used blue food coloring. The team ordered new membranes with a different pore size and were transparent. This flow test was completed to ensure that the new membranes would not cause any issues within the system. Although the new membranes the team purchased were not different in dimensions this was still a good test to complete.
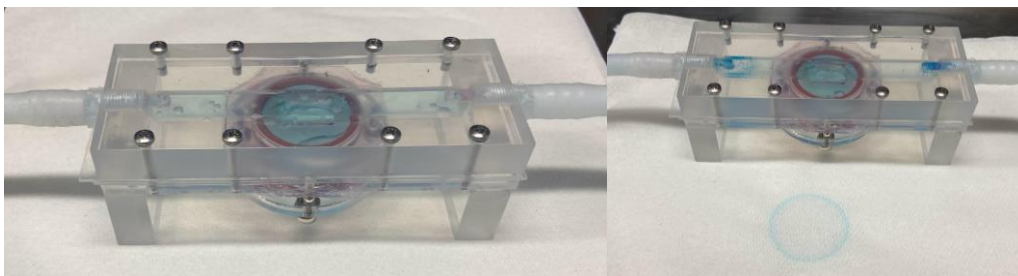
Figure 46: Flow Test 5: Blue. These images show the blue flow test that was conducted in addition to the leak that resulted. The membrane is in place, but it is hard to see because of its transparent properties.

The result of this test was that the system leaked but not due to the new membrane, rather due to the seal and O-ring. Another test would have to be conducted to determine why this leak was occurring. In addition, the team looked at the membrane under an Echo Rebel microscope to see if there were any visible tears due to the shear stress in the flow system. It appeared that there were no rips or tears which showed that the membranes were able to hold up to the shear stress in the system.

5.2.6 Flow Test 6: Purple

This flow test was conducted following the exact same procedures as the previous test with blue food coloring. The primary goal of this test was to determine if tightness was a factor that was causing the petri dish attachment to leak. Therefore, the team tightened the petri dish holder tighter but made sure not to allow the O-ring to warp.
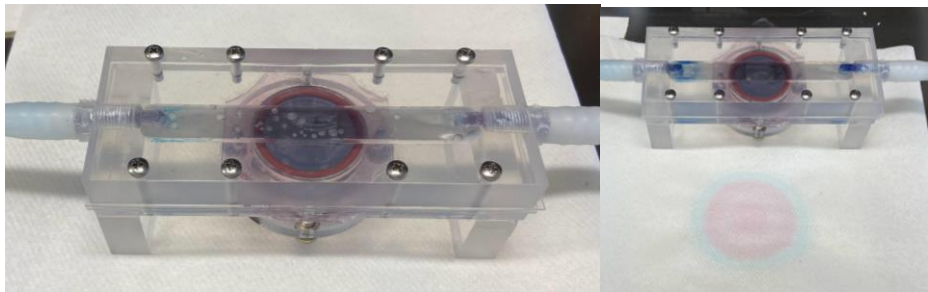
Figure 47: Flow Test 6: Purple. The above images depict the leakage as a result of this test.

The result of this flow test, as seen in Figure 47 above, was that there were still leaks from the petri dish seal. Again, it leaked only a few drops over the 24-hour period of flow running through the system, but a new solution was needed which led to the next flow test. When taking the device apart this time after running the flow, the petri dish attachment was taken off last. From doing this the team found out that the O-ring was going inside the petri dish when it was tightened. From the bottom it was impossible to tell that the O-ring was inside of the petri dish but when it was taken apart the O-ring was found directly inside the top of the petri dish. This meant that the top plastic lip of the petri dish was pressing up against the acrylic making it leak. This was a breakthrough for the team because the source of the leak was discovered.

5.2.7 Flow Test 7: Chartreuse

Flow test number 7 (Figure 48) was the last flow test to be conducted. This flow test was successful on all fronts and met all goals that were stated by the team. The change that was made

from previous flow tests was the seal. As opposed to using the O-ring, the team moved to using a rubber seal that was cut out from a big sheet to be exactly the size of the hole in the device. This rubber seal was placed directly into the circular area. Following that, the petri dish was inserted and then the holder was screwed onto the bottom of the petri dish to hold it in place. See Appendix X for the specifics on how to set up the device properly so it does not leak as tightening the device ever so slightly will result in a leak.
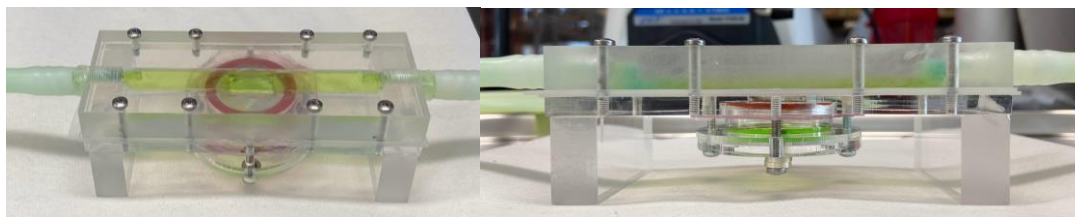
Figure 48: Flow Test 7: Chartreuse. The image on the left shows the final flow test with the new seal and the image on the right shows the petri dish not being completely filled with water after 24 hours.

The overall result after a 24-hour period of constant flow was that no leaks occurred. In addition, there was less water that leaked into the petri dish. In a normal flow test using the other seal methods, the petri dish would fill up within 30 minutes to an hour but with this new seal it filled up less than halfway. This also shows the success of the membrane that the team is moving forward with to the final testing.

5.3 Membrane Tests

In parallel to completing flow experiments, membrane tests were being completed primarily in order to ensure that the membranes met required specifications and would work under the conditions the team established. These specifications consisted of the membrane biocompatibility, allowance of the formation of a confluent monolayer of HLMVECs on the membrane's surface, and cancer cell migration through the membrane pores. Three different types of membrane tests were completed to determine lung cell-membrane interaction, cancer cell-membrane interaction and cell-cell interaction.

5.3.1 Static HLMVEC Membrane Test

The first membrane experiment that was performed consisted of using HLMVECs to assess if they migrated through the membrane or properly formed a cell monolayer on the membrane. The experimental setup consisted of two 60 mm x 15 mm petri dishes, one containing a PETE membrane, and the other was the control with a glass slide (Figure 49). In this test, the PETE membrane was coated with 300 µl of 20 µg/mL fibronectin and was incubated at 37°C for 30 minutes. Following the 30 minutes, the system was returned to the biosafety cabinet, the fibronectin was aspirated, and 100k HLMVECs were seeded in 500 µl of media. An hour after

seeding, HLMVEC media (5 mL) was carefully added to the petri dishes to ensure enough nutrients for the cells to live for 3 days. Two separate PETE membranes were tested in these experiments. The first test was performed with a 0.4-micron PETE membrane, and the second test was performed with a transparent 3.0-micron PETE membrane. In the first test with the 0.4-micron PETE membrane after 24 hours brightfield images of the membrane were taken as seen in Figure 50.
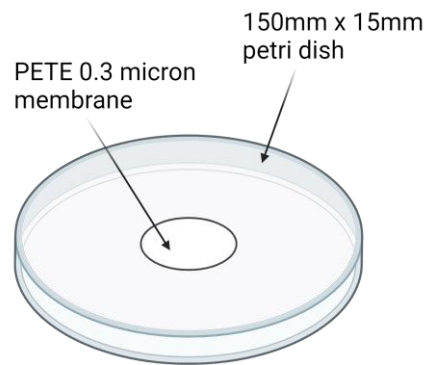
Figure 49: Static HLMVEC Membrane Test System Setup. The above image is a BioRender image of the simple setup used in this process.
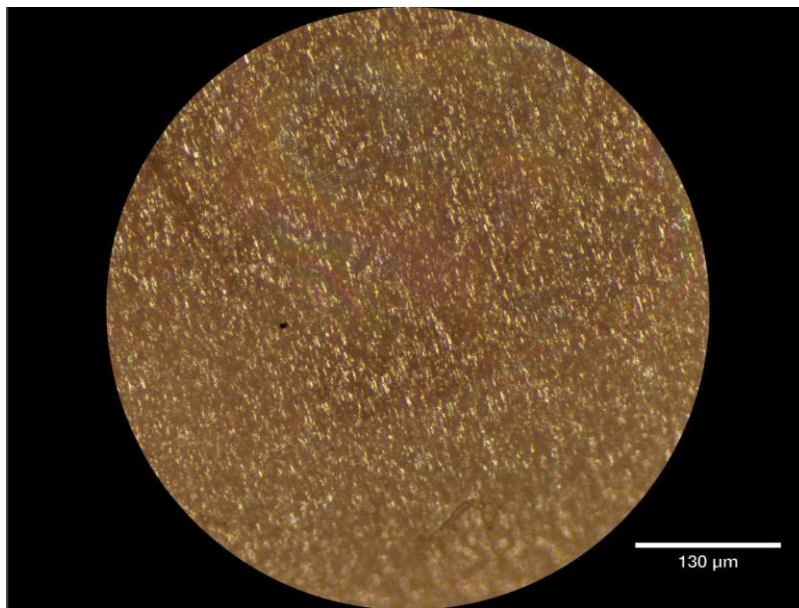
Figure 50: 20x Brightfield Image of 0.4 Micron PETE Membrane. Using the Echo Rebel microscope the membrane was imaged.

As a result of the membrane not being fully transparent, the cells were almost impossible to view with the use of a brightfield microscope. The only visible part of the membrane was the PE

fibers. Although cells were not initially located on the membrane, the membrane was stained using DAPI. This was done by first fixing the cells with a solution of 3% PFA in PBS and letting them sit for 30 minutes. Following the 30 mins, the cells were washed 2-3x with PBS. The membrane was then placed on a glass slide and a 50 µl drop of DAPI mounting medium was placed on top of the membrane. Finally, a glass coverslip was placed over the membrane and nail polish was spread around the edges of the glass coverslip. The glass slide with the membrane was then placed in a -4C fridge in darkness for 30 mins. After 30 minutes, the cells were transported to the Keyence BZ X810 for fluorescent viewing. The results can be viewed in Figure 51.
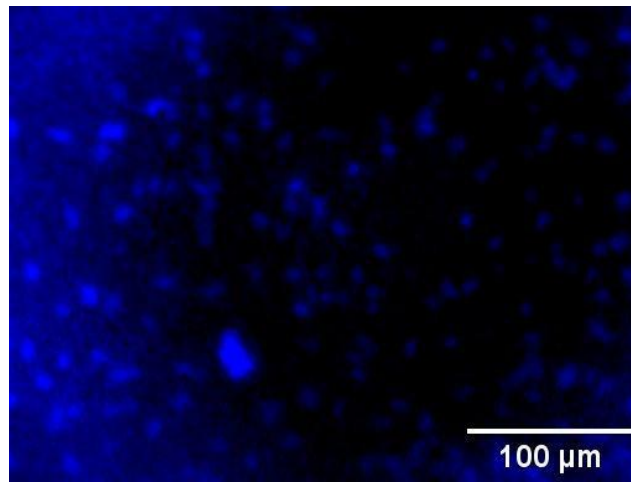
Figure 51: 20x Result of Static HLMVEC Membrane Test. 20x image taken of DAPI stained HLMVECs with the Keyence BZX810 microscope.

The DAPI staining confirmed the presence of cell nuclei on the membrane, but as a result of the membrane not being fully transparent, the cells could not be brought into complete focus. From this primary test, we decided to explore more transparent membrane options.

The second test performed with the transparent 3.0-micron PETE membrane was performed in the same manner as the first test. This test produced much better results, and the membrane was imaged at time intervals of 45 mins, 1 day, and 2 days following HLMVEC seeding. These results as well as the images from the control glass slide can be observed in Figures 52-54 below.
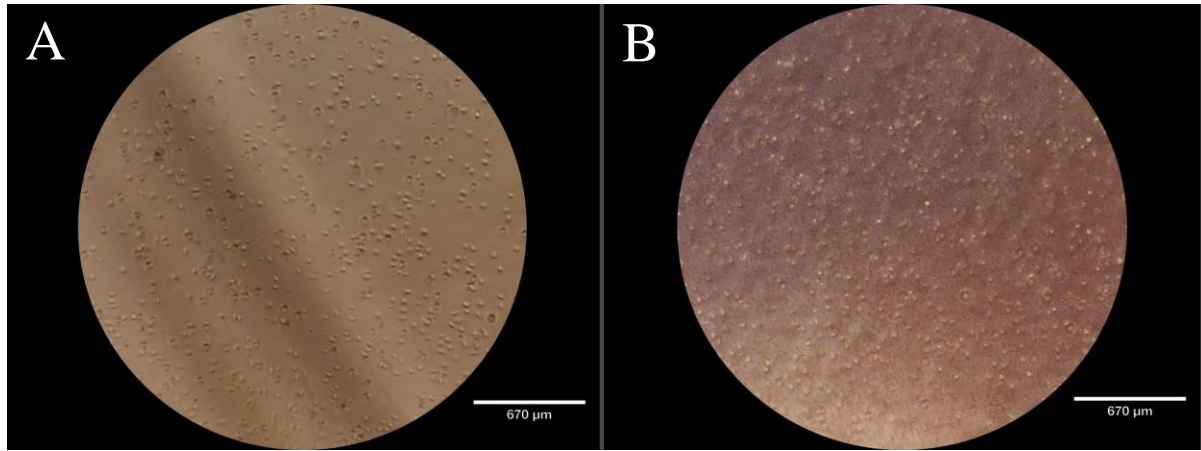
Figure 52: Static HLMVEC Membrane Test at 45 Minutes. (A) 4x image of control glass slide (B) 4x image of 3.0 Micron PETE membrane 45 minutes after seeding cells.
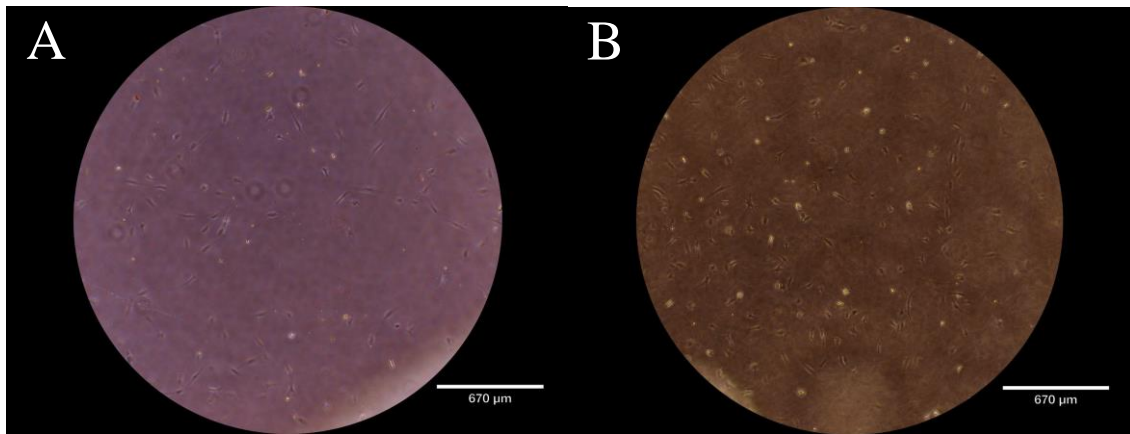
Figure 53: Static HLMVEC Membrane Test at 24 hours. (A) 4x image of control glass slide (B) 4x image of 3.0 Micron PETE membrane 24 hours after seeding cells.
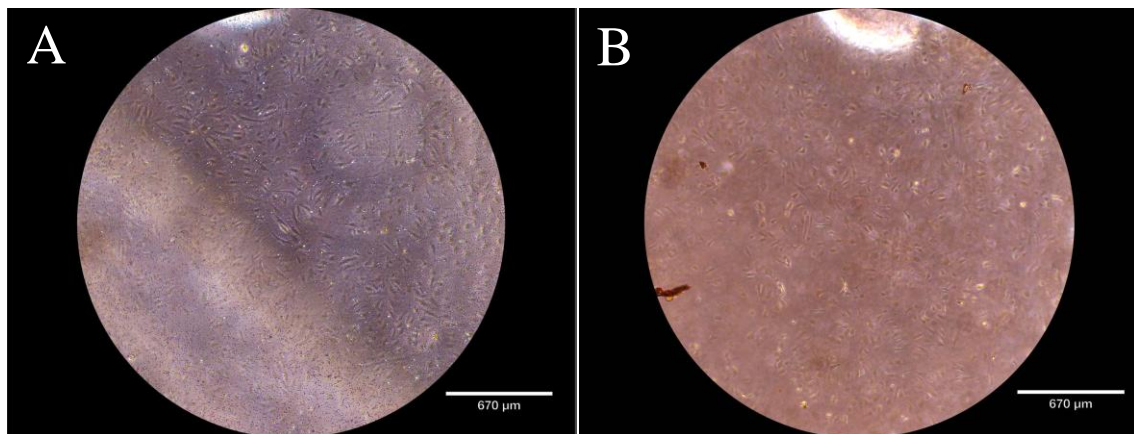
Figure 54: Static HLMVEC Membrane Test at 48 hours. (A) 4x image of control glass slide (B) 4x image of 3.0 Micron PETE membrane 48 hours after seeding cells.

These figures display that the cells are properly attached to the membrane, and that the new transparent membrane could be easily imaged using brightfield. In addition, since the initial seeding concentration was performed at a concentration of 100k cells per 500 μl of media, it took 2-3 days for the membrane to reach 100% confluency. Knowing this timing, we could properly seed cells that would be 100% confluent in time for testing. It was also determined that the PETE membranes are biocompatible, as no cell death was located in any of the microscopic images.

5.3.2 Static MDA-MB-231 Membrane Test

To test if the 0.4-micron porous membranes permitted the migration of cancer cells, we developed a simple system constructed with a 150 mm x 15 mm petri dish, a 35 mm x 15 mm petri dish, silicone sealant, and a 0.4-micron membrane. The setup consisted of the top 150 mm x 15 mm plate with a small cutout hole (about 20 mm diameter) in the center. The 0.4-micron porous membrane was then attached to the bottom of this hole using Loctite silicone sealant. Below the membrane was the bottom of a 35 mm x 15 mm petri dish filled about halfway with MDA-MB-231 media (90% DMEM, 10% FBS, 1% 100x Penicillin Streptomycin), where the cancer cells would be collected if they were able to migrate. The setup can be visualized in Figure 55.
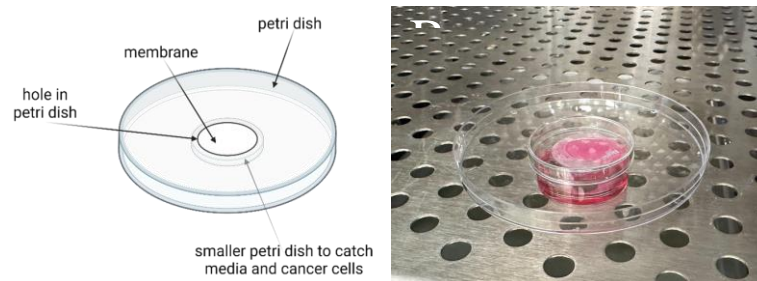
Figure 55: Setup of Static MDA-MB-231 Membrane Test. (A) BioRender depiction of migration assay utilized for the MDA-MB-231 Membrane Test. (B) Migration assay set up in the incubator.

Prior to experimentation, the two Petri dishes were sterilized by spraying them with 70% IPA and UV treatment for 15 minutes in the biosafety cabinet. The membrane was autoclaved at 121°C for 30 minutes. The silicone sealant was also brought into the biosafety cabinet. The 150 mm x 15 mm petri dish was obtained and flipped upside down. Using the tip of a micropipette, a small amount of silicone sealant was applied in a thin layer around the edge of the 20 mm cutout hole. Using sterile forceps, the membrane was carefully placed to cover the cutout hole and to

adhere to the surrounding silicone sealant. After securing the membrane, the silicone sealant was allowed to cure for 24 hours. Once fully cured, the MDA-MB-231 cells were cultured, stained with Far Red CellTrace (Appendix IV), and resuspended in media to attain a $1x10^6$ cells/mL concentration. The bottom reservoir (bottom of a 60 mm x 15 mm petri dish) was filled with 5 mL of MDA-MB-231 media. This reservoir was then placed directly under the cutout to catch any cells that may pass through the membrane. 100k MDA-MB-231 cells (in 500 μL of media) were then directly added on top of the membrane within the 150 mm x 15 mm petri dish. Finally, the top of the 35 mm x 15 mm petri dish was placed over the cutout containing media in the top petri dish to prevent any contamination during incubation. The system was then placed in an incubator at 37°C and 5% CO2 for 24 hours.

After waiting 24 hours, the system was carefully removed from the incubator and brought to the Echo Rebel microscope. The bottom 60 mm x 15 mm petri dish was removed from the system and placed under the objective of the microscope to examine if any of the MDA-MB-231 cells had migrated through the membrane. Upon viewing under the microscope with a 4x objective, dead cells were observed as seen in Figure 56.
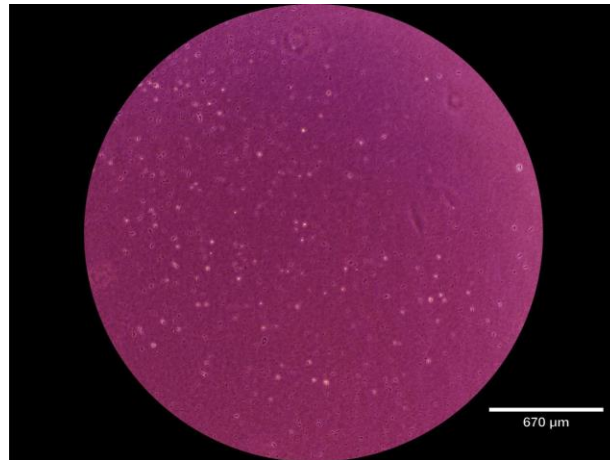
Figure 56: Static 4x MDA-MB-231 Cells in Reservoir 0.4-Micron Membrane Test.
4x image taken with Echo Rebel microscope displaying dead cells that had previously migrated to the bottom 60 mm x 15 mm petri dish through the 0.4-micron membrane.

Although these cells were observed to be dead, this trial confirmed that the cells were able to migrate across the membrane effectively. The cells may have died as a result of improper sterilization.

Since it was decided that the 0.4-micron porous membrane could not be used for the purposes of our project due to imaging difficulties associated with the fact that it was not fully transparent, the same test was repeated using the transparent 3.0-micron porous membrane in order to verify that the MDA-MB-231 cancer cells were able to migrate through this membrane. The cells in

this test were stained with CellTrace Far Red to locate the cells with the use of a Keyence BZX810. The images obtained from the tests with the 3.0-micron PETE membrane can be located in Figure 57 below.
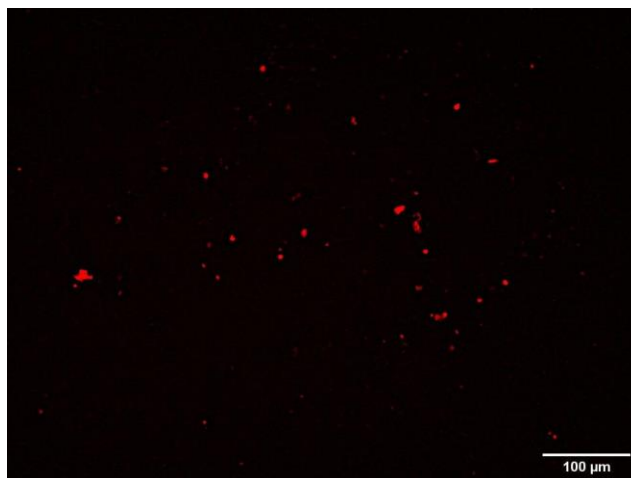
Figure 57: Far Red CellTrace Stained MDA-MB-231 Cells in Reservoir for Static Test. 20x image taken with Keyence fluorescence microscope taken of cancer cells that passed through the membrane and into the reservoir for the static MDA-MB-231 membrane test.

5.3.3 Static HLMVEC + MDA-MB-231 Migration Test

This test was conducted to determine whether MDA-MB-231 cancer cells could migrate through the HLMVECs monolayer on a 3.0-micron porous membrane. This was a static test performed on the same system as described in section 5.3.2. After sterilizing and setting up the system, the PETE membrane was coated with 300 µl of 20 µg/mL fibronectin and was incubated at 37°C for 30 minutes. Then, the system was brought into the hood, the fibronectin was aspirated, and 300k HLMVECs were seeded in 500 µl of media into the membrane. After allowing the HLMVECs to attach to the membrane for an hour, 5 mL of HLMVEC media was added to the petri dish and the system was transferred into the incubator.

After one day, when the HLMVECs had fully attached, proliferated, and reached 100% confluency, $1x10^6$ MDA-MB-231 cancer cells stained with Far Red Cell Trace (in 1 mL of media) were added on top of the HLMVEC monolayer. The bottom reservoir (bottom of a 60 mm x 15 mm petri dish) was filled with 5 mL of MDA-MB-231 media and placed directly under the cutout to collect the cancer cells that may migrate through the membrane. Finally, the top of the 35 mm x 15 mm petri dish was placed over the cutout containing media in the top petri dish to prevent any contamination during incubation, and the system was brought into the incubator to stay for 1 hour.

After 1 hour, the system was carefully brought to the Keyence fluorescence microscope and the bottom reservoir was removed for imaging. The resulting image can be observed in Figure 58 below.
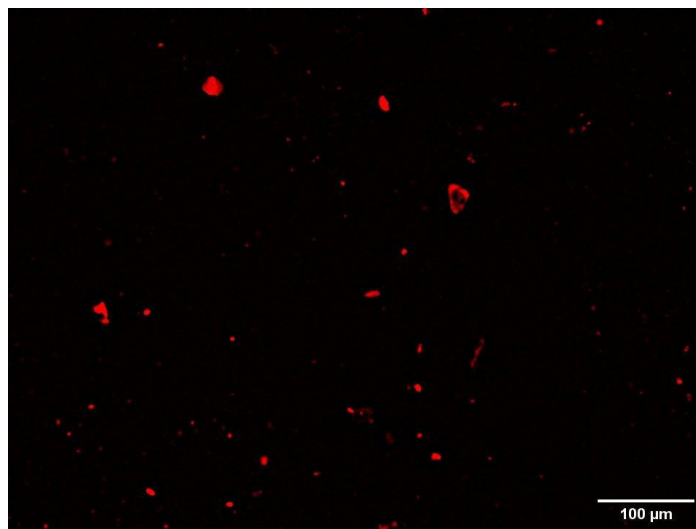
Figure 58: Far Red CellTrace Stained MDA-MB-231 Cells in Reservoir for Static HLMVEC + MDA-MB-231 Membrane Test. 20x image taken with Keyence fluorescence microscope taken of cancer cells that passed through the membrane and into the reservoir for the static HLMVEC + MDA-MB-231 membrane test.

5.4 Staining Tests

In order to both qualitatively and quantitatively assess the HLMVECs and the MDA-MB-231 cells, staining was performed. The staining was responsible for validating factors such as cancer cell migration and shear stress on the endothelial glycocalyx.

5.4.1 Far Red CellTrace Cancer Cell Staining

To decipher the MDA-MB-231 cells and understand how these cells interact with the endothelial glycocalyx, it was crucial that these cells were stained. The staining of these cells helps in identifying and tracking the behavior of the cancer cells during metastasis, such as their movement and invasion into surrounding tissues. Staining can also help distinguish cancer cells from the HLMVECs utilized in our experiments as well as aid in cancer cell quantification. This is essential for accurately assessing the metastatic potential of cancer cells as we can generate data regarding the amount of migrated cancer cells in a static culture versus a dynamic culture. More specifically, the team utilized CellTrace™ Far Red staining solution which is a live stain. This stain efficiently permeates cell membranes, binding covalently inside cells to provide a stable fluorescent signal, facilitating consistent tracking of cellular behavior over time. Its minimal cytotoxicity and negligible impact on cell biology make it ideal for long-term in vitro experiments, allowing accurate assessment of cellular processes such as proliferation and

metastasis [63]. In this experiment, MDA-MB-231 cells were stained following the procedures from Appendix IV, and images were obtained using the Keyence BZX810 microscope as seen in Figure 59.
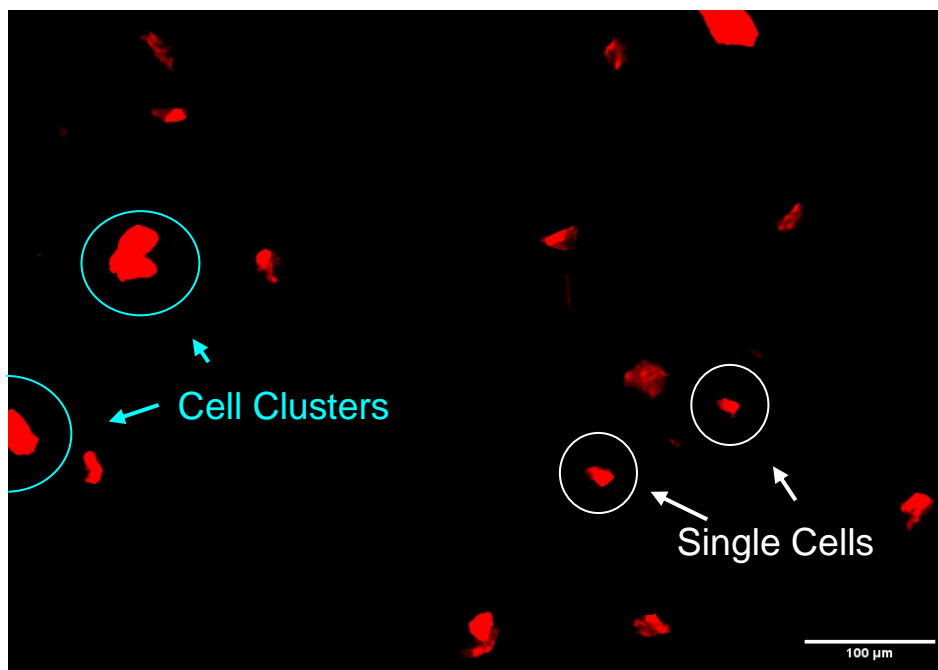
Figure 59: 20x Far Red CellTrace Testing. Following staining, the cells were imaged under the Keyence BZX810 microscope and could be easily viewed showing positive results from the Far Red CellTrace stain.

5.4.2 WGA + DAPI Staining HLMVEC Cells

In order to assess the morphology and view individual components of the HLMVECs, it was crucial that staining was performed to generate both a qualitative and quantitative picture of the cells. In this experiment, a 3.0-micron membrane that was confluent with HLMVEC cells was fixed and stained using wheat germ agglutinin (WGA), which binds to glycoproteins of the cell membrane, and 4',6-diamidino-2-phenylindole (DAPI) which is typically utilized to determine the number of nuclei and to assess gross cell morphology [64] [65]. The cells on the PETE membrane were first fixed with 3% PFA in PBS, and then blocked with 3% BSA in PBS after 30 mins of room temperature incubation. The primary WGA antibody solution and secondary WGA antibody solution were then applied to the cells on the membrane using the procedures from Appendix XII. Following the addition of the WGA staining solutions, the cells were washed with PBS to remove any excess antibodies, DAPI mounting media was added and a glass slide was carefully placed on top. The membrane was placed in tin foil and brought to the Keyence microscope for imaging. The image results can be observed in Figure 60. This image confirms that the cells were able to be properly fixed and stained.
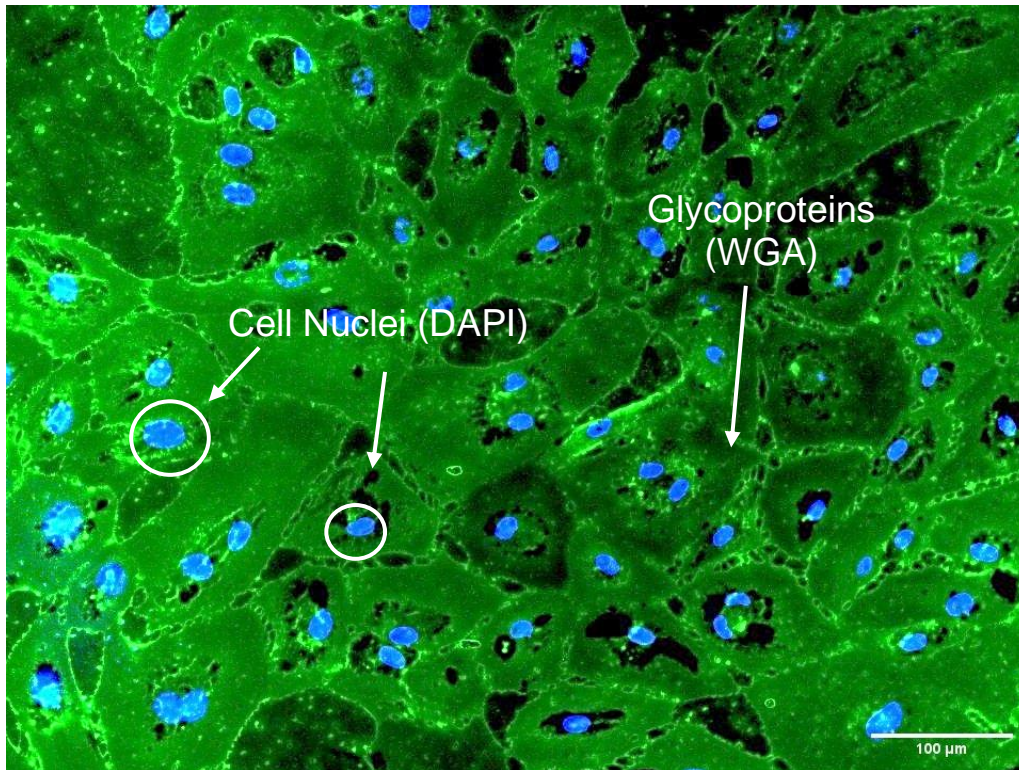
Figure 60: Confluent HLMVECs on 3.0-Micron Membrane. 20x image of confluent HLMVECs on 3.0-micron transparent PETE membrane. WGA, represented by the green, was used to stain the glycoproteins, while DAPI, represented by the blue, was used to stain the cell nuclei.

Chapter 6: Final Design

From the design process, the team finalized the design and fabricated the device to begin the testing process. There are several different components of the final model as well as the flow system which leads to the final setup. The manufacturing process will also be discussed due to the safety constraints and complexities of the device creation. Hence, this chapter seeks to explain in detail the various components and final setup the team used for testing.

6.1 Final Model Components

The final model has several different components which together make up the device as can be seen in Figure 61. These components or subassemblies include the distributor and connectors, gaskets, membrane, seal, and finally the reservoir. Each component contributes a different aspect to the device and when separated the device does not work properly. These components help to meet a variety of the design specifications that the team defined previously.
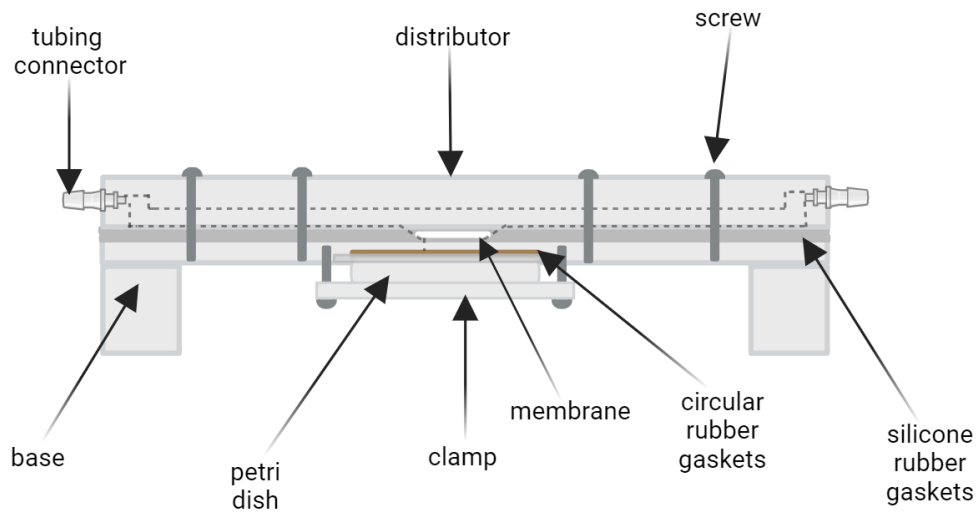
Figure 61: Diagram of Device Components Made Using BioRender. The diagram above has all components labeled and helps meet design specifications such as shear stress and emulating that of a capillary.

6.1.1 Distributor and Connectors

The distributor is a crucial component when it comes to the in-vitro flow system, as it distributes fluid across it. It is designed to have an inlet to allow the fluid into the system, an outlet to let the fluid out, and a channel that goes across the inlet and the outlet and allows for fluid circulation through the system. The distributor setup can be located in Figure 62 below. The inlet and outlet consist of two threaded holes where two connectors are screwed in. The connectors are then attached to the tubing, whose role is to transport fluid in and out of the system. For the purposes of our study, the distributor receives the fluid from a fluid-filled syringe reservoir through a peristaltic pump and distributes it evenly throughout the channel. Ultimately, the fluid is pumped out and goes back into the reservoir, and the cycle is repeated for a specified amount of time. The distributor itself ensures that the flow rate throughout the channel is equal and consistent the whole time. This is particularly important for maintaining experimental consistency and reliable results.
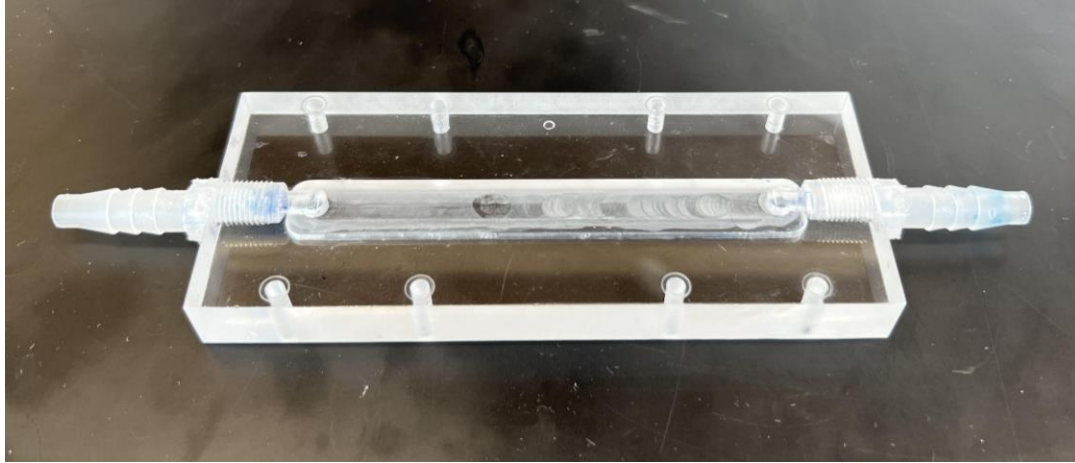
Figure 62: Distributor and Connectors. The above image shows the top of the device with the connectors screwed into the acrylic.

6.1.2 Gaskets

The two gaskets (Figure 63) were made using a roll of High-Purity High-Temperature Silicone Rubber Strip. This strip is a 2" wide, 36" long, and 0.040" thick silicone rubber strip. To make the gaskets, two 5-inch-long strips were cut from the High-Purity High-Temperature Silicone Rubber Strip. A 2 mm by 1.5 mm rectangular hole was cut in the middle of both of the strips that aligned with the cutout in the bottom piece of our device. The next step was to slope only the top gasket, so we set the second one off to the side. To slope the gaskets towards the cutout a sharp razor blade was used to cut the High-Purity High-Temperature Silicone Rubber Strip at an angle towards the rectangular cut-out.

Figure 63: Gaskets. These silicone rubber gaskets were used to hold the membrane in place as well as provide a slope for the flow to ensure no large height differences.

6.1.3 Membrane

In the study of cancer metastasis in vitro, the cancer cells must have a barrier to cross in which HLMVECs may be seeded to emulate a capillary wall. In in-vitro studies, porous membranes are frequently employed in tissue barrier and co-culture models [66]. These are utilized because they facilitate the exchange of soluble factors and sometimes physical contact between cell populations. They are most typically used in studying phenomena including transmigration and permeability, relevant for immune response, cancer metastasis, and drug screening [66].

In looking for a membrane to emulate a capillary wall the team needed to look at various factors including material, diameter, pore size, porosity, transparency, and thickness [66]. Each of these factors plays a crucial role in how the HLMVECs attach to the membrane, how the metastatic cancer cells migrate through the pores, and the ease of imaging the membrane. One of the most crucial factors was maintaining a pore size of 0.4 to 3 μm and a membrane thickness of 10 μm. This pore size and thickness are commonly utilized in studies on cancer cell transendothelial migration [66]. This is because the metastatic cancer cells are small enough to migrate through the pores while the HLMVECs are large enough to form a monolayer on the top surface of the membrane [66]. In addition, to fit within the dimensions of our flow system, the membrane needed to be at least 20 mm in diameter to avoid possible buckling during flow tests. Last, a membrane constructed of an elastomer to emulate physiological strain with optical transparency to enable high-resolution microscopy was needed. Based on these membrane specifications, a commercially available membrane had to be attained. The team eventually decided on utilizing a transparent PETE 3.0-micron membrane as seen in Figure 64 below.

Figure 64: Sterlitech PETE 3.0-Micron Membranes. These are the membranes that were used in final testing because they met all the above qualifications and are biocompatible.

The membranes the team decided on were the transparent track-etched polyester (PETE) membrane filters for Sterlitech. These membranes were optically transparent and had a pore size of 3 μm, a thickness of 12 μm, and a diameter of 25 mm. In addition, these membranes came in a pack of 25 and could be sterilized with the use of an autoclave. This specific material was chosen because it is commonly used in cell culture applications due to its well-defined pore sizes and

high pore density, which allow for controlled cell migration [66]. Polyester membranes are known for their excellent mechanical strength, chemical resistance, and biocompatibility [66]. Various studies have shown that there is greater cell attachment and cell spreading on hydrophilic, relative to hydrophobic surfaces, both with and without serum [67]. These PETE membranes are naturally hydrophilic and can be further modified with fibronectin to enhance HLMVEC attachment.

6.1.4 Seal

The seal for the device, as seen in Figure 65 below, consists of two components: a seal attached directly to the device and a rubber gasket seal. Both types of seals were utilized to ensure the device did not leak. The purpose of the seal was to make sure the petri dish fit securely into the device, therefore preventing leaks. The seal that was directly attached to the device was made using a High-Purity High-Temperature Silicone Rubber Strip. The team cut a 2 inch by 2-inch square out of the silicone rubber sheet and then the corners were cut off to allow for the screws to go through the holes without interference. Next, we cut a 35 mm diameter circle to allow the petri dish to fit properly in the device. Finally, the seal was adhered to the device using Loctite clear silicone which is waterproof.
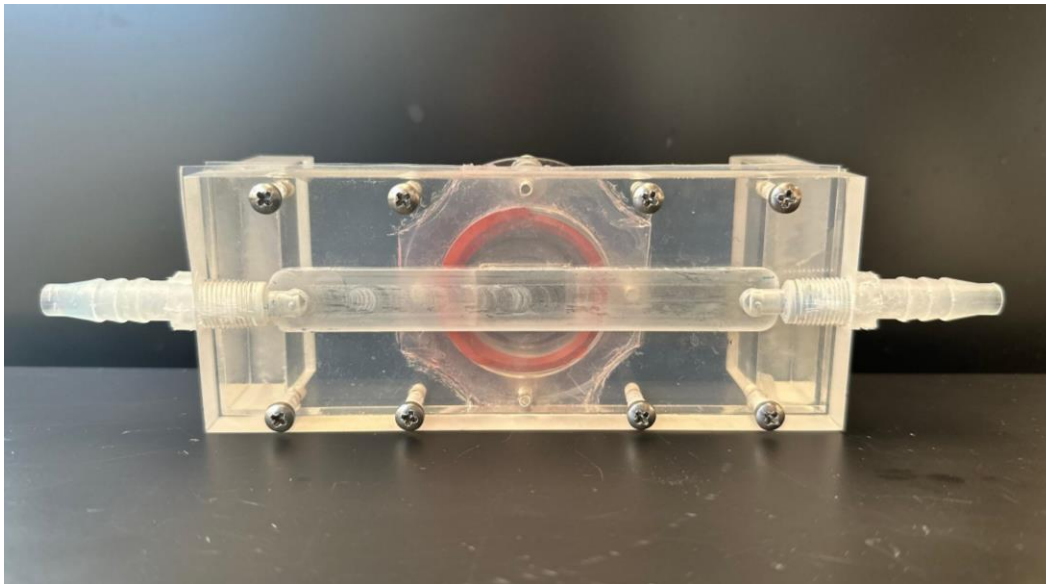
Figure 65: Top View of Device. The image above shows the top view of the device. In this view you can clearly see the flow channel that leads from the inlet to the outlet as well as the reservoir. You can also see the outer seal on the bottom of the device which was made out of silicone rubber and the rubber gasket that is inserted before the petri dish.

Rubber gaskets are used in a variety of different applications in order to create a seal between two mating surfaces. For the petri dish attachment, a rubber gasket was necessary in order to create a seal between the top of the petri dish and the bottom of the device. The rubber gasket is

a rubber material which was cut in order to perfectly fit the hole created in the bottom of the device. Once inserted, the petri dish also fits into the circular hole in the acrylic and creates a slight suction. The reservoir is then attached to ensure that there are no leaks.

6.1.5 Reservoir

The reservoir consists of the petri dish and the petri dish plate which holds the petri dish in place. The components of this sub-assembly can be seen in Figure 66 below. The petri dish is a Nunc 35 mm cell culture plate and only the bottom of the dish was used in these experiments. As shown in Figure 66, the bottom of the device is flipped upside down and then the rubber gasket fits into the bottom cavity. Then the petri dish is placed on top of both gaskets which hold it in place snugly. There is a lip on the acrylic plate that the petri dish is positioned on, which allows for high accuracy and precision when attaching the petri dish to the device.
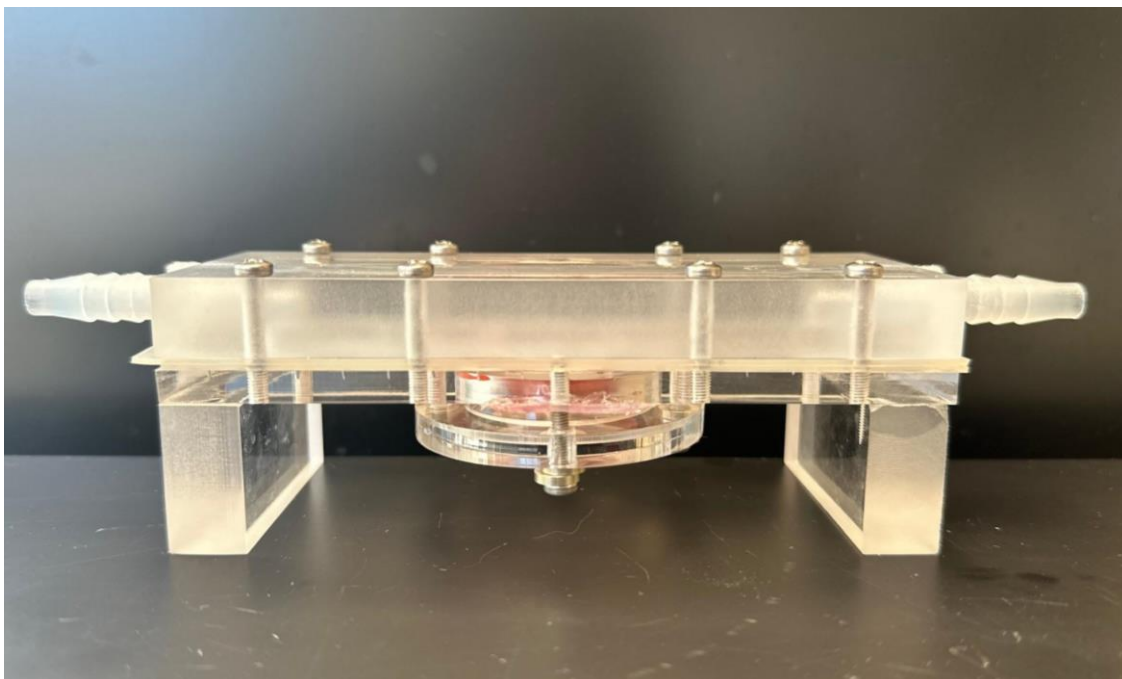
Figure 66: Side View of Device. This image shows the side view of the device. As you can see the distributor, silicone rubber gaskets, and base are all screwed together to ensure no leakage. There is a base for the petri dish to sit on, that screws into the base of the device to ensure a snug fit between the reservoir and the base.

The bottom plate is made such that the tolerances between the petri dish and the plate allow for no movement of the petri dish within the plate. The purpose of this plate is to help secure the petri dish and press the dish up against the seal when the screws are intact. Four screws are used in order to hold the plate to the bottom of the device. These are two M3-.5x20 and two M3-.5x16. The two longer screws have two washers while the shorter screws only have one washer

each. The reason behind the shorter screws is to ensure that they do not interfere with the flow patterns within the channel of the device.

In order to attach the reservoir to the bottom of the device using the screws there needs to be equal amounts of tension applied at once. Because the screws add tension to the bottom of the petri dish, they should be tightened across from each other in an x-shape. Additionally, the seal will buckle and move out of place in the event that one side is tightened too much compared to the other side. When the plate is fully secured to the bottom of the reservoir, there should be an equal amount of space on all sides.

6.2 Device Manufacturing

Once the final design was completed in CAD, the team met with Ian Anderson in the Chemical Engineering department at WPI in order to see how feasible it would be to manufacture the device. During this meeting Ian expressed that it would be hard to machine close end pieces, which means the part holding the petri dish had to be redesigned. The team and Ian came up with the idea of making a plate that the petri dish could sit on that could be screwed into the bottom of the device to tighten it, as can be seen in Figure 67. The next change we made was related to where the tubing connected to the device. Initially we had an extruded piece that extended from the distributor, and it had a curved inner tubing; however, during the discussion with Ian we learned that it was nearly impossible to machine an inner tube to be curved. Using this information, we removed the extruded piece and made the inner tube into a right angle, in place of the inner tubing we would use threads and tubing connectors. The final changes we made to the device were related to the bottom piece. Instead of machining the bottom part as one piece we decided to separate it into multiple pieces and then adhere them using an acrylic solvent. Figure 67 shows the sketches made by Ian and the team during the consultation which include the new changes. After this consultation, we made the changes to the device design and had Ian manufacture it in the Goddard Hall machine shop.
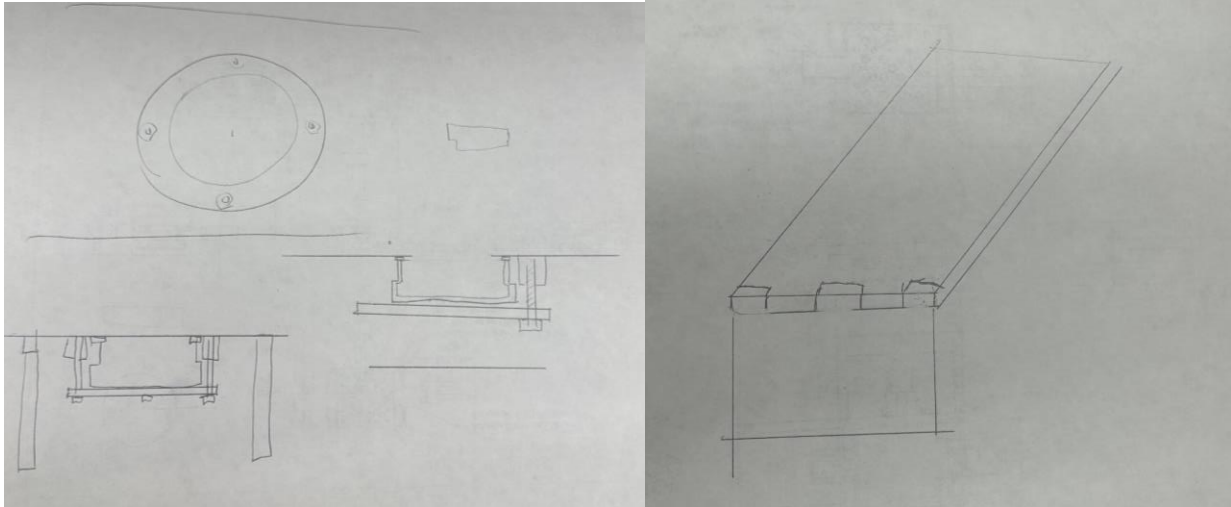
Figure 67: Sketches for CAD Changes. The sketches were made by Ian Anderson and the team to outline changes that needed to be made to the device in order for manufacturing to occur.

6.3 Flow System Components

Once the device was designed and manufactured it could be assembled as a flow system. The final model components together with the flow system components comprise the flow system. After the device is assembled, the tubing, peristaltic pump, and syringe reservoir can be connected in order to begin running the flow.

6.3.1 Tubing and Barbs

The primary component that permitted the flow of media throughout the flow system was the tubing. The tubing had to be carefully picked to fit the MasterFlex L/S Easy-Load® II Pump Head, and it had to be capable of facilitating a flow rate greater than 260 mL/min (this is the flow rate that was calculated to produce realistic shear stress on HLMVECs). It was also necessary that the tubing was biocompatible and autoclavable. Based on these specifications, the tubing decided upon was the MasterFlex L/S 17 (Figure 68A). This tubing can withstand flow rates in the range of 17 to 1700 mL/min and withstand temperatures greater than 120°C, rendering it autoclavable. In addition, the interior diameter of the tubing is 6.40 mm (0.252") and the length is 25 feet. These dimensions allowed the tubing to be tightly fit on the hose barbs of our model. The barbs used on the device were 1/4" Barb X 1/8" NPT male thread adapter connector pipe fittings (Figure 68B).

Figure 68: Tubing and Barbs. (A) Masterflex L/S Tubing. (B) Plastic Barbs to fit Masterflex Tubing [68] [69].

6.3.2 Peristaltic Pump

In order to run flow through the system, the team decided on using a peristaltic pump. These pumps are typically used to emulate blood flow in flow systems due to their ability to replicate the pulsatile nature of blood flow, their gentle pumping action that minimizes sample damage, and their easy maintenance. They ensure accurate simulation of physiological conditions, offer non-contaminating pumping, and enable adjustable flow rates essential for our project's purpose [70]. The specific model that was utilized was the Masterflex™ L/S™ Variable-Speed Console Drive with the Masterflex® L/S® Easy-Load® II Pump Head (Figure 69). The pump and pump head were capable of producing flow rates up to 2300 mL/min, well over our required flow rate of 260.25 mL/min.
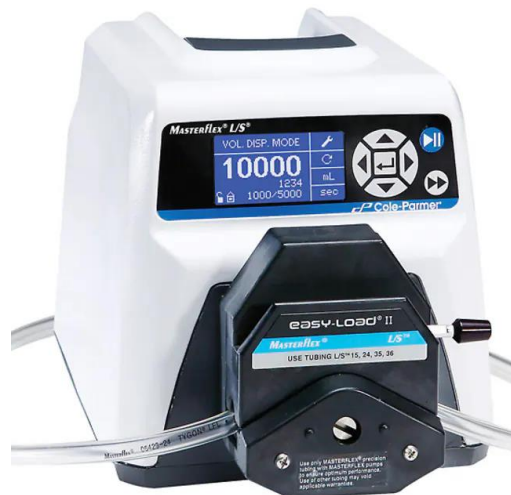
Figure 69. Masterflex Peristaltic Pump. The above pump is the one used by the group when conducting all experiments [71].

6.3.3 Syringe Reservoir

The syringe reservoir, as seen in Figure 70, was used as a holding tank for the fluid and the media to ensure that the system could run for a few hours without running out of fluid. Tubing

was attached to the bottom of the syringe while the top was plugged with a rubber gasket that had a hole for the other end of the tubing to enter into the top of the syringe. The syringe was aligned vertically and attached to a steel support ring stand to keep it upright. When the flow system was started, the team ensured that there was enough fluid in the syringe reservoir to allow the entire experiment to run without the fluid running out of the syringe reservoir.

Figure 70. Syringe Reservoir. These reservoirs were used to hold and store fluids while the experiment was running [72].

6.4 Final Design Setup

The final design setup is a culmination of all the final design components explained above. There are five components that make up this system, including the peristaltic pump, tubing, flow chamber, syringe reservoir, and the steel support ring stand, as shown in Figure 71. In order to set up the system, the following steps were taken.
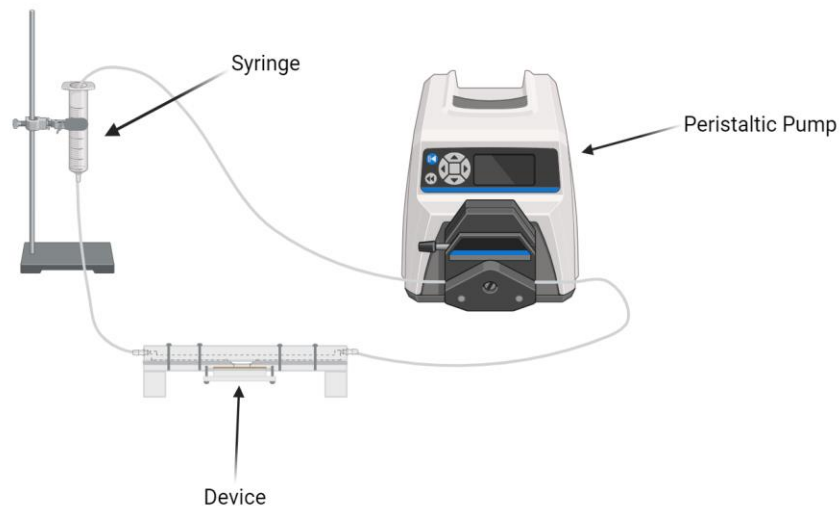
Figure 71: Final Design Setup. The above image is the final design setup. This includes all the components described above in greater detail.

First, the flow chamber is screwed together to the proper tightness to ensure no leaks. The peristaltic pump is plugged into a power source and turned on using the switch on the back. The

flow rate is set to 270.3 mL/min and the direction of flow is set to be clockwise initially, but the pump is not powered on yet. Then the ring stand is set up to hold the syringe reservoir and tightened appropriately. Next, the two sections of tubing are connected to the device on either end. One side is fed through the peristaltic pump and then into the syringe reservoir and the other is fed directly into the syringe reservoir. The setup of the flow system is now complete, and an experiment is ready to be run.

6.5 Final Design Test

To test the complete functionality of our flow chamber, two tests were developed to determine if the flow chamber properly emulated a capillary wall in terms of cancer cell migration potential and effects on the integrity of the endothelial glycocalyx.

6.5.1 HLMVEC Flow Tests

The first tests performed were dynamic HLMVEC flow tests. These tests consisted of seeding 300k HLMVECs in 500µl of media onto two fibronectin-coated 3.0-micron transparent PETE membranes. When the membranes were 100% confluent with HLMVECs, one membrane was left in a petri dish containing HLMVEC media to be used as a control, and the other was carefully placed within the flow chamber and media was run through the system at a volumetric flow rate of 270.3 mL/min. Following 2 hours of incubation (control) and flow (experimental), both of the membranes were fixed and immunostained with DAPI and WGA to view under the Keyence BZX810 fluorescent microscope. This test was repeated three times, each trial with a control and experimental.

6.5.2 HLMVEC and MDA-MB-231 Flow Tests

The next set of experiments were dynamic HLMVEC and MDA-MB-231 flow tests. Similar to the HLMVEC flow tests, the two fibronectin-coated 3.0-micron transparent PETE membranes were seeded with 300k HLMVECs in 500µl of media. The control for these experiments consisted of the migration assay, explained in Section 5.3.3. A view of the control setup can be seen in Figure 72 below.
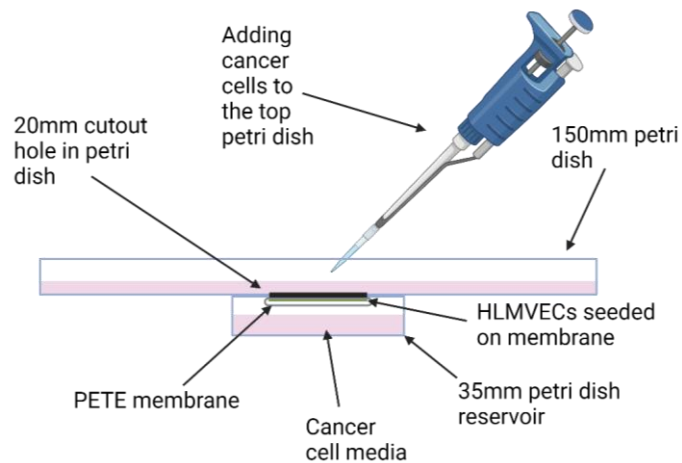
Figure 72: Control Setup for HLMVEC and MDA-MB-231 Static Flow Tests. The above image shows the various components involved in this test. The migration of Far Red stained cancer cells was analyzed through the membrane seeded with HLMVEC cells.

In terms of the experimental setup, one of the 100% confluent membranes was carefully placed within the flow chamber using the same procedures as the HLMVEC flow tests. MDA-MB-231 cells were then live-stained with Far Red CellTrace using the procedures from Appendix IV. The flow chamber was then completely set up (refer to Figure 71 for the depiction of the flow setup). The system was then placed in an incubator (37°C, 5% CO2), and primed with 250 mL of media. The pump was set to 270.3 mL/min and ran for 1 hour to precondition the HLMVECs. Following an hour, the flow rate was reduced to 62.1 mL/min, and 1x10^6 stained MDA-MB-231 cells in 1 mL of solution were added into the syringe reservoir. The system was left to run for another hour. Once the hour was complete, the reservoir and membrane were extracted from the flow system. The control migration assay was removed from the incubator and the reservoir and membrane were extracted from the system. Both of the membranes and reservoirs were then brought to the Keyence BZX810 fluorescent microscope. This test was repeated three times, each trial with a control and experimental.

Chapter 7: Design Validation and Verification

The purpose of design validation and verification is to determine if the design and system meet the established requirements and specifications. For each specification, the team broke the specification into both functional and performance specifications. Functional specifications are qualitative specifications meaning that they are non-numerical. Performance specifications, on the other hand, are quantitative meaning they can be measured. Validation is based upon the functional specifications while verification is based on the performance specifications. In this section the team will describe each of the design specifications and how testing was completed to validate and verify each specification.

7.1 Flow System

The flow system had to be validated and verified using a variety of specifications. The flow system geometry, shear stress, ability to mimic capillary geometry, and flow time will all be discussed in this section.

7.1.1 Flow System Geometry

To ensure our in-vitro device properly resembles the conditions of a capillary our team had to ensure the geometry of the device was made to the correct scale. The functional specification was that the device would allow for flow conditions to mimic a capillary, we did this by determining the shape and shear stress of a capillary and scaling that up to make our device. Our performance specification was that the gasket geometry is calculated based on that of a capillary and the hole in the gasket that allows for cells to be exposed to shear stress has a width of 13.01 mm and a height of 2 mm. We verified this specification by not only measuring before making the cut-out but by also measuring the hole after we cut it to make sure it was correct.

7.1.2 Shear Stress

Shear stress in a capillary can be described as the tangential force of the flowing blood on the vessel wall [73]. The functional specification for shear stress stated that the flow rate going through the device shall provide a shear stress value similar to that seen in capillaries. The way the team validated this specification was through visual analysis. Cells lining a vessel wall that have not yet experienced any shear stress will be circular and or rounded. After the flow system has run for two hours, the cells lining the wall will elongate in the direction of flow due to the shear stress in the vessel.
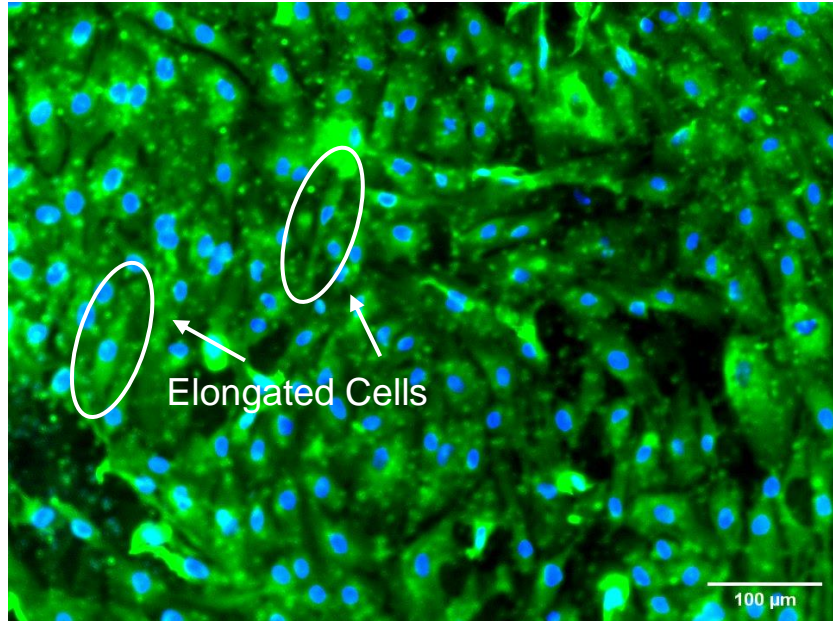
Figure 73: Elongated and Flattened Lung Cells due to Shear Stress. From the above image one can determine the direction of flow due to the alignment of the cells and their deformation.

As can be seen in Figure 73, after the flow was run, the cells were significantly flatter and not as rounded compared to the initial image. This shows that the functional specification stated above was met.
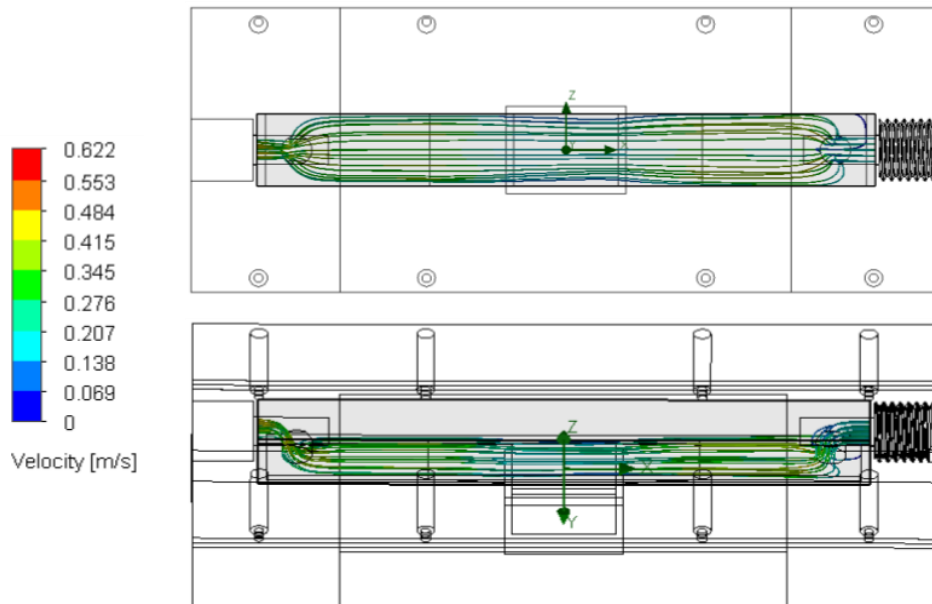
Figure 74: Views of Fluid Flow Simulation within Device. The image on the top is a top view and the image on the bottom is a tilted side view. A key for velocity values represented by the different colors is also shown.

The performance specification stated that the shear stress experienced in the flow chamber is within the range of 0.2-0.6 Pa or 2.0×10^{-7} to 6.0×10^{-7} MPa as seen in a typical capillary [51]. In order to verify this specification, the team created a SolidWorks Fluid Flow Simulation. This allowed the team to model the shear stresses within the CAD model of our design. Figure 74 above is the depiction of the fluid flow as represented within the model.

Shear Stress vs Length
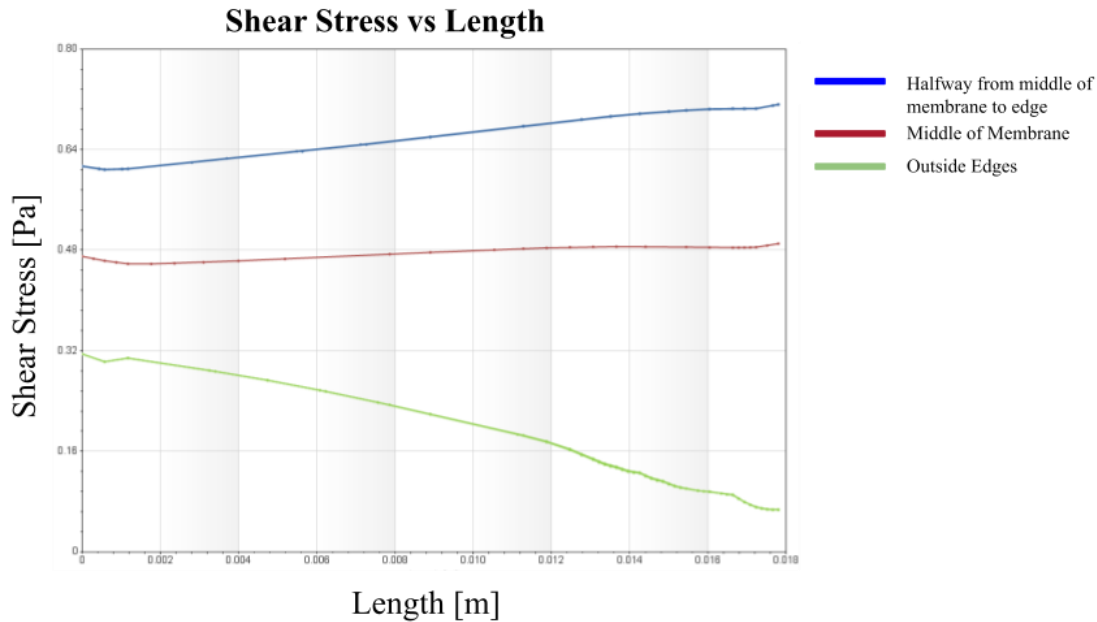
Figure 75: Graph of Shear Stress in Flow Simulation. The red represents the middle of the membrane, the blue represents halfway from the middle of the membrane to the middle of the edges, and the green represents the outside most edges.

In addition, using the graphing feature on SolidWorks Fluid Flow, the team was able to graph the shear stress at different locations along the membrane using lines. The graph in Figure 75 above shows the shear stress in the middle of the membrane as well as along the edges. Again, the model confirms the team's specification was met based on the shear stress from the graph modeled in the middle of the membrane.

7.1.3 Mimicking Capillary Flow

The purpose of this in-vitro device is to mimic a capillary, this means that the device has to have the same flow rate as a capillary. This brings us to the functional specification which is that the device shall emulate proper blood flow rates through the utilization of a certain method of flow. Our team then decided that our method of flow would be a peristaltic pump, so in order to validate our functional specification we needed to run a flow test using a peristaltic pump to ensure that the system could run successfully. Then we decided on our performance specification

which states that the flow system will allow for the use of a peristaltic pump and a laminar flow rate of 260.25 mL/min which is a factor of 0.75 mm/s which is typically observed in capillaries. To verify this specification, we ran a flow test using two graduated cylinders to determine if the flow rate entered into the peristaltic pump matched the flow going through the system. During this test we learned that in order for the flow rate through the device to be 260.25 mL/min we needed to set the peristaltic pump to 270.25 mL/min.

7.1.4 Flow Time

The flow time functional specification states that the device would allow for continuous and intact flow to be able to observe all of the stages of transendothelial migration (TEM). Before the team validated this specification it was important to define continuous and intact flow. This type of flow involves the law of conservation of mass for fluids which states that in a pipe system the volume of flow entering the pipe and leaving the pipe must be the same regardless of if the pipe changes diameter [74]. Therefore this specification was validated through running a flow test through the final design setup with water and food coloring as seen below in Figure 76.
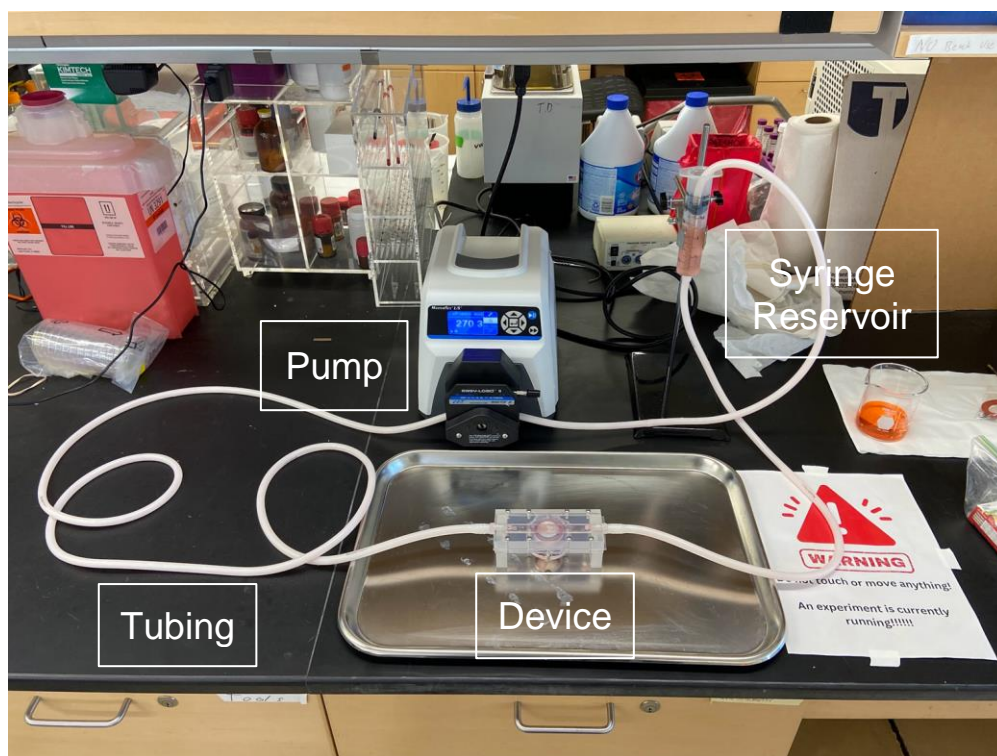
Figure 76. Flow Test Through the System. The image above shows the flow system while it is running. During this trial, red food coloring (appears pink) was used to better see the fluid running through the system.

Additionally, the performance specification for flow time stated that the device will allow for 6 hours of flow via a peristaltic pump. In order to ensure the system does not leak over a longer

period of time, the flow system was run for a 24-hour period of uninterrupted flow to verify the design. This type of test was run several times to guarantee that the device and all its components would not leak. This is the same test that was recorded for the functional specification and can be seen in Figure 76 above.

7.2 Cells

To ensure that the appropriate types of cells and the correct working populations were chosen, our team needed to run different tests regarding cell seeding and cell concentrations. In this section, we talk about how we verified and validated these two specifications.

7.2.1 Cell Seeding

Cell seeding is an important specification of our device. The functional specification associated with cell seeding states that the device shall allow for a certain adherent cell type that can form a proper glycocalyx to be seeded on the membrane. To validate this specification, the HLMVECs were seeded directly on the membrane to see if they adhere and form a proper monolayer. Additionally, they were stained using WGA and DAPI to confirm their confluency and the formation of a robust glycocalyx. The performance specification stated that the device would allow seeding of at least 100k HLMVECs on the membrane. To verify this specification, 100k HLMVECs were seeded on the membrane to confirm that the membrane could hold this number of cells, and a proper monolayer was formed.

7.2.2 Cell Concentrations

Our system works by utilizing two types of cells, the adherent endothelial cells, and the metastatic cancer cells. The functional specification regarding cell concentrations stated that the device should contain a distinct concentration of adherent cells, and a certain concentration of metastatic cancer cells should flow through the system. To validate this specification, we needed to run two different tests. The first one consisted in seeding HLMVECs on the membrane, allowing them to attach and proliferate, and continuously imaging them at different time points until a 90% confluency was observed on the membrane (refer back to section 5.3.1 for more information on this test). The second one was associated with the concentration of cancer cells, and to validate that a certain concentration of cancer cells could flow through the system, we simply needed to view unattached cancer cells anywhere in the flow system and in a petri dish before entering the system. The performance specification regarding cell concentrations stated that the concentration of HLMVECs will be at least 100k/mL, and the concentration of breast cancer cells will be at least 100k/mL. To verify this specification, we simply needed to count the cells using a hemocytometer to ensure that the concentration of cells was 100k/mL before introducing them to the system.

7.3 Membranes

Choosing the right porous membrane that properly emulated the capillary function and allowed the cancer cells to migrate through it was another essential aspect of our flow system, therefore, our team needed to test the effectiveness of the membranes in this context.

7.3.1 Membranes

The functional specification was that the membrane would emulate the capillary wall, permitting cancer cell migration. In order to validate this specification, we needed to choose a porous membrane that would allow cancer cells to migrate through it and simply test it by seeding cancer cells on the membrane and collecting them on a reservoir underneath the membrane. If there were cancer cells collected in the reservoir, the membrane choice was appropriate, and the specification was validated. The performance specification stated that a 3.0-microns porous membrane would allow for an HLMVEC monolayer to be established on top while the breast cancer cells can pass through. To verify this specification, a migration test was performed (see section 5.3.3) to verify that the 3.0-micron membrane allowed HLMVECs to be seeded and cancer cells to complete transendothelial migration.

7.3.2 Cancer Cell Migration

The functional specification regarding cancer cell migration stated that an aggressive type of cancer that has the ability to perform transendothelial migration needed to be chosen for this model. To validate this specification, we chose MDA-MB-231, a metastatic human breast cancer cell line, known to be aggressive. Additionally, the static MDA-MB-231 membrane test described in section 5.3.2, was able to validate this specification and demonstrate the aggressiveness of this type of cancer cell line. The performance specification stated that after 1 hour of flow, the breast cancer cells shall collect in the petri dish. To verify this specification, a full flow test needed to be performed, and after 1 hour, at least 10 cancer cells would be collected in the petri dish.

7.4 Imaging

To ensure that our device would allow for easy and proper imaging of all key components, our team had to determine the correct working distance of the Keyence microscope as well as run appropriate staining tests to differentiate HLMVECs from the cancer cells.

7.4.1 Imaging

Imaging is another important specification of our device, which was designed to be taken apart in order to allow for easier and better imaging of separate parts. The functional specification regarding imaging stated that the device would allow for easy imaging of cells from underneath

using a microscope. To validate this specification, we simply needed to be able to locate the cells under the microscope. This could be done by imaging either the membrane to observe the HLMVECs, or the petri dish reservoir to observe the cancer cells that had performed transendothelial migration. The performance specification stated that a Keyence Microscope should be utilized at an established working distance of 1 mm. To verify this specification, we ran a few Keyence working distance tests using different culture flasks/plates with different heights. HLMVECs were seeded in a T-75 flask, T-25-flask, and a petri dish, with heights 40 mm, 30 mm, and 11 mm, respectively. The cells could not be located in any of the tests, and this could be attributed to the lack of fluorescence in the cells since no staining agent was used. For the remainder of the project, we assume the working distance to be 45 mm as stated by the Keyence manufacturing [52]. Please refer to section 4.4.1 for more information regarding this test.

7.4.2 Identification of Cancer Cells

The functional specification regarding identification of cancer cells within our system states that the device shall allow for easy immunofluorescence staining on cells, in order to differentiate cancer cells from endothelial cells when imaging them under the microscope, as well as to observe the degradation of the glycocalyx. To validate this specification, the cancer cells were stained with CellTrace (see section 5.4.1) and imaged on a fluorescent microscope. The performance specification stated that Far Red CellTrace would be applied to the cancer cells to image using the Keyence microscope in order to verify transendothelial migration. To verify this specification, our team ran a membrane test which is described in section 5.3.3. The cancer cells were stained beforehand with Far Red CellTrace. HLMVECs were seeded on a membrane and allowed to reach 100% confluency before adding the cancer cells on top of the HLMVECs. The stained cancer cells were collected into the reservoir and brought for imaging on the Keyence. Additionally, the membrane with the HLMVECs was stained using WGA and DAPI (see section 5.4) and was also imaged on the Keyence to observe the degradation of the glycocalyx.

Chapter 8: Safety and Ethics Statement

8.1 Health and Safety Concerns

Although the device is not directly being inserted into the human body, there are still important ramifications that need to be taken into consideration. The largest health and safety concern that may arise due to the completion of this project is during the machining and manufacturing process. The components of the device are manufactured in a machine shop which requires specific safety measures to ensure no injury occurs. Another health and safety concern would be using the equipment in the lab and ensuring that each team member has the appropriate personal protective equipment while completing experimentation. Our team will be working with mammalian cells, so it is important that we wear proper personal protective equipment and

adhere to biosafety cabinet rules. Other than ensuring the proper PPE and procedures are followed this is a relatively safe and unharmful project from start to finish.

8.2 General Ethical Concerns and Mitigation

Throughout the entire design process, it is critical to take into consideration all the ethical implications that may arise during the process. Although the device will not come into direct contact with patients and no animal testing is required, there are still several ethical considerations in the categories of environmental, social, global, and economic considerations. In ensuring that the device works as intended, the team is taking into consideration all of these factors and carefully analyzing all possible risks associated with the design of this flow system.

8.2.1 Environmental

One of the goals of this project is to ensure that the creation of this device does not have a significant impact on the environment. A few components of the system including the pump and microscope will require electricity use within a lab setting. In terms of the materials used to construct the device, all the materials are readily available and can be easily ordered. Additionally, the majority of the materials that we will be using in the creation of this flow system can be reused over and over again during the testing phase of the MQP. Due to the fact that the device has to be produced outside of the typical lab, manufacturing plants will experience an uptick in resource usage. The nature of the team's experimentation will result in biohazard waste which may pose risks to human health or the environment. Microbiological waste is an example and includes materials such as specimen cultures, disposable culture dishes, discarded cells, and culture media. Biohazardous materials will be placed in red biohazard bags, provided by WPI, and then disposed of in the proper locations in the laboratory. Although WPI properly disposes of all biowaste, there is still a small potential that it could impact the environment if not correctly processed. Therefore, the overall production of the flow system will have a fairly negligible impact on the greater environment.

8.2.2 Social

Society as a whole will be positively impacted through the development of this device due to the nature of this research regarding cancer. A greater understanding of how cancer migrates through capillaries in various locations of the body could lead to improved methods of treating cancer. Individuals with cancer will once again be able to get back to work if treatments become available, and therefore contribute to society and have overall improvements in their general quality of life. Additionally, the device can be used to study other diseases besides cancer. There are numerous diseases that spread and become more dangerous to the body when they migrate through layers of the blood vessel walls. For example, many inflammatory conditions that involve leukocytes (white blood cells), complete transendothelial migration [75].

8.2.3 Global

Cancer is one of the leading causes of death in the world, with approximately one in six deaths being caused by cancer [10]. With more than 18 million people being diagnosed with cancer each year, the hope is that treatment options will be available across the world and this device is one step closer to determining how to best treat cancer, especially in preventing it from metastasizing and forming secondary tumors [76].

8.2.4 Economic

Our in vitro model presents a minor initial cost, including the costs of materials, production, culture media, HLMVECs, metastatic cancer cells, and imaging agents. Various lab equipment was also accessible for our group for free or with drastically reduced cost such as the Keyence microscope, and 3D printers. This may impose an economic barrier for researchers/citizens who may not have a network, or a research facility containing this type of equipment.

Outside of the initial manufacturing and materials costs, our in vitro model will permit an improved method of studying cancer metastasis and how it interacts with the endothelial glycocalyx, researchers and medical professionals can use this system to better understand and develop novel cancer treatments that may be more accessible to society. As a result of this accessibility, these treatments may become cheaper on the market. The process of drug development is a high-risk high-reward undertaking. It was estimated that the cost of developing a new cancer drug is in the realm of $2.6 billion [77]. With this being said, only 1 in 15 oncology drugs studied in phase 1 clinical trials will make it to market [78]. Our in vitro model will provide a more accurate way to study cancer and its tendencies, making it more likely that beneficial cancer drugs will be produced that will make it past phase 1 clinical trials. This means that billions of dollars will not be thrown away producing drugs that do not pass clinical trials.

In the long run, with improved, and cheaper cancer treatments as a direct result of our in-vitro model, more citizens will be able to get back to work, which would have an overall beneficial impact on the economy. This will also have a positive impact on the families of those affected by cancer as they will not have to tend to them as much with better treatments on the market, also they will have to spend much less on these treatments. Although beneficial for cancer patients and their families, with these improved drugs, pharmaceutical companies will lose customers as cancer patients will be cured much more effectively and efficiently. Ultimately this could disincentivize pharmaceutical producers from innovating as their revenue would be drastically reduced. This could have major implications for the economy as pharmaceutical companies possess an immense market share, especially in the US.

Chapter 9: Results

9.1 HLMVEC Flow Tests

In this section we discuss the qualitative and quantitative results collected by the HLMVEC only flow tests. A total of three control trials under no flow conditions and three experimental trials where flow was present were performed to obtain these results.

9.1.1 Collecting HLMVEC Flow Test Data

To determine if our device worked as intended, we ran a total of three experiments. Each consisted of an experimental (flow) and control (static). These flow tests, containing only HLMVECs seeded on the PETE membrane, yielded results that displayed alterations in cell morphology and alignment. In addition, it was observed that the cells aligned to the direction of flow and exhibited greater intensity and distribution of WGA and DAPI staining compared to the control that did not experience flow.

In flow trial 1, it was observed that there was a lower confluency of cells than expected. The brightfield images of the control and experimental membrane prior to flow can be seen in Figure 77.
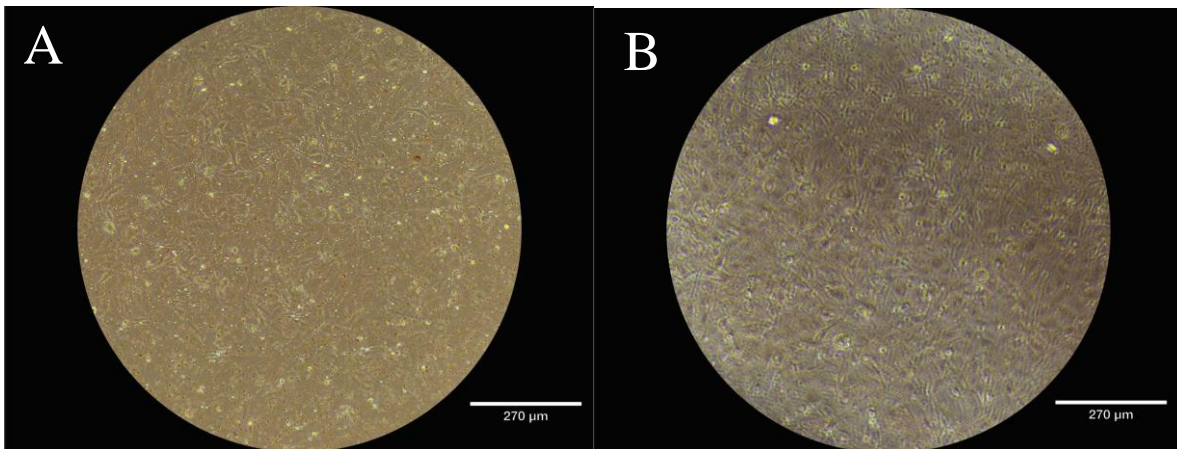
Figure 77: Brightfield Images of HLMVEC Coated Membranes for HLMVEC-Only Tests Trial 1. (A) 10x image of flow trial 1 control membrane. (B) 10x image of flow trial 1 experimental membrane.

Following two hours of flow and incubation (for the control), the HLMVECs on the membranes were immunostained with DAPI and WGA. The fluorescent images taken on the Keyence BZX810 and post-processed in ImageJ can be seen in Figure 78.
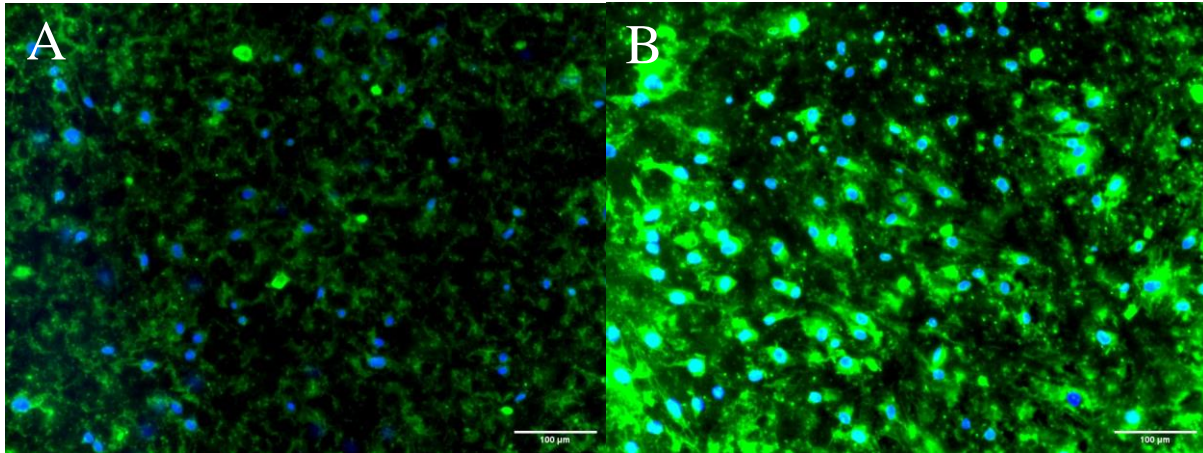
Figure 78: Control and Experimental HLMVEC-Only Flow Test Quantitative Results for Trial 1. (A) 20x image of DAPI and WGA-stained membrane from the control experiment for trial 1. (B) 20x image of DAPI and WGA-stained membrane from control experiment for trial 1.

Flow trials 2 and 3 provided more consistent results that were observed to be much more confluent with stronger DAPI and WGA signals. The brightfield images of the control and experimental membrane for trial 3 prior to flow can be seen in Figure 79. The fluorescent images taken on the Keyence BZX810 and post-processed in ImageJ can be seen in Figure 80.
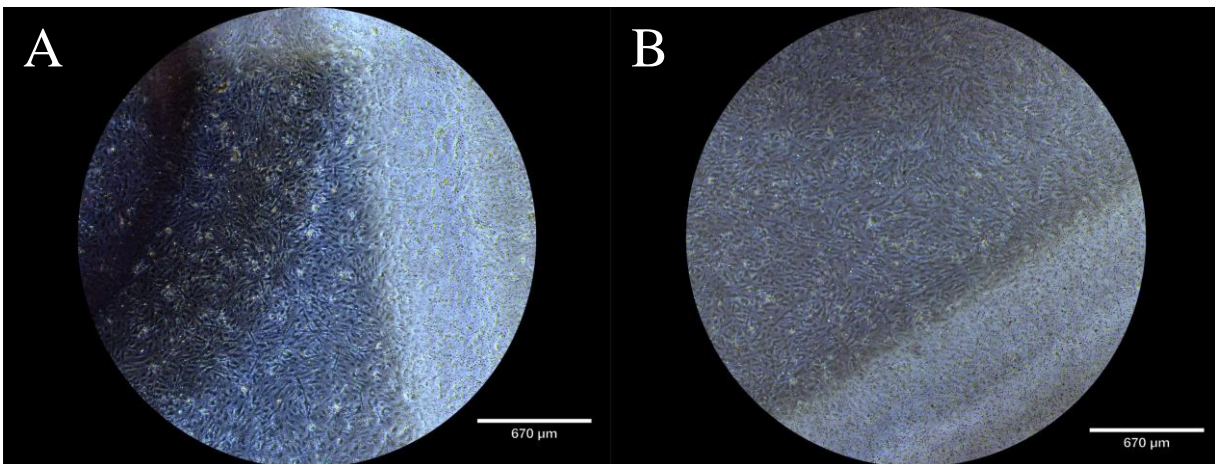
Figure 79: Brightfield Images of HLMVEC Coated Membranes for HLMVEC-Only Tests Trial 3. (A) 4x image of flow trial 3 control membrane. (B) 4x image of flow trial 3 experimental membrane.
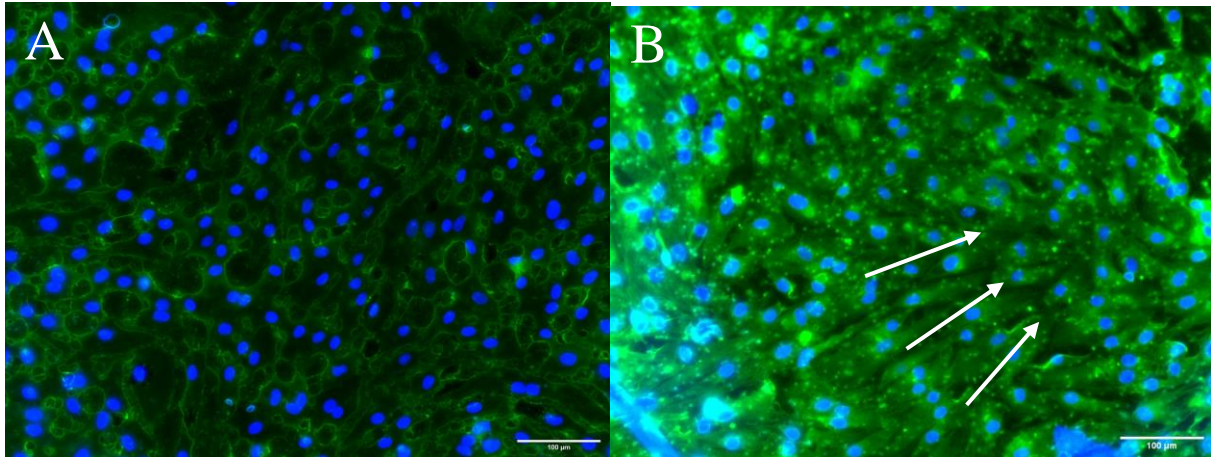
Figure 80: Control and Experimental HLMVEC-Only Flow Test Quantitative Results for Trial 3. (A) 20x image of DAPI and WGA-stained membrane from control experiment for trial 3. (B) 20x image of DAPI and WGA-stained membrane from control experiment for trial 3.

In all of the flow trials, it is apparent that the experimental membranes presented much greater DAPI and WGA fluorescent signals than their associated controls. It can also be observed that the cells aligned in the direction of flow. Figure 73 displays the cells elongated towards the right of the membrane which is denotative of the direction of flow.

9.1.2 Quantifying HLMVEC Flow Test Data

Once the images were obtained our team moved them into ImageJ, an analysis software, to quantify the data. The HLMVEC data was quantified based on two categories which were coverage and thickness. The coverage measured what percent of the slide was covered by the glycocalyx. This test allowed us to ensure that the slides were confluent, and as seen from Figure 81A, there was no significant statistical difference between the static cells coverage and the flow cells coverage.
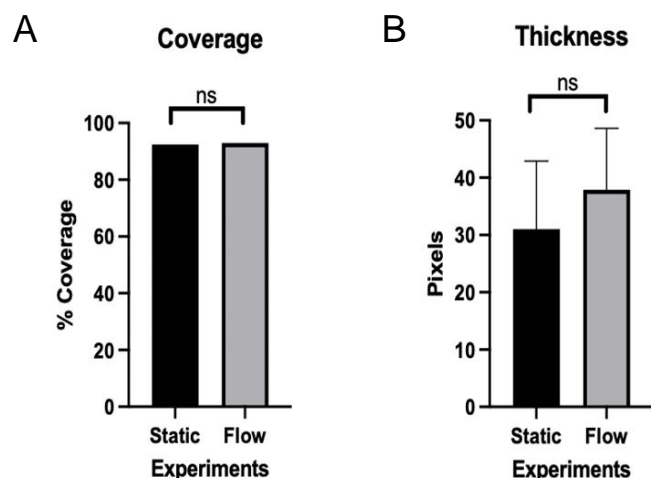
Figure 81: Quantification of HLMVEC Flow Test. (A) A bar chart of the percent coverage of the glycocalyx for the static experiment and flow experiment (B) A bar chart of the thickness of the glycocalyx for the static experiment and flow experiment.

For thickness, the orthogonal view of the images was measured to determine if the thickness of the glycocalyx changed when exposed to flow. As mentioned previously, when the glycocalyx is exposed to shear stress it is supposed to shed and regrow thicker, so it was important our device properly mimics that. As you can see in Figure 81B, the cells exposed to flow expressed a thicker glycocalyx than the static cells, and this shows that our device was working as intended.

In terms of the statistical relevance of our quantified data the unpaired t test for the coverage and thickness can be seen in Tables 5 and 6. Although the data for both the percent coverage and the glycocalyx thickness were not statistically significant, they showed trends that support our research that the glycocalyx thickens when exposed to shear stress.

Table 5: Percent Coverage Data. The Statistical Analysis for the percent coverage unpaired t test shows the data was not significant.

Percent Coverage Unpaired T-Test	
P value	0.8995
P value summary	ns
Significantly different (P<0.05)?	No
One- or two-tailed P value?	Two-tailed

t, df	t=0.1345, df=4

Table 6: Glycocalyx Thickness Data. The Statistical Analysis for the glycocalyx thickness unpaired t test shows the data was not significant.

Glycocalyx Thickness Unpaired T-Test	
P value	0.6905
P value summary	ns
Significantly different (P<0.05)?	No
One- or two-tailed P value?	Two-tailed
t, df	t=0.4283, df=4

9.2 HLMVEC and MDA-MB-231 Flow Tests

In this section we discuss the qualitative and quantitative results collected by the HLMVEC and MDA-MB-231 tests. A total of three control trials under no flow conditions and three experimental trials where flow was present were performed to obtain these results.

9.2.1 Collecting HLMVEC and MDA-MB-231 Flow Test Data

In the HLMVEC and MDA-MB-231 flow tests, HLMVECs were seeded on the membranes and 1×10^6 MDA-MB-231 cancer cells were either placed within the flow system media, or statically placed on top of the control membrane in the migration assay setup. In total, three tests, each with an experimental (flow) and control (static) were performed. Prior to running the experiments, the membranes seeded with HLMVECs were checked under an Echo Rebel microscope to confirm confluency. Each of the trials exhibited almost 100% confluency and images can be seen in Figure 82.
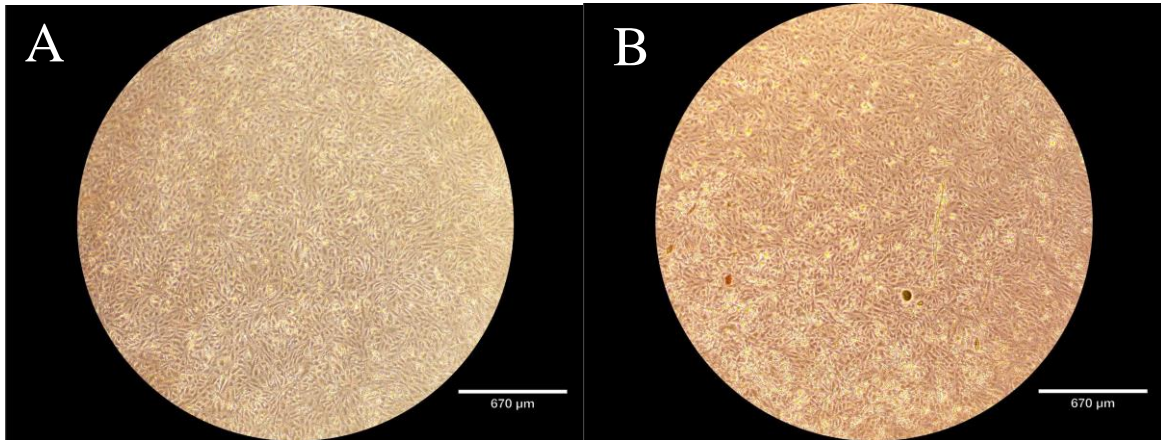
Figure 82: 4x Images of Membranes Prior to Flow Test 2. (A) 4X image taken with the Echo Rebel microscope of the control membrane prior to the control test 2. (B) 4X image taken with the Echo Rebel microscope of the control membrane prior to the experimental test 2.

Following the experiments, both the membranes and reservoirs from the control and experimental tests were fluorescently imaged with a Keyence BZX810.
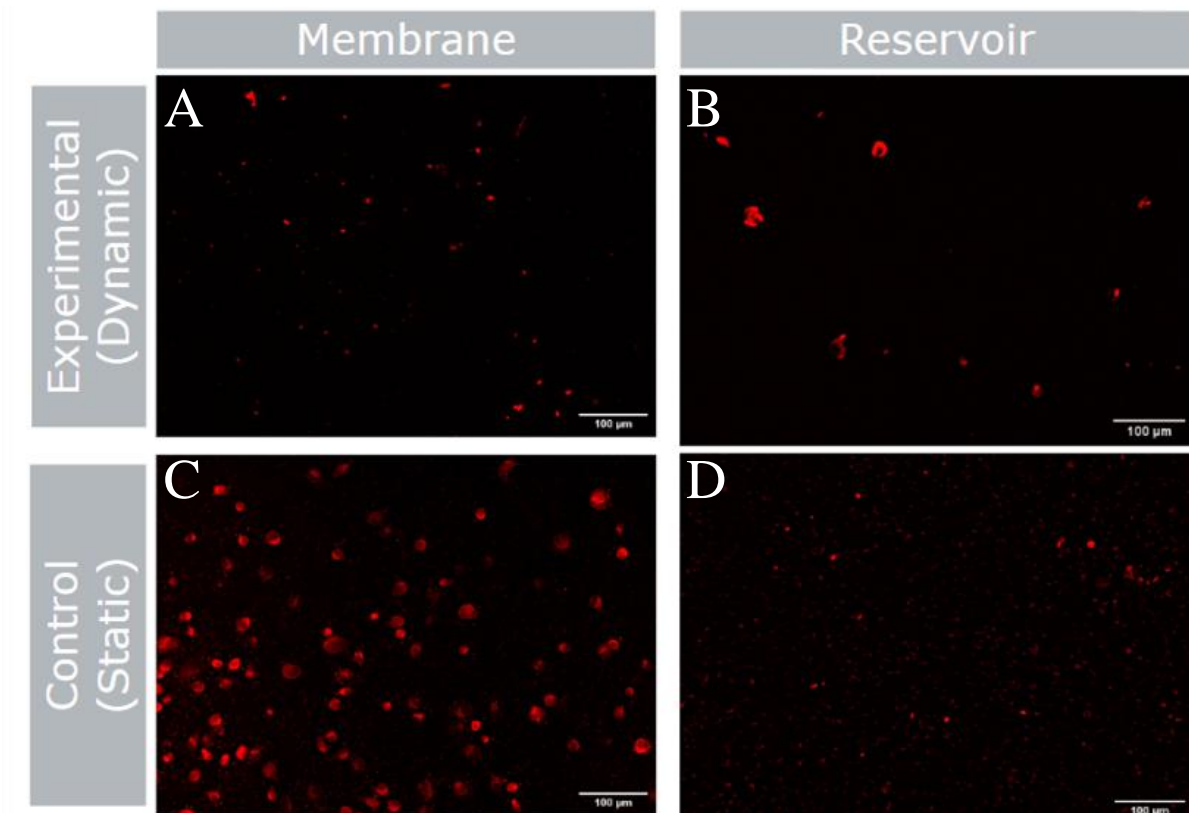
Figure 83: 20x Fluorescent Images of the Membranes and Reservoirs from Flow Test 2. (A) 20X image taken with the Keyence BZX810 microscope of the Far Red CellTrace stained MDA-MB-231 cells on the experimental membrane. (B) 20X image taken with the Keyence BZX810

microscope of the Far Red CellTrace stained MDA-MB-231 cells in the experimental reservoir. (C) 20X image taken with the Keyence BZX810 microscope of the Far Red CellTrace stained MDA-MB-231 cells on the control membrane. (D) 20X image taken with the Keyence BZX810 microscope of the Far Red CellTrace stained MDA-MB-231 cells in the control reservoir.

The results from the trials exhibited that the tests that experienced 2-hours of flow resulted in less migrated cancer cells. This can be observed by comparing Figures 83 B & D above. In Figure 83B, representing the experimental reservoir, it can be seen that there are minimal cells and that some of the cells have formed clusters. In Figure D, denotative of the control reservoir (static), there are no significant clusters and there are more individualized cells. In terms of the membrane, it can be seen that far less cells are attached to the membrane in flow conditions. As seen in Figure 83C, representing the control membrane, there are a plethora of cells attached to the membrane. On the other hand, in Figure 83A, representative of the experimental membrane, there are minimal cells observed on the membrane, significantly less than its associated control.

9.2.2 Quantifying HLMVEC and MDA-MB-231 Flow Test Data

Quantification of the data collected from both the experimental and control trials also confirmed the results above. To quantify the number of stained cancer cells on both the membrane and the reservoir, ImageJ was used. For each trial, three images of the membrane and three images of the reservoir in multiple positions were captured using the Keyence BZX810. Each image was then transferred to ImageJ and analyzed using the Cell Counter Notice tool. To access this tool, go to Plugins →Analyze →Cell Counter Notice. After that, the red stained cancer cells were counted by clicking on each of them. The information gathered from ImageJ for each image was transferred to Excel for further analysis. A table with four categories was created for each trial (Experimental Membrane, Experimental Reservoir, Control Membrane, Control Reservoir). Since three images were analyzed for each category, the average was taken and recorded for each trial. Ultimately, all the averages of all trials were transferred on a separate sheet. The mean, the standard deviation, and the standard error of the mean were calculated using Excel. This data was then transferred to GraphPad Prism software for further statistical analysis. A two-tailed student t-test was performed for both the membrane and the reservoir results (see Tables 7 and 8). Plots of the data can also be seen in Figure 84 below.

Table 7: T-Test Membrane Data. Two-tailed student t-test to compare the number of cancer cells on the membrane between the experimental and the control.

Unpaired T-Test (Membrane)	
P value	0.3196
P value summary	ns
Significantly Different (P < 0.05)?	No
One- or two-tailed P value?	Two-tailed
t, df	t=1.136, df=4

Table 8: T-Test Reservoir Data. Two-tailed student t-test to compare the number of cancer cells on the reservoir between the experimental and the control.

Unpaired T-Test (Reservoir)	
P value	0.1454
P value summary	ns
Significantly Different (P < 0.05)?	No
One- or two-tailed P value?	Two-tailed
t, df	t=1.805, df=4
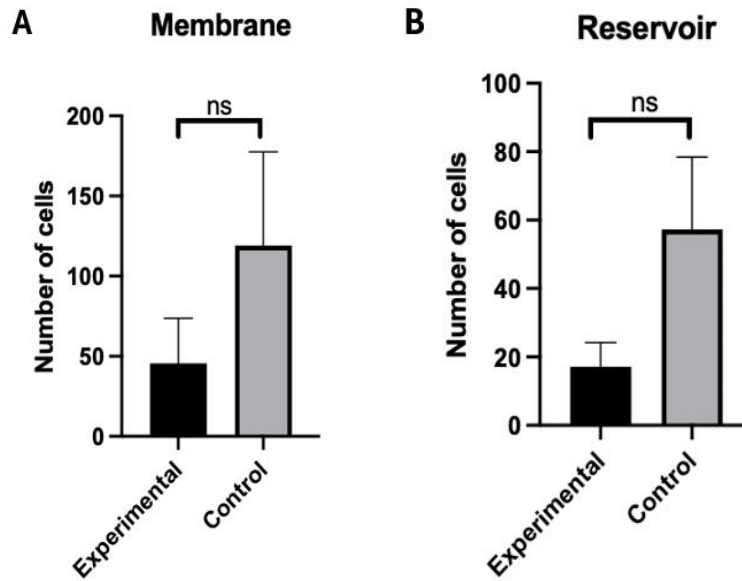
Figure 84: Plots Showing the Number of Cancer Cells in the Membrane and the Reservoir from all Experimental and Control Trials. (A) Plot comparing the number of cancer cells on the membrane between the experimental and the control. (B) Plot comparing the number of cancer cells on the reservoir between the experimental and the control.

As seen from Table 7, the P value for the membrane tests was determined to be 0.3196, which means that the results are statistically non-significant. However, the plot in Figure 84A clearly shows that there is an evident trend between the experimental and the control tests. As expected, the control exhibited a higher number of cells on the membrane compared to the experimental.

Similarly, the P value for the reservoir tests was determined to be 0.1454 (see Table 8), which also shows statistical non-significance. However, the plot in Figure 84B shows that the control also exhibited a higher number of cells on the reservoir compared to the experimental, which is what was hypothesized prior to running the experiments.

Chapter 10: Discussion

The purpose of this project was to develop an in vitro system that would allow for the investigation of the role of the endothelial glycocalyx in transendothelial migration of cancer by properly emulating the physiological environment.

To understand how shear stress exerted by flow impacts the endothelial glycocalyx, the team ran a set of experiments using only HLMVECs seeded on PETE membranes. The controls were static tests performed under no flow conditions, while the experimental were dynamic tests that involved activation of the whole flow system and were performed under flow conditions as described in section 9.1. The results from the HLMVEC only tests showed the percent coverage being slightly higher in the flow test compared to the static test. Similarly, the thickness of the glycocalyx was greater in the flow test compared to the control. Even though the results are statistically non-significant, the trends can be seen. The results from this set of tests are what the team expected to see. As mentioned in the background, when the glycocalyx is exposed to shear stress exerted by flow, it sheds and grows back thicker, and this was confirmed by both the percent coverage and the thickness of the glycocalyx being higher in the experimental trials. These results confirmed that our device is able to properly emulate the physiological conditions as seen in vivo. The fact that the results were statistically non-significant is attributed to the limited number of trials run by the team due to time constraints. If the number of trials is increased for both the control and the experimental tests, we expect to see statistical significance in the future.

To properly investigate the migration potential of cancer cells through the HLMVEC monolayer and the role of the glycocalyx in this process, the team ran another set of experiments using HLMVECs seeded on PETE membranes, as well as MDA-MB-231 metastatic cancer cells added to the respective systems as described in section 9.2. Similar to the HLMVEC only tests, the controls were run under no flow conditions, while the experimental were performed under flow. The results from HLMVEC and MDA-MB-231 tests, although statistically non-significant, showed that the control exhibited a higher number of cancer cells on both the membrane and the reservoir compared to the experimental. This was an expected outcome because the glycocalyx of the HLMVECs that were exposed to flow and shear stress (experimental) was more robust, therefore, it was harder for the cancer cells to pass through it, attach to the endothelial cells, and ultimately perform transendothelial migration. On the other hand, the control was performed under no flow conditions thus the glycocalyx was less robust due to the lack of shear stress as a result more cancer cells were able to attach to the endothelial monolayer and pass through it. Similar to the HLMVEC only tests, the results were statistically non-significant despite the trends being there. This was due to the limited number of trials run by the team. Increasing the number of trials will most likely result in statistical significance in the results, and that is what we expect to see in the future.

The fact that the trends were evident, though statistically non-significant, shows that the device was able to properly emulate the physiological processes as seen in vivo. Flow causes the glycocalyx to shed and regrow thicker, which was confirmed by our results. Shear stress helps maintain a robust glycocalyx, which further prevents cancer cells from passing through the endothelial monolayer, thus lowering their migration potential. Overall, the device allows for easy assessment of the state of the glycocalyx and migration potential of metastatic breast cancer cells as a function of shear stress. This system can be further utilized by researchers to gain useful insight when developing novel cancer treatments aimed at blocking cancer cell migration, decreasing metastasis, and ultimately lowering the fatality of cancer.

There are certain limitations with our device as well as the data quantification methods used by the team, which might have an impact on the results. From time to time, we would notice minor leaks from the device, specifically at the petri dish attachment. It was determined that the leaks resulted from inconsistencies with the rubber gasket seal and how tightly it was clamped in place. Tightening the screws enough to create a perfect seal between the rubber gasket and the reservoir was slightly challenging; sometimes it could be slightly loose and other times it would be too tight, both cases resulting in potential leakages from the reservoir attachment. Our data might have been slightly impacted because of these leakages, despite them being minor. A modification to the rubber gasket at the petri dish attachment might be helpful in the future, in order to ensure consistency and avoid any leaks that might impact data collection, especially when it comes to counting the cancer cells.

Another limitation is associated with the approach our team took when quantifying the data from both the HLMVEC only and the HLMVEC and MDA-MB-231 tests. To determine the percent coverage, thickness of the glycocalyx, as well as the number of cancer cells on the membrane and the reservoir, ImageJ was used. However, the software relies on the user quantifying the data, therefore, it is a rather subjective method of data quantification. For percent coverage, the threshold was manually set by the user as they saw fit. Similarly, to measure thickness, the user manually measured each green area they were able to see. This approach is likely to vary across users. Even though we tried our best to be as consistent as possible with the data quantification by having only one person working on it, this method of quantification leaves room for error, as it remains subjective. Lastly, quantifying the number of cells on both the membrane and the reservoir was also challenging. The user had to use their best judgment when distinguishing between stained cancer cells, membrane pores, and debris. Again, we tried to be consistent, counting only the cells that were similar in shape and/or size; however, this method is also likely to generate some error. Using a less subjective method of data quantification, such as writing a MATLAB code and using it to analyze qualitative results might be helpful for future improvements and more accurate data.

Chapter 11: Conclusions and Future Recommendations

11.1 Conclusions

The goal of our project was to develop an in-vitro device that can study the role of the endothelial glycocalyx in the transendothelial migration of cancer cells. Utilizing this device, qualitative and quantitative results displayed that there was an increase in the thickness and density of the endothelial glycocalyx when subjected to flow conditions. As a result of this increase in "robustness" of the glycocalyx, it was seen that the HLMVECs that experienced flow better prevented the metastatic breast cancer cells from interacting with endothelial cells and ultimately, penetrating the membrane within our device.

From the flow tests containing only HLMVECs, quantitative and qualitative data was obtained showing that under normal conditions, blood flow exerts shear stress on the endothelial cells. This is known because of the alteration of cell morphology and alignment in the direction of flow. This redirection likely represents a biomechanical adaptation, where HLMVECs reorient to minimize shear stress and optimize their structural integrity and functionality within a dynamic fluid environment. It also displayed that this shear stress aids in maintaining a robust glycocalyx in terms of thickness and density.

For the flow tests containing both metastatic breast cancer cells (MDA-MB-231) and HLMVECs the results displayed that the glycocalyx acts as a barrier that regulates the adherence of cells to the endothelial surface. In healthy conditions, such as with a typical flow rate, shear stress helps maintain a robust glycocalyx, which can prevent cancer cells from interacting with endothelial cells and penetrating the blood vessel wall. On the other hand, when the glycocalyx is degraded, such as when not experiencing flow, the endothelial monolayer was seen to become more permeable as many more cancer cells were observed in the reservoir. This increased permeability can facilitate the extravasation of cancer cells, a critical step where cancer cells escape from the blood circulation into surrounding tissues, establishing new metastatic sites.

Ultimately, the designed system allowed one to easily assess the state of the glycocalyx and migration potential of metastatic breast cancer cells as a function of shear stress. This system can be further explored to better determine how the endothelial glycocalyx plays a role in the transendothelial migration of cancer cells. This could advance our understanding of how cancer is able to metastasize. Utilizing this knowledge, better cancer treatments can be produced aimed at halting cancer cell migration throughout the body.

11.2 Future Recommendations

Although this project showed promising results and correct general trends, there are several recommendations that can be made to further the progress of this design. In order for the data

collected by the team to be statistically significant, more iterations of the test need to be completed. Further improvements include running more tests, adding an inflammatory cytokine to further the study of the degradation of the glycocalyx, staining both the cancer cells and lung cells simultaneously, and running the flow experiments for longer periods of time.

Due to time constraints, the team wrapped up experimentation by completing 3 tests of each of the flow tests, but further experimentation needs to be completed in order to demonstrate the effectiveness of the device. In addition to just more testing being completed, there are a few ways that the testing can be varied in order to gain additional insight related to the device. Running more flow tests with both the lung cells and cancer cells is recommended to provide further results for quantification. Additionally, flow tests should be run for longer periods of time. The team ran flow tests for two hours due to time constraints, but the flow tests should be run for a recommended six-hour period in the future. Running more flow tests should allow for statistically significant data following future quantification of the results.

The degradation of the glycocalyx in vivo is often attributed to both shear stress and inflammatory cytokines. In order to model the degradation of the glycocalyx using our device more accurately, an inflammatory cytokine should be added. One example of such an inflammatory cytokine is TNF-α (Tumor Necrosis Factor Alpha), which is readily available in the lab and would properly take on a greater role of degrading the glycocalyx. Therefore, although the shear stress of a capillary was properly modeled in the entirety of the flow system, the addition of an inflammatory cytokine would help to further emulate that of the in vivo environment.

Being able to study the interactions between the two types of cells following a flow period would allow for further investigation of the relationship between the endothelial layer of cells and how cancer cells metastasize specifically by degrading the glycocalyx. By simultaneously staining both the cancer cells and the lung cells with their respective staining methods, these interactions could be shown. In addition, the interactions with the membrane would also be viewed further using this method. The cancer cells would be live stained using Far Red CellTrace and the lung cells would be stained using DAPI and WGA. Finally, these experiments could be imaged using the confocal microscope to get orthogonal images in order to understand the state of the glycocalyx to a greater extent. Overall, with these recommendations, future teams will successfully be able to generate additional results that are statistically significant in modeling the role of the endothelial glycocalyx in transendothelial migration of cancer cells in-vitro.

References

[1] J. Fares, M. Y. Fares, H. H. Khachfe, H. A. Salhab, and Y. Fares, "Molecular principles of metastasis: a hallmark of cancer revisited," *Sig Transduct Target Ther*, vol. 5, no. 1, pp. 1–17, Mar. 2020, doi: 10.1038/s41392-020-0134-x. Available: https://www.nature.com/articles/s41392-020-0134-x. [Accessed: Apr. 22, 2024]

[2] S. Reitsma, D. W. Slaaf, H. Vink, M. A. M. J. van Zandvoort, and M. G. A. oude Egbrink, "The endothelial glycocalyx: composition, functions, and visualization," Pflugers Arch - Eur J Physiol, vol. 454, no. 3, pp. 345–359, Jun. 2007, doi: 10.1007/s00424-007-0212-8. Available: https://doi.org/10.1007/s00424-007-0212-8. [Accessed: Apr. 22, 2024]

[3] T. A. Martin, L. Ye, A. J. Sanders, J. Lane, and W. G. Jiang, "Cancer Invasion and Metastasis: Molecular and Cellular Perspective," in Madame Curie Bioscience Database [Internet], Landes Bioscience, 2013. Available: https://www.ncbi.nlm.nih.gov/books/NBK164700/. [Accessed: Apr. 22, 2024]

[4] W. Le, B. Chen, Z. Cui, Z. Liu, and D. Shi, "Detection of cancer cells based on glycolytic-regulated surface electrical charges," Biophys Rep, vol. 5, no. 1, pp. 10–18, Feb. 2019, doi: 10.1007/s41048-018-0080-0. Available: https://doi.org/10.1007/s41048-018-0080-0. [Accessed: Apr. 22, 2024]

[5] Y. Wu and B. P. Zhou, "TNF-α/NF-κB/Snail pathway in cancer cell migration and invasion," Br J Cancer, vol. 102, no. 4, pp. 639–644, Feb. 2010, doi: 10.1038/sj.bjc.6605530. Available: https://www.ncbi.nlm.nih.gov/pmc/articles/PMC2837572/. [Accessed: Apr. 22, 2024]

[6] A. T. Salminen et al., "In vitro Studies of Transendothelial Migration for Biological and Drug Discovery," Front. Med. Technol., vol. 2, Nov. 2020, doi: 10.3389/fmedt.2020.600616. Available: https://www.frontiersin.org/articles/10.3389/fmedt.2020.600616. [Accessed: Apr. 22, 2024]

[7] Y.-H. Li and C. Zhu, "A modified Boyden chamber assay for tumor cell transendothelial migration in vitro," Clin Exp Metastasis, vol. 17, no. 5, pp. 423–429, Jul. 1999, doi: 10.1023/A:1006614232388. Available: https://doi.org/10.1023/A:1006614232388. [Accessed: Apr. 22, 2024]

[8] C. Hajal, L. Ibrahim, J. C. Serrano, G. S. Offeddu, and R. D. Kamm, "The effects of luminal and trans-endothelial fluid flows on the extravasation and tissue invasion of tumor cells in a 3D in vitro microvascular platform," Biomaterials, vol. 265, p. 120470, Jan. 2021, doi: 10.1016/j.biomaterials.2020.120470

[9] S. Bersini et al., "A microfluidic 3D in vitro model for specificity of breast cancer metastasis to bone," Biomaterials, vol. 35, no. 8, pp. 2454–2461, Mar. 2014, doi: 10.1016/j.biomaterials.2013.11.050

[10] "Cancer." Available: https://www.who.int/news-room/fact-sheets/detail/cancer. [Accessed: Apr. 22, 2024]

[11] "Cancer Facts & Figures 2024." Available: https://www.cancer.org/research/cancer-facts-statistics/all-cancer-facts-figures/2024-cancer-facts-figures.html. [Accessed: Apr. 22, 2024]

[12] "What Is Cancer? Symptoms, Signs, Types & Causes," Cleveland Clinic. Available: https://my.clevelandclinic.org/health/diseases/12194-cancer. [Accessed: Apr. 22, 2024]

[13] "Cancer - Symptoms and causes," Mayo Clinic. Available: https://www.mayoclinic.org/diseases-conditions/cancer/symptoms-causes/syc-20370588. [Accessed: Apr. 22, 2024]

[14] "What Is Cancer? - NCI," Sep. 17, 2007. Available: https://www.cancer.gov/about-cancer/understanding/what-is-cancer. [Accessed: Apr. 22, 2024]

[15] "Tests and Procedures Used to Diagnose Cancer - NCI," Mar. 09, 2015. Available: https://www.cancer.gov/about-cancer/diagnosis-staging/diagnosis. [Accessed: Apr. 22, 2024]

[16] V. A. Moyer, "Screening for Lung Cancer: U.S. Preventive Services Task Force Recommendation Statement," Ann Intern Med, vol. 160, no. 5, pp. 330–338, Mar. 2014, doi: 10.7326/M13-2771. Available: http://annals.org/article.aspx?doi=10.7326/M13-2771. [Accessed: Apr. 22, 2024]

[17] "What is a biopsy and why would I need one?," Cleveland Clinic. Available: https://my.clevelandclinic.org/health/diagnostics/15458-biopsy-overview. [Accessed: Apr. 22, 2024]

[18] "Types of Cancer Treatment - NCI," Jul. 31, 2017. Available: https://www.cancer.gov/about-cancer/treatment/types. [Accessed: Apr. 22, 2024]

[19] "Cancer Treatment Options | Houston Methodist." Available: https://www.houstonmethodist.org/cancer/treatment-options/. [Accessed: Apr. 22, 2024]

[20] "Chemotherapy to Treat Cancer - NCI," Apr. 29, 2015. Available: https://www.cancer.gov/about-cancer/treatment/types/chemotherapy. [Accessed: Apr. 22, 2024]

[21] "Bone Marrow Transplantation," Aug. 08, 2021. Available: https://www.hopkinsmedicine.org/health/treatment-tests-and-therapies/bone-marrow-transplantation. [Accessed: Apr. 22, 2024]

[22] "Cost of Cancer Care." Available: https://www.cancer.org/cancer/financial-insurance-matters/managing-costs.html. [Accessed: Apr. 22, 2024]

[23] N. Iragorri, C. de Oliveira, N. Fitzgerald, and B. Essue, "The Out-of-Pocket Cost Burden of Cancer Care—A Systematic Literature Review," Curr Oncol, vol. 28, no. 2, pp. 1216–1248, Mar. 2021, doi: 10.3390/curroncol28020117. Available: https://www.ncbi.nlm.nih.gov/pmc/articles/PMC8025828/. [Accessed: Apr. 22, 2024]

[24] M. M. Alam et al., "Quality of Life (QoL) of cancer patients and its association with nutritional and performance status: A pilot study," Heliyon, vol. 6, no. 10, p. e05250, Oct. 2020, doi: 10.1016/j.heliyon.2020.e05250. Available: https://linkinghub.elsevier.com/retrieve/pii/S2405844020320934. [Accessed: Apr. 22, 2024]

[25] N. M. Novikov, S. Y. Zolotaryova, A. M. Gautreau, and E. V. Denisov, "Mutational drivers of cancer cell migration and invasion," Br J Cancer, vol. 124, no. 1, pp. 102–114, Jan. 2021, doi: 10.1038/s41416-020-01149-0. Available: https://www.nature.com/articles/s41416-020-01149-0. [Accessed: Apr. 22, 2024]

[26] L. Godwin, M. A. Tariq, and J. S. Crane, "Histology, Capillary," in StatPearls, Treasure Island (FL): StatPearls Publishing, 2024. Available: http://www.ncbi.nlm.nih.gov/books/NBK546578/. [Accessed: Apr. 22, 2024]

[27] W. D. Tucker, Y. Arora, and K. Mahajan, "Anatomy, Blood Vessels," in StatPearls, Treasure Island (FL): StatPearls Publishing, 2024. Available: http://www.ncbi.nlm.nih.gov/books/NBK470401/. [Accessed: Apr. 22, 2024]

[28] January 2023, "Introduction to the Peripheral Vascular System," Jan. 2023, Available: https://pressbooks.library.torontomu.ca/assessmentnursing2/chapter/introduction-to-the-peripheral-vascular-system/. [Accessed: Apr. 22, 2024]

[29] "Structure and Function of Blood Vessels | Anatomy and Physiology II." Available: https://courses.lumenlearning.com/suny-ap2/chapter/structure-and-function-of-blood-vessels/. [Accessed: Apr. 22, 2024]

[30] A. Krüger-Genge, A. Blocki, R.-P. Franke, and F. Jung, "Vascular Endothelial Cell Biology: An Update," Int J Mol Sci, vol. 20, no. 18, p. 4411, Sep. 2019, doi: 10.3390/ijms20184411. Available: https://www.ncbi.nlm.nih.gov/pmc/articles/PMC6769656/. [Accessed: Apr. 22, 2024]

[31] J. Jin et al., "The Structure and Function of the Glycocalyx and Its Connection With Blood-Brain Barrier," Front. Cell. Neurosci., vol. 15, Oct. 2021, doi: 10.3389/fncel.2021.739699. Available: https://www.frontiersin.org/articles/10.3389/fncel.2021.739699. [Accessed: Apr. 22, 2024]

[32] J. Qu, Y. Cheng, W. Wu, L. Yuan, and X. Liu, "Glycocalyx Impairment in Vascular Disease: Focus on Inflammation," Front Cell Dev Biol, vol. 9, p. 730621, Sep. 2021, doi: 10.3389/fcell.2021.730621. Available: https://www.ncbi.nlm.nih.gov/pmc/articles/PMC8473795/. [Accessed: Apr. 22, 2024]

[33] L. F. Sembajwe et al., "Glycocalyx–Sodium Interaction in Vascular Endothelium," Nutrients, vol. 15, no. 13, p. 2873, Jan. 2023, doi: 10.3390/nu15132873. Available: https://www.mdpi.com/2072-6643/15/13/2873. [Accessed: Apr. 22, 2024]

[34] N. Singh, D. Baby, J. P. Rajguru, P. B. Patil, S. S. Thakkannavar, and V. B. Pujari, "Inflammation and Cancer," Ann Afr Med, vol. 18, no. 3, pp. 121–126, 2019, doi: 10.4103/aam.aam_56_18. Available: https://www.ncbi.nlm.nih.gov/pmc/articles/PMC6704802/. [Accessed: Apr. 22, 2024]

[35] A. K. Shenoy and J. Lu, "Cancer cells remodel themselves and vasculature to overcome the endothelial barrier," Cancer Lett, vol. 380, no. 2, pp. 534–544, Oct. 2016, doi: 10.1016/j.canlet.2014.10.031. Available: https://www.ncbi.nlm.nih.gov/pmc/articles/PMC4417104/. [Accessed: Apr. 22, 2024]

[36] N. Pouliot, H. B. Pearson, and A. Burrows, "Investigating Metastasis Using In Vitro Platforms," in Madame Curie Bioscience Database [Internet], Landes Bioscience, 2013. Available: https://www.ncbi.nlm.nih.gov/books/NBK100379/. [Accessed: Apr. 22, 2024]

[37] "2D vs 3D cell culture | Learning Center," 2D vs 3D cell culture | Learning Center | UPM Biomedicals. Available: https://www.upmbiomedicals.com/resource-center/learning-center/what-is-3d-cell-culture/2d-versus-3d-cell-culture/. [Accessed: Apr. 22, 2024]

[38] M. Kapałczyńska et al., "2D and 3D cell cultures – a comparison of different types of cancer cell cultures," Arch Med Sci, vol. 14, no. 4, pp. 910–919, Jun. 2018, doi: 10.5114/aoms.2016.63743. Available: https://www.ncbi.nlm.nih.gov/pmc/articles/PMC6040128/. [Accessed: Apr. 22, 2024]

[39] C.-C. Liang, A. Y. Park, and J.-L. Guan, "In vitro scratch assay: a convenient and inexpensive method for analysis of cell migration in vitro," Nat Protoc, vol. 2, no. 2, pp. 329–333, 2007, doi: 10.1038/nprot.2007.30

[40] "Transwell Assay Protocol | Creative Bioarray." Available: https://www.creative-bioarray.com/transwell-migration-and-invasion-assays.htm. [Accessed: Apr. 22, 2024]

[41] M. E. Fallon, R. Mathews, and M. T. Hinds, "In Vitro Flow Chamber Design for the Study of Endothelial Cell (Patho)Physiology," J Biomech Eng, vol. 144, no. 2, p. 020801, Feb. 2022, doi: 10.1115/1.4051765. Available: https://www.ncbi.nlm.nih.gov/pmc/articles/PMC8628846/. [Accessed: Apr. 22, 2024]

[42] S. Basehore, J. Garcia, and A. M. Clyne, "Chapter 17 - Vascular mechanobiology and metabolism," in The Science, Etiology and Mechanobiology of Diabetes and its Complications, A. Gefen, Ed., Academic Press, 2021, pp. 291–312. doi: 10.1016/B978-0-12-821070-3.00008-8. Available: https://www.sciencedirect.com/science/article/pii/B9780128210703000088. [Accessed: Apr. 22, 2024]

[43] J. Sun et al., "Anti-inflammatory and Anti-thrombotic Efficacy of Targeted Ultrasound Microbubbles on LPS-induced HUVEC Cells," Anticancer Research, vol. 41, no. 10, pp. 4761–4769, Oct. 2021, doi: 10.21873/anticanres.15291. Available: https://ar.iiarjournals.org/content/41/10/4761. [Accessed: Apr. 22, 2024]

[44] F. Bragheri, R. Martínez Vázquez, and R. Osellame, "Chapter 12.3 - Microfluidics," in Three-Dimensional Microfabrication Using Two-Photon Polymerization (Second Edition), T. Baldacchini, Ed., in Micro and Nano Technologies. William Andrew Publishing, 2020, pp. 493–526. doi: 10.1016/B978-0-12-817827-0.00057-6. Available: https://www.sciencedirect.com/science/article/pii/B9780128178270000576. [Accessed: Apr. 22, 2024]

[45] R. Zeineldin, "7 - Nanotechnology for cancer screening and diagnosis," in Biomaterials for Cancer Therapeutics, K. Park, Ed., Woodhead Publishing, 2013, pp. 137–164. doi: 10.1533/9780857096760.3.137. Available: https://www.sciencedirect.com/science/article/pii/B9780857096647500070. [Accessed: Apr. 22, 2024]

[46] LCDub, "Determining units in a cone and plate flow system," Physics Stack Exchange, Aug. 24, 2016. Available: https://physics.stackexchange.com/q/276099. [Accessed: Apr. 22, 2024]

[47] M. Franzoni, I. Cattaneo, B. Ene-Iordache, A. Oldani, P. Righettini, and A. Remuzzi, "Design of a cone-and-plate device for controlled realistic shear stress stimulation on endothelial cell monolayers," Cytotechnology, vol. 68, no. 5, pp. 1885–1896, Oct. 2016, doi: 10.1007/s10616-015-9941-2. Available: https://www.ncbi.nlm.nih.gov/pmc/articles/PMC5023562/. [Accessed: Apr. 22, 2024]

[48] A. R. Aref et al., "3D microfluidic ex vivo culture of organotypic tumor spheroids to model immune checkpoint blockade," Lab Chip, vol. 18, no. 20, pp. 3129–3143, Oct. 2018, doi: 10.1039/c8lc00322j

[49] S. A. Mensah et al., "Flow-regulated endothelial glycocalyx determines metastatic cancer cell activity," FASEB J, vol. 34, no. 5, pp. 6166–6184, May 2020, doi: 10.1096/fj.201901920R

[50] E. M. J. Siren et al., "An improved in vitro model for studying the structural and functional properties of the endothelial glycocalyx in arteries, capillaries and veins," FASEB J, vol. 35, no. 6, p. e21643, Jun. 2021, doi: 10.1096/fj.201802376RRRR

[51] Z. Chen, Y. Song, Z. Hu, S. Zhang, and Y. Chen, "An estimation of mechanical stress on alveolar walls during repetitive alveolar reopening and closure," Journal of Applied Physiology, vol. 119, no. 3, pp. 190–201, Aug. 2015, doi: 10.1152/japplphysiol.00112.2015. Available: https://www.physiology.org/doi/10.1152/japplphysiol.00112.2015. [Accessed: Apr. 22, 2024]

[52] "Keyence BZ-X810," Cellular and Molecular Imaging Facility. Available: https://research.ncsu.edu/cmif/equipment-list/workstations/keyence-bz-x810/. [Accessed: Apr. 22, 2024]

[53] C. M. Leung et al., "A guide to the organ-on-a-chip," Nat Rev Methods Primers, vol. 2, no. 1, pp. 1–29, May 2022, doi: 10.1038/s43586-022-00118-6. Available: https://www.nature.com/articles/s43586-022-00118-6. [Accessed: Apr. 22, 2024]

[54] R. C. Lagoy and D. R. Albrecht, "Microfluidic Devices for Behavioral Analysis, Microscopy, and Neuronal Imaging in Caenorhabditis elegans," Methods Mol Biol, vol. 1327, pp. 159–179, 2015, doi: 10.1007/978-1-4939-2842-2_12

[55] A. Helmenstine, "Capillary Action - What It Is and How It Works," Science Notes and Projects, Feb. 27, 2022. Available: https://sciencenotes.org/capillary-action-what-it-is-and-how-it-works/. [Accessed: Apr. 22, 2024]

[56] S. Chung, R. Sudo, V. Vickerman, I. K. Zervantonakis, and R. D. Kamm, "Microfluidic Platforms for Studies of Angiogenesis, Cell Migration, and Cell–Cell Interactions," Ann Biomed Eng, vol. 38, no. 3, pp. 1164–1177, Mar. 2010, doi: 10.1007/s10439-010-9899-3. Available: https://doi.org/10.1007/s10439-010-9899-3. [Accessed: Apr. 22, 2024]

[57] C. G. Conant, M. A. Schwartz, and C. Ionescu-Zanetti, "Well Plate–Coupled Microfluidic Devices Designed for Facile Image-Based Cell Adhesion and Transmigration Assays," SLAS

Discovery, vol. 15, no. 1, pp. 102–106, Jan. 2010, doi: 10.1177/1087057109353789. Available: https://linkinghub.elsevier.com/retrieve/pii/S2472555222078716. [Accessed: Apr. 22, 2024]

[58] R. C. Lagoy and D. R. Albrecht, "Automated fluid delivery from multiwell plates to microfluidic devices for high-throughput experiments and microscopy," Sci Rep, vol. 8, no. 1, p. 6217, Apr. 2018, doi: 10.1038/s41598-018-24504-x. Available: https://www.nature.com/articles/s41598-018-24504-x. [Accessed: Apr. 22, 2024]

[59] C. Lam, "BioFlux Plates," Jan. 17, 2024. Available: https://cellmicrosystems.com/bioflux/bioflux-plates. [Accessed: Apr. 22, 2024]

[60] K. P. Ivanov, M. K. Kalinina, and Yu. I. Levkovich, "Blood flow velocity in capillaries of brain and muscles and its physiological significance," Microvascular Research, vol. 22, no. 2, pp. 143–155, Sep. 1981, doi: 10.1016/0026-2862(81)90084-4. Available: https://www.sciencedirect.com/science/article/pii/0026286281900844. [Accessed: Apr. 22, 2024]

[61] B. J. Ballermann, A. Dardik, E. Eng, and A. Liu, "Shear stress and the endothelium," Kidney International, vol. 54, pp. S100–S108, Sep. 1998, doi: 10.1046/j.1523-1755.1998.06720.x. Available: https://www.sciencedirect.com/science/article/pii/S0085253815308887. [Accessed: Apr. 22, 2024]

[62] "PLA | Prusa Knowledge Base." Available: https://help.prusa3d.com/article/pla_2062. [Accessed: Apr. 22, 2024]

[63] "c,34572,celltrace,far,proliferation,cytometryes." Available: https://www.fishersci.ca/shop/products/celltrace-far-red-cell-proliferation-kit-flow-cytometry-2/c34564. [Accessed: Apr. 22, 2024]

[64] B. Emde, A. Heinen, A. Gödecke, and K. Bottermann, "Wheat Germ Agglutinin Staining as a Suitable Method for Detection and Quantification of Fibrosis in Cardiac Tissue after Myocardial Infarction," Eur J Histochem, vol. 58, no. 4, p. 2448, Dec. 2014, doi: 10.4081/ejh.2014.2448. Available: https://www.ncbi.nlm.nih.gov/pmc/articles/PMC4289847/. [Accessed: Apr. 22, 2024]

[65] B. I. Tarnowski, F. G. Spinale, and J. H. Nicholson, "DAPI as a useful stain for nuclear quantitation," Biotech Histochem, vol. 66, no. 6, pp. 297–302, 1991.

[66] H. H. Chung, M. Mireles, B. J. Kwarta, and T. R. Gaborski, "Use of Porous membranes in tissue barrier and co-culture models," Lab Chip, vol. 18, no. 12, pp. 1671–1689, Jun. 2018, doi: 10.1039/c7lc01248a. Available: https://www.ncbi.nlm.nih.gov/pmc/articles/PMC5997570/. [Accessed: Apr. 22, 2024]

[67] K. Webb, V. Hlady, and P. A. Tresco, "Relative importance of surface wettability and charged functional groups on NIH 3T3 fibroblast attachment, spreading, and cytoskeletal organization," J Biomed Mater Res, vol. 41, no. 3, pp. 422–430, Sep. 1998, Available: https://www.ncbi.nlm.nih.gov/pmc/articles/PMC2632339/. [Accessed: Apr. 22, 2024]

[68] "Masterflex® L/S® Precision Pump Tubing, C-Flex®, L/S 17; 25 ft," VWR. Available: https://us.vwr.com/store/item/NA5143552/masterflex-l-s-precision-pump-tubing-c-flex-avantor. [Accessed: Apr. 22, 2024]

[69] "Amazon.com: ANPTGHT Plastic Hose Barb Fitting, 1/2" Barb X 1/2" NPT Male Thread Adapter Connector Pipe Fittings for Fuel Gas Liquid Air (Pack of 5) : Industrial & Scientific." Available: https://www.amazon.com/ANPTGHT-Plastic-Fitting-Connector-Fittings/dp/B092PF346S/ref=sr_1_1?keywords=1%2F8%22%2BBarb%2BX%2B1%2F4%22%2BNPT%2BMale%2BThread%2BAdapter%2BConnector%2BPipe%2BFittings&qid=170749930 1&sr=8-1&th=1. [Accessed: Apr. 22, 2024]

[70] Admin, "Benefits of Peristaltic over Centrifugal pumps | Global Pumps." Available: https://www.globalpumps.com.au/blog/benefits-of-peristaltic-over-centrifugal-pumps. [Accessed: Apr. 22, 2024]

[71] "AVANTOR MASTERFLEX (VWR LLC) Masterflex L/S Digital Drive with Easy-Load II Pump Head for High-Performance Tubing, 600 rpm; 115/230 VAC." Available: https://www.fishersci.com/shop/products/masterflex-l-s-digital-pump/NC0623391. [Accessed: Apr. 22, 2024]

[72] "BD Plastipak Luer Lock Syringes," Darwin Microfluidics. Available: https://darwin-microfluidics.com/products/bd-plastipak-luer-syringes. [Accessed: Apr. 22, 2024]

[73] J. J. Paszkowiak and A. Dardik, "Arterial wall shear stress: observations from the bench to the bedside," Vasc Endovascular Surg, vol. 37, no. 1, pp. 47–57, 2003, doi: 10.1177/153857440303700107

[74] "Continuity for Fluids." Available: https://www.aplusphysics.com/courses/honors/fluids/continuity.html#:~:text=When%20fluids% 20move%20through%20a,conservation%20of%20mass%20for%20fluids. [Accessed: Apr. 22, 2024]

[75] A. B. Schwartz et al., "Elucidating the Biomechanics of Leukocyte Transendothelial Migration by Quantitative Imaging," Front. Cell Dev. Biol., vol. 9, Mar. 2021, doi: 10.3389/fcell.2021.635263. Available: https://www.frontiersin.org/articles/10.3389/fcell.2021.635263. [Accessed: Apr. 22, 2024]

[76] "World Cancer Day: closing the care gap." Available: https://www.who.int/news/item/03-02-2022-world-cancer-day-closing-the-care-gap. [Accessed: Apr. 22, 2024]

[77] J. A. DiMasi, H. G. Grabowski, and R. W. Hansen, "Innovation in the pharmaceutical industry: New estimates of R&D costs," J Health Econ, vol. 47, pp. 20–33, May 2016, doi: 10.1016/j.jhealeco.2016.01.012

[78] M. Hay, D. W. Thomas, J. L. Craighead, C. Economides, and J. Rosenthal, "Clinical development success rates for investigational drugs," Nat Biotechnol, vol. 32, no. 1, pp. 40–51, Jan. 2014, doi: 10.1038/nbt.2786

Appendix I: Fluid Flow Calculations

Fluid Flow Calculations for Initial Flow Rate

<u>Cross-sectional area of tubing (A)</u>

Knowns: Tubing I.D = 6.40 mm, Tubing Shape = Cylindrical

$$Cross\ sectional\ A\ of\ tubing\ =\ \pi r^2 = \pi(3.20mm)^2 = 32.17mm^2$$

<u>Velocity flow through size 17 tubing to replicate shear forces seen in vivo</u>

Knowns: A = 32.17 mm^2, Viscosity = 1x10^-9 MPa s, Height of gasket = 2 mm, 5x10^-7 MPa = typical shear stress at the wall in a capillary

$\tau = \frac{6\gamma Q}{wh^2}$: Rearrange to solve for V (Q = V * A)

$$V\ =\ \frac{\tau wh^2}{6\gamma A} = \frac{(5x10^{-7}MPa)(13.0124\ mm)(2mm)^2}{(6)(1x10^{-9}MPa \cdot s)(32.17mm^2)} =\ 134.8\ mm/s$$

<u>Example of scaling up</u>

Blood flow rate in capillaries in vivo = 0.75 mm/s

Factor that we scaled the blood flow up:

$$\underline{Velocity\ Calculated/velocity\ blood\ flow\ in\ vivo\ =\ scale\ up\ factor}$$
$$\underline{134.8/0.75\ =\ 180}$$

<u>Volumetric flow rate</u>

$$Q\ =\ V \cdot A = 134.8mm/s \cdot 32.17mm^2 = 4337.47mm^3/s = 260.6\ mL/min$$

Calculations for Cancer Cell Flow Rate

<u>Cross-sectional area of tubing (A)</u>

Knowns: Tubing I.D = 6.40 mm, Tubing Shape = Cylindrical

$$Cross\ sectional\ A\ of\ tubing\ =\ \pi r^2 = \pi(3.20mm)^2 = 32.17mm^2$$

<u>Velocity flow through size 17 tubing to replicate shear forces seen in vivo</u>

Knowns: A = 32.17 mm^2, Viscosity = 1x10^-9 MPa s, Height of gasket = 2 mm, 1.0x10^-7 MPa = shear stress

$\tau = \frac{6\gamma Q}{wh^2}$: Rearrange to solve for V (Q = V * A)

$V = \frac{\tau wh^2}{6\gamma A} = \frac{(1.0x10^{-7}MPa)(13.0124\,mm)(2mm)^2}{(6)(1x10^{-9}MPa \cdot s)(32.17mm^2)} = 26.966\,mm/s$

Scaling Up

Blood flow rate in capillaries in vivo = 0.75 mm/s

Factor that we scaled the blood flow up:

$$Velocity\ Calculated/velocity\ blood\ flow\ in\ vivo\ =\ scale\ up\ factor$$
$$26.966/0.75\ =\ 35.95$$

Volumetric flow rate

$$Q\ =\ V \cdot A = 26.966mm/s \cdot 32.17mm^2 = 867.50mm^3/s = 52.05mL/min$$

Appendix II: Breast Cancer Cell Culture Protocol

1. Grab a 50 mL tube of trypsin, and modified DMEM media (protocols to make in Appendix VII) from the fridge and place it in a water bath for around 5 minutes.
2. Prepare the hood by properly cleaning it (spray with IPA and let dry).
3. Remove the confluent flask from the incubator and bring it inside the hood (spray with IPA before bringing it into the biosafety cabinet).
4. Carefully aspirate the medium from the flask (tip flask).
5. Do a quick wash with trypsin.
   a. T-25: 1 mL
   b. T-75: 2 mL
6. Carefully aspirate the trypsin from the flask (tip flask)
7. Add trypsin to the flask.
   a. T-25: 1 mL
   b. T-75: 3 mL
8. Close the flask and let the cells detach for about 5-15 minutes in the incubator.
9. Observe the cells in the microscope and when the cells start to detach, gently tap the sides of the flask to loosen the remaining cells.
10. Add media to the flask, 2x-3x the amount of trypsin added.
11. Pipette up and down to mix the solution thoroughly.
12. With a pipette transfer the solution to a centrifugation tube.
13. Count cells using 30 μL in the hemocytometer (15 μL on each side).
14. Spin down the cells for 5 minutes at 200 rcf.
15. Aspirate down to pellet and resuspend in media.
    a. T-25: 4 mL
    b. T-75: 6 mL
16. Plate cells in the flask.
    a. T-25: at least 5mL solution in the entire flask
    b. T-75: at least 10 mL solution in the entire flask

Appendix III: HLMVEC Culture Protocol

1. Grab a 50 mL tube of trypsin, and HLMVEC media from the fridge and place it in a water bath for around 5 minutes.
2. Prepare the hood by properly cleaning it (spray with IPA and let dry).
3. Remove the confluent flask from the incubator and bring it inside the hood (spray with IPA before bringing it in).
4. Carefully aspirate the medium from the flask (tip flask).
5. Do a quick wash with trypsin.
   a. T-25: 1 mL
   b. T-75: 2 mL
6. Carefully aspirate the trypsin from the flask (tip flask).
7. Add trypsin to the flask.
   a. T-25: 1 mL
   b. T-75: 3 mL
8. Close the flask and let the cells detach for about 5 minutes (no incubator needed).
9. Observe the cells in the microscope and when the cells start to detach, gently tap the sides of the flask to loosen the remaining cells.
10. Add media to the flask, 2x the amount of trypsin added.
11. Pipette up and down to mix the solution thoroughly.
12. With a pipette transfer the solution to a centrifugation tube
13. Count cells using 30 μL in the hemocytometer (15 μL on each side).
14. Spin down the cells for 5 minutes at 200 rcf.
15. Aspirate down to pellet and resuspend in media.
    a. T-25: 4 mL
    b. T-75: 6 mL
16. Plate cells in the flask.
    a. T-25: at least 5mL solution in the entire flask
    b. T-75: at least 10 mL solution in the entire flask

Appendix IV: CellTrace Protocol

1. Prepare CellTrace™ stock solution immediately before use by adding the appropriate volume of DMSO (Component B) to one vial of CellTrace™ reagent (Component A) and mixing well (see Table 2, page 3).
   a. 20µL of DMSO with Cell Trace reagent
2. Add 1 µL of CellTrace™ stock solution in DMSO (prepared in Step 1.1) to each mL of cell suspension in PBS for a final working solution (see Table 3, page 3, for concentration).
   a. Take 1 microliter (µL) of the 1 millimolar solution. (20 µl)
   b. Add it to 999 microliters (µL) of PBS (20 mL)

   (can adjust this based on mL of solution) i.e. 5 µL and 995 µL for 1 mL solution that's 5µM)
3. Spin down cells up to 1 million cells and pour off supernatant (count before spinning and withdraw media that contains 1 million cells total).
4. Resuspend cells in 1 mL of CellTrace Far Red staining solution.
5. Incubate cells for 20 minutes in a 37°C water bath, protected from light.
6. Add five times (5*X) the original staining volume of culture medium (containing at least 1% protein) to the cells and incubate for 5 minutes. This step removes any free dye remaining in the solution.
7. Pellet the cells by centrifugation and resuspend them in 1mL of fresh pre-warmed complete MDA-MB-231 culture medium.
8. Incubate the cells for at least 10 minutes before analysis to allow the CellTrace™ reagent to undergo acetate hydrolysis.
9. Proceed with cell stimulation, incubation, or analysis.

Appendix V: Cell Freezing Protocols

HLMVEC

1. Put trypsin, FBS, and HLMVEC media into the water bath.
2. Prepare the hood by spraying it with 70% ethanol and wiping it with Kim wipes.
3. Once trypsin, FBS, and HLMVEC media are warmed/thawed spray with 70% ethanol before bringing in the hood.
4. Grab cells from the incubator and spray them with 70% ethanol before bringing them into the hood.
5. Follow the HLMVEC Cell passaging protocol.
6. Create freezing media.
    a. Freezing media = 10% DMSO + 50% FBS + 40% HLMVEC media
        i. The total should be 500 μL (1 million cells/mL)
7. Label cryovial: HLMVEC, Passage #, Date, and Initials.
8. Place the cryovial in the -20ºC freezer.
9. The following day, place the cryovial in -80ºC freezer.
10. The day after, place the cryovial in the liquid nitrogen tank.

MDA-MB-231

1. Put trypsin, FBS, and DMEM media into the water bath.
2. Prepare the hood by spraying it with 70% ethanol and wiping it with Kim wipes.
3. Once trypsin, FBS, and DMEM media are warmed/thawed spray with 70% ethanol before bringing in the hood.
4. Grab cells from the incubator and spray them with 70% ethanol before bringing them into the hood.
5. Follow the MDA-MB-231 Cell passaging protocol.
6. Create freezing media.
    a. Freezing media = 10% DMSO +20% FBS + 70% DMEM media
        i. Total should be 1 mL (1 million cells/mL)
7. Label cryovial:MDA-MB-231, Passage #, Date, and Initials
8. Place the cryovial in the -20ºC freezer.
9. The following day, place the cryovial in -80ºC freezer.
10. The day after, place the cryovial in the liquid nitrogen tank.

Appendix VI: Cell Thawing Protocols

HLMVEC

1. Thaw the vial by gentle agitation in a 37°C water bath. To reduce the possibility of contamination, keep the O-ring and cap out of the water. Thawing should be rapid (approximately 2 minutes).

2. Remove the vial from the water bath as soon as the contents are thawed and decontaminate by dipping in or spraying with 70% ethanol. All of the operations from this point on should be carried out under strict aseptic conditions.

3. Transfer vial contents into a culture flask (T75 or T25) and mix with 10 mL HLMVEC media for a T75 and 5 mL HLMVEC media for a T25 flask.

4. Incubate the culture at 37°C in a suitable incubator.

MDA-MB-231

1. Thaw the vial by gentle agitation in a 37°C water bath. To reduce the possibility of contamination, keep the O-ring and cap out of the water. Thawing should be rapid (approximately 2 minutes).

2. Remove the vial from the water bath as soon as the contents are thawed and decontaminate by dipping in or spraying with 70% ethanol. All of the operations from this point on should be carried out under strict aseptic conditions.

3. Transfer the vial contents to a centrifuge tube containing 9.0 mL complete culture medium and spin at approximately 120x g (rcf) for 5 to 7 minutes.

4. Resuspend the cell pellet with the recommended complete medium (see the specific batch information for the culture recommended dilution ratio) and dispense into a new culture flask (resuspended in 3mL for T25 and 6mL for T75).

5. Incubate the culture at 37°C in a suitable incubator.

Appendix VII: MDA-MB-231 Media Preparation

1. Attain DMEM media, FBS (frozen), and 100x pen strep. Thaw/warm up in the water bath.
2. Using a sterile pipette, measure 89 mL of liquid DMEM and transfer it to a sterile container.
3. Using a sterile pipette, add 10 mL of FBS to the 89 mL of DMEM. Mix gently to combine.
4. Add 1 mL of 100x Penicillin-Streptomycin solution to the DMEM with FBS. Mix gently to ensure uniform distribution (1% by volume, so 1mL for 100mL).
5. You can store the media in the fridge until needed.

Appendix VIII: Flow Rate Test Protocols

1. Construct the flow system according to Appendix X (see below).

2. Attain another 500 mL graduated cylinder and a beaker of 475 mL of water.

3. On the peristaltic pump go to the settings and select "calibration." Select the desired tubing size and flow rate (size 17 and 260.25 mL/min).

4. Prime the system with water by pouring water into the 1000 mL graduated cylinder reservoir until it is about half full (500 mL).

5. Press the double triangle button on the pump to fill the tubing and eliminate any air bubbles in the system.

6. Place the collection reservoir (other 500 mL graduated cylinder) next to the flow setup.

7. Transfer the outlet tubing from the initial reservoir to the collection reservoir.

8. Attain a stopwatch.

9. Press the start button on the pump and start the timer at the same time.

10. Run the system for 1-2 minutes.

11. Stop the pump and record the volume of water in the collection reservoir as well as the time that the experiment was run.

12. Divide the volume by the duration to achieve the flow rate through the flow system in mL/min.

13. Run the test 3x and average the data.

Appendix IX: Full System Test

<u>HLMVEC ONLY:</u>

1. Sterilize the device and components according to the following table.

Autoclave @121℃ for 30 minutes	Spray with 70% IPA and UV Treat for 15 min
Tubing Gaskets x2 Syringe Rubber Stopper Membrane	Acrylic Body Reservoir Holder 35mm Petri Dish 60mm Petri Dish Rubber Seal

2. Transport the two membranes and 60 mm Petri dishes to the biosafety cabinet.
3. Place 20 μg/ml fibronectin, 0.25% EDTA-trypsin, and HLMVEC media in a water bath to thaw.
4. Bring reagents to the biosafety cabinet when finished warming in a water bath.
5. Using sterile forceps place the membranes in the two 60 mm petri dishes.
6. Using a micropipette transfer ~600 μL fibronectin directly on top of each membrane (try only to cover the membrane).
7. Let fibronectin sit at room temperature for an hour.
8. Carefully aspirate the fibronectin by tilting the plates and aspirating it from the bottom of the dish (do not directly aspirate on top of the membrane).
9. Culture HLMVECs cells and dilute them into 600k cells/ mL (300k / 500 μL).
10. Place 500 μL of cell solution onto each membrane (try to only place on top of the membrane).
11. Place in the incubator (37C at 5% CO2) and let the cells attach for 1 hour.
12. After an hour, place 5 mL of media into each plate (place this on the side of the plate to prevent pushing cells off of the membrane).
13. Place in the incubator for 1 day to become fully confluent and finish attaching.
14. After 1 day, check the cells under the microscope to confirm confluency on the membrane.
15. Bring one petri dish containing the membrane to the biosafety cabinet and aspirate the media. The other membrane can be placed directly in the incubator to be a control.
16. Using forceps transfer to the membrane in between the gaskets of the device.

17. Set up the flow system in the hood according to the Flow System Setup Protocol (see Appendix X.

18. Transport the entire setup from the biosafety cabinet to the incubator (37°C, 5% CO2), feed the tubing of the flow system through the back of the incubator to the peristaltic pump, feed the tubing through the pump, and use a paper towel to fill the remainder of the hole in the back of the incubator.

19. Attach the peristaltic pump and set the flow rate to 270.3 ml/min.

20. Press the white button with two black arrows on the peristaltic pump to remove any air trapped in the system, then press the start button.

    NOTE: Nothing else was kept in the incubator and it was not opened at any point during a flow trial to limit the opportunity for contaminants to enter and to minimize any disturbances that could affect the flow.

21. Turn on the pump and let it run for 2 hours.

22. Follow steps 23-27 if you are running multiple experiments in a row. If not, follow the steps below.

23. Remove the tubing from the hose barbs on the ends of the device and clamp them with binder clips.

24. Remove the device from the incubator and disassemble it.

25. Remove the membrane from the system and add a new confluently seeded membrane.

26. Transfer the device back to the hood and place the tubing on the ends of the hose barbs.

27. Add more media to the reservoir to account for the lost media.

28. Following the two hours, remove the flow system from the incubator and bring it to the biosafety cabinet.

29. Remove the membrane from the system using forceps and place it in a 60 mm petri dish.

30. Aspirate all media from the system and run sterile PBS through the system.

31. Take the control membrane out of the incubator and place it in the biosafety cabinet.

32. Aspirate all media from the control (make sure the petri dish is labeled control).

33. Fix and stain the cells following these protocols (see Appendix XII below).

34. Bring to the Keyence microscope and Image.

<u>HLMVEC + MDA-MB-231</u>

1. Sterilize the device and components according to the following table.

Autoclave @121°C for 30 minutes	Spray with 70% IPA and UV Treat for 15 min
Tubing Gaskets x2 Syringe Rubber Stopper Membrane	Acrylic Body 35mm Petri Dish 60mm Petri Dish Rubber Seal

2. Transport the membranes and 60 mm petri dishes, and DIY migration assay setups to the biosafety cabinet.

3. Place 20 μg/ml fibronectin, 0.25% EDTA-trypsin, and HLMVEC media in a water bath to thaw/warm up.

4. Bring reagents to the biosafety cabinet when finished warming in the water bath.

5. Using sterile forceps place the membranes in the 60 mm petri dishes.

6. Using a micropipette transfer ~600 μL fibronectin directly on top of each membrane (try only to cover the membrane).

7. Let fibronectin sit at room temperature for an hour.

8. Carefully aspirate the fibronectin by tilting the plates and aspirating it from the bottom of the dish (do not directly aspirate on top of the membrane).

9. Culture HLMVECs cells and dilute them into 600k cells/ mL (300k / 500 μL).

10. Place 500 μL of cell solution onto each membrane (try to only place on top of the membrane).

11. Place in the incubator (37C at 5% CO2) and let the cells attach for 1 hour.

12. After an hour, place 5 mL of media into each petri dish (place this on the side of the plate to prevent pushing cells off of the membrane) (can put more than 5mL for DIY migration assay).

13. Place in an incubator for 1 day to become fully confluent and finish attaching.

14. After 1 day, check the cells under the microscope to confirm confluency on the membrane.

15. Stain cancer cells using CellTrace.

16. Before spinning down count how many cells total (use the equation from page 105 to calculate how many mL need to be withdrawn).

17. Remove X mL of media to get multiple aliquots containing 1 million cells each.

18. Add media until at least there is 4 mL in each tube (if not already).

19. Spin down.

20. Aspirate media and resuspend each tube in 1 mL of Far Red CellTrace staining solution (aliquoted in the freezer).

21. Incubate cells for 20 minutes in a 37°C water bath, protected from light.

22. Add five times (5*X = 5mL) the original staining volume of culture medium (containing at least 1% protein) to the cells and incubate for 5 minutes. This step removes any free dye remaining in the solution.

23. Pellet the cells by centrifugation and resuspend them in a fresh pre-warmed complete MDA-MB-231 culture medium.

24. Incubate the cells for at least 10 minutes before analysis to allow the CellTrace™ reagent to undergo acetate hydrolysis.

25. Proceed with cell stimulation, incubation, or analysis.

26. Bring one petri dish containing the membrane to the biosafety cabinet and aspirate the media. The migration assay can be left in the incubator to be a control.

27. Using forceps transfer to the membrane in between the gaskets of the device.

28. Set up the flow system in the hood according to the Flow System Setup Protocol (see Appendix X below).

29. Transport the entire setup from the biosafety cabinet to the incubator (37°C, 5% CO2), feed the tubing of the flow system through the back of the incubator to the peristaltic pump, feed the tubing through the pump, and use a paper towel to fill the remainder of the hole in the back of the incubator.

30. Attach the peristaltic pump and set the flow rate to 270.3 ml/min.

31. Press the white button with two black arrows on the peristaltic pump to remove any air trapped in the system, then press the start button.

32. NOTE: Nothing else was kept in the incubator and it was not opened at any point during a flow trial to limit the opportunity for contaminants to enter and to minimize any disturbances that could affect the flow.

33. After 1 hour of flow at 270.3 ml/min stop the flow system using the pause button on the pump. Change the flow rate to 62.05 ml/min but do not start the flow.

34. Add 1 million cancer cells into the syringe reservoir.

35. Start the flow for another 1 hour at the flow 62.05 ml/min flow rate.

36. Stop the flow.

37. Bring to the Keyence microscope and Image.

Appendix X: Flow System Setup Protocol

1. Sterilize the device and components according to the following table.

Autoclave @121°C for 30 minutes	Spray with 70% IPA and UV Treat for 15 min
Tubing Gaskets x2 Syringe Rubber Stopper Membrane	Acrylic Body Reservoir Holder 35mm Petri Dish 60mm Petri Dish Rubber Seal Screws and Washers

2. Bottom Petri Dish Assembly
   a. Parts Needed: bottom of the device, 35 mm petri dish, reservoir holder, rubber seal, 2x M3-0.5-16 screws, 2x M3-0.5-20 screws, 6 washers.
   b. Flip over the bottom of the device and place the rubber seal inside the circular area. Ensure the seal is not buckled in any spot or has a wave. Use the tip of your finger to push the entire seal on the device.
      i. *Note: you may have to take the seal out and reposition it so that it fits- they are not cut perfectly and as a result do not fit perfectly.
   c. Put the 35 mm petri dish into the circular compartment below the seal. Due to the outside seal that is glued to the device, the petri dish should stay in place and not fall out of this slot.
   d. Take the reservoir holder and with the device still upside down, align the screw holes on the reservoir holder with the screw holes on the bottom of the device.
   e. Place 2 M3-0.5-16 screws each with one washer onto the device in the holes above the flow area closest to the middle of the device.
   f. Place 2 M3-0.5-20 screws, each one with two washers onto the device in the holes closest to the outside of the bottom of the device.
   g. Fasten the screws onto the device using even pressure to ensure that the rubber seal does not buckle. Screw them in an X-shape going across the device which helps an application of even pressure on the seal.
      i. Tighten the screws so that an even ring can be seen around the entire seal when the device is flipped over.
      ii. It is helpful to allow the screws to latch onto the device a few turns and then flip the device over so the seal can be seen.

iii. Tighten the screws enough so the seal forms a darker ring with the acrylic device. Do not tighten it anymore than that. Some of the washers might still be loose but that is okay. If it is tightened too much the rubber seal will buckle and the device will leak.

3. Top Assembly

   a. Flip the device so it is standing on the two legs.

   b. Place the gasket with the square opening onto the top of the bottom of the device lining up the screw holes and the square cutout.

   c. Carefully place the membrane onto the device following proper protocols. Ensure that the membrane is flat when placing it on the gaskets. Because of the material of the gaskets, the membrane should 'stick' to them so placement of the membrane the first time is critical.

   d. Gently place the sloped gasket with the slopes down (meaning that if flow were to run it would follow a gradual path to the membrane) again aligning the screw holes and the cutout.

   e. Place the top of the device onto the sloped gasket aligning it via the screw holes.

   f. Use 8 M3-0.5-20 screws to screw all components of the device together.

      i. When you screw the device start with the screws in the middle and continue working in opposite sides and opposite corners in an X shape. This helps make sure no air is captured in between the gaskets.

4. Flow System Setup

   a. Attach the syringe reservoir to the ring stand using the appropriate attachment.

   b. Connect the shorter length of tubing to the bottom of the syringe reservoir and the other end to one end of the assembled device.

   c. Take the longer section of tubing and connect one end to the other end of the device.

   d. Plug in the peristaltic pump and turn it on. Feed a portion of the longer section of the tubing through the pump. The other end of the tubing should be placed in the top of the syringe reservoir and held there using the rubber stopper.

   e. Place all components except for the pump onto a tray for easy transport into and out of the incubator.

   f. Follow proper protocol on running the flow test.

Appendix XI: Static Migration Tests

HLMVEC

1. Autoclave membranes at 121°C for 30 minutes.
2. Attain a 60 mm x 15 mm petri dish and transport to a biosafety cabinet.
3. Attain 20 μg/mL fibronectin and HLMVEC media.
4. Using forceps, transfer the sterile membrane into the petri dish.
5. Using a micropipette transfer ~500 μL fibronectin directly on top of the membrane (try only to cover the membrane).
6. Let fibronectin sit at room temperature for an hour.
7. Carefully aspirate the fibronectin by tilting the plate and aspirating it from the bottom of the dish (do not directly aspirate on top of the membrane).
8. Culture HLMVECs and dilute them into a concentration of 600k cells/ mL.
9. Place 500 μL of cell solution onto the membrane (try to only place on top of the membrane).
10. Place in the incubator (37°C at 5% CO2) and let it attach for 1 hour.
11. After an hour, place 5 mL of media into the plate (place this on the side of the plate to prevent pushing cells off of the membrane).
12. Place in an incubator for 1 day until cells are 100% confluent.

MDA-MB-231

1. Sterilize two Petri dishes (1x150 mm, 1x 35 mm) by spraying them with 70% IPA and UV-treating them under the hood for 15 minutes.
2. Autoclave the membrane at 121°C for 30 minutes and bring it under the hood.
3. Attach the membrane to the bottom of the cutout hole of the 150 mm Petri dish using Loctite silicone sealant and allow the sealant to cure for about 24 hours.
   NOTE: Can use a micropipette tip to spread to the silicone sealant.
4. Place the 35 mm Petri dish right below the cutout hole of the 150 mm Petri dish in case there are any media leakages through the membrane.
5. Add 1x10^6 MDA-MB-231 cancer cells in 1 mL of media on top of the membrane with HLMVECs. Prior to this, the cancer cells should have been stained with Far Red CellTrace.
6. Place the 35 mm Petri dish right below the cutout hole of the 150 mm Petri dish to collect any cancer cells that pass through the membrane.
7. Move the system into the incubator and let it sit for 1 hour.
8. After 1 hour, image the 35 mm Petri dish to see if any cancer cells have migrated through the membrane.

HLMVEC + MDA-MB-231

For this experiment, the following components are needed:

- 150 mm x 15 mm petri dish with a small cutout hole (about 20 mm diameter) in the center.
- 35 mm x 15 mm petri dish
- Silicone sealant
- 3.0-micron membrane

1. Sterilize two Petri dishes (1x150 mm, 1x 35 mm) by spraying them with 70% IPA and UV-treating them under the hood for 15 minutes.
2. Autoclave the membrane at 121°C for 30 minutes and bring it under the hood.
3. Attach the membrane to the bottom of the cutout hole of the 150 mm Petri dish using Loctite silicone sealant and allow the sealant to cure for about 24 hours.
   NOTE: Can use a micropipette tip to spread to the silicone sealant.
4. Coat the membrane with 500 μl of 20 μg/mL fibronectin and incubate at room temperature for 30 minutes.
5. Bring the system under the hood and aspirate fibronectin.
6. Place the 35 mm Petri dish right below the cutout hole of the 150 mm Petri dish in case there are any media leakages through the membrane.
7. Seed 300k HLMVECs in 500 uL media onto the membrane, bring the system to the incubator and allow the cells to attach to the membrane for 1 hour.
8. After 1 hour, bring the system back into the hood and carefully add 5 mL of HLMVEC media to the 150 mm Petri dish, avoiding direct contact with the cells on the membrane to not disrupt their attachment. Cover the 150 mm Petri dish to prevent contamination.
9. Move the system to the incubator and let it sit there for 2-3 days until the cells reach 100% confluency.
10. After 2-3 days, image the membrane to ensure the cells have reached 100% confluency.
11. Bring the system back to the hood and aspirate the HLMVEC media.
12. Add 1x10^6 MDA-MB-231 cancer cells in 1 mL of media on top of the membrane with HLMVECs. Before this, the cancer cells should have been stained with Far Red CellTrace.
13. Place the 35 mm Petri dish right below the cutout hole of the 150 mm Petri dish to collect any cancer cells that pass through the membrane.
14. Move the system into the incubator and let it sit for 1 hour.
15. After 1 hour, image the 35 mm Petri dish to see if any cancer cells have migrated through the membrane.

Appendix XII: Staining WGA and DAPI Procedures

1. Aspirate media from plate.
2. Wash the membrane in PBS (about 1 mL is plenty) and let sit for 2-5 mins.
3. Aspirate the PBS from the Petri dish.

   NOTE: Tilt the plate to let the PBS flow off to the side and aspirate the liquid. Don't put the tip anywhere near the membrane or make contact with a surface that cells are on. You can tap the plate on the hood surface to try to encourage the PBS to drain out.

3. Mix PFA (paraformaldehyde) with PBS (pipette up + down to mix).

   NOTE: Did 40 µL PFA in 960 µL of PBS for 1000 µL 3-4% PFA in PBS

4. Transfer the PFA + PBS mixture onto the membrane (500 µL per membrane).
5. Incubate the cells in 3-4% PFA in PBS at room temperature for 20-30 minutes.
6. Aspirate staining/fixing solution.

   NOTE: Use the same tilt and tap technique to avoid aspirating cells.

7. Wash fixed cells 2-3x in PBS for about 2-5 minutes (use the same procedure from steps 1-2).
8. If not staining immediately follow steps (9-11) if staining these can be skipped.
9. Fill the cell culture plate containing the membrane with PBS so that the membrane is completely submerged.
10. Close the plate, cover it thoroughly with parafilm, and place it in a +4°C fridge.
11. Aspirate PBS from PDMS membrane and dish.

    NOTE: tilt and gently tap the dish to get the PBS out of the vasculature without aspirating directly.

12. Prepare 6 mL of 3% BSA in PBS (180 µL in 5820 µL PBS).
13. Using the blocking solution of 3% BSA in PBS: fill membrane with ~500-600 µL of blocking solution and let sit for 30 minutes at room temperature.
14. While this is going on, Prepare WGA primary antibody: 10 µL WGA primary antibody in 2000 µL of blocking solution (3% BSA).
15. Following the 30 min from step 13, aspirate the blocking solution from the plate containing the membrane.
16. Immediately cover the membrane(s) with 1000 µL of the primary antibody mixture.
17. Let sit in darkness at room temperature for 30 minutes.

18. After 30 minutes have passed, aspirate excess antibodies gently.

19. Wash 3 times with PBS (1-2 mL per wash), 5 min per wash.

20. Prepare WGA secondary antibody: 4 μL of secondary antibody in 2000 μL PBS.

21. Place ~1000 μL of secondary antibody solution (pipette up and down to mix thoroughly) onto each membrane.

22. Repeat steps 17-19.

23. Attain a glass slide and DAPI mounting media.

24. Place a 40 μL drop of mounting media and place the membrane (cells facing up) onto the glass slide.

25. Place a 40 μL drop of DAPI mounting media on top of the membrane and cover with a glass coverslip.

26. Seal the edges of the glass coverslip with clear nail polish.

27. Place in a slide holder and put in the fridge until needed for imaging.

Appendix XIII: Quantification Procedure

Percent Coverage:

1. Open ImageJ
2. Open an image
3. Image → color → make composite
4. Image → color → split channels
5. Image → adjust → threshold
   a. adjust the threshold until it looks accurate compared to the initial composite
   b. subtract percentage given from 100% to get percent coverage

Thickness of Glycocalyx:

1. Open ImageJ
2. Open an image
3. Image → color → make composite
4. Image → color → split channels
5. Image → adjust → color balance
   a. Decrease the background noise in the blue and green channels
6. Image → color → merge channels
   a. make sure only the green and blue channels are selected
7. Image → stacks → orthogonal view
8. Image → duplicate
9. Using the line tool, measure each green spot you see in the orthogonal view and press ctrl M to document it.
10. Repeat steps 8 and 9 at two more locations in the image
   a. we chose top, middle, and bottom
11. Average out all the measurements to determine the average thickness

Number of Cancer Cells:

1. Using Keyence BXZ810 take at least three images at different positions for each category of each trial: Experimental Membrane, Experimental Reservoir, Control Membrane, Control Reservoir. Name them accordingly and save them on your drive (you can group them into folders for easier reference).

Follow the following steps for each image separately.

2. Open ImageJ.

3. Drag and drop each image onto ImageJ.

4. Go to Plugins → Analyze → Cell Counter Notice. Press "OK" on the pop-up window. You should see another pop-up window like the one below:

5. To count the cells, click on each cell (stained red). The counter will display the number of cells you have counted once you are done.

6. Open an Excel sheet. Create a table with the following categories: Experimental Membrane, Experimental Reservoir, Control Membrane, Control Reservoir. If you are running multiple experiments, create extra sheets indicating each trial as needed.

7. Transfer the number of cells you have counted into the Excel sheet under the corresponding category. You should have at least three numbers for the same category for each sheet.

8. Find the mean value for each category, utilizing Excel's formula [=AVERAGE()]

9. After you are done with all your images from all the trials, transfer the mean values for each trial and each category into a separate sheet (formatted similarly with all the categories: Experimental Membrane, Experimental Reservoir, Control Membrane, Control Reservoir)

10. Find the mean, standard deviation, and the standard error of the mean for each category by using the following formulas:

    a. Mean: [=AVERAGE()]

    b. Standard Deviation: [=STDEVA()]

    c. Standard Error of the Mean: [=STDEVA()/SQRT(n)], where n indicates the number of trials.

11. Transfer this information to GraphPad Prism software for plotting and statistical analysis.